# Engineering aglycosylated antibody variants with immune effector functions



by

Stephen L. Sazinsky

A.B. Chemistry
Princeton University, 2001

Submitted to the Department of Biological Engineering
in Partial Fulfillment of the Requirements for the Degree of

Doctor of Philosophy in Biological Engineering

at the

Massachusetts Institute of Technology

February 2008
[February 2008]



Signature of Author. .....
Department of Biological Engineering
December 9, 2008

Certified by.....
K. Dane Wittrup
J.R. Mares Professor of Chemical Engineering and Bioengineering
Thesis Supervisor

Accepted by.....
Alan Grodzinsky
Professor of Biological Engineering
Chair, Department Graduate Program Committee

Certified by.....

Doug Lauffenburger
Uncas & Helen Whitaker Professor of Bioengineering
Chair, Thesis Committee

Certified by.....

Forest White
Mitsui Career Development Associate Professor of Biological Engineering
Member, Thesis Committee

# Engineering aglycosylated antibody variants with immune effector functions

by

Stephen L. Sazinsky

Submitted to the Department of Biological Engineering
on December 9, 2008 in Partial Fulfillment of the
Requirements for the Degree of Doctor of Philosophy in
Biological Engineering

## ABSTRACT

Monoclonal antibodies have emerged as a promising class of therapeutics for the treatment of human disease, and in particular human cancer. While multiple mechanisms contribute to antibody efficacy, the engagement and activation of immune effector cells – mediated by the interaction of the conserved Fc regions of the antibody with the Fc gamma receptors (FcγRs) on immune cells – is critical to the efficacy of several. This thesis describes the engineering of antibody Fc domain interactions with FcγRs, using the yeast *S. cerevisiae*. In an initial step, a microbial system for the production of full-length antibodies in *S. cerevisiae* in milligram per liter titers has been developed, which serves as a platform for the engineering of antibody Fc domains with defined properties. The presence of a single N-linked glycan on each chain of the antibody Fc, as well as the specific composition of the glycoforms comprising it, are critical to the binding of the Fc to FcγRs, and have largely limited the production of therapeutic antibodies to mammalian expression systems. Using a display system that tethers full-length antibodies on the surface of yeast, we identify and characterize aglycosylated antibody variants that bind a subset of the human low-affinity FcγRs, FcγRIIA and FcγRIIB, with approximately wild-type binding affinity and activate immune effector functions *in vivo*. In a separate approach, we identify aglycosylated variants that weakly bind a third low-affinity receptor, FcγRIIIA, and through subsequent engineering generate variants that bind all of the low-affinity FcγRs with approximately wild-type binding affinity. By decoupling the function of the antibody from its post-translational processing, these variants have the potential to open up therapeutic antibody production to a far wider array of expression systems than currently available. Finally, in parallel work, we use a similar system to screen for glycosylated Fc variants with improved affinity and specificity for the activating receptor FcγRIIIA compared to the inhibitory receptor FcγRIIB, properties which have been hypothesized to lead to more potent antibody therapeutics.

Thesis Supervisor: K. Dane Wittrup
Title: J.R. Mares Professor of Chemical Engineering and Bioengineering

## Acknowledgements

As I hope the following chapters bear out, this project, serendipitous as it was, was an incredibly interesting one to work on, and (I think) a productive one too. A lot of credit, naturally, goes to my advisor Dane Wittrup, whose enthusiasm, in addition to guidance and suggestions, was invaluable in pushing this work forward. One of the best things Dane does as a PI is assemble a wonderful group of people to work with, and I've certainly learned an incredible amount from them, and have really enjoyed the time I've spent with them along the way. Lest anyone feel left out, I would like to very sincerely thank all of the lab members that I've overlapped with, past and present, for your help and your friendship.

In particular, I would like to thank my officemates throughout the years. You've borne an even heavier burden than others in answering my questions and putting up with my eccentricities; I've also really had a lot of fun working (and not working) so close to all of you. So, thank you: Shanshan Howland, Andrea Piatesi, Letha Sooter, Ginger Chao, Annie Gai, and Ben Hackel. I'd also like to thank my long-term neighbors over the years within the lab, for much the same: Andy Yeung, Wai Lau, Margie Ackerman, and Kelly Davis; and finally, some of the 'older' students from the lab, whose perspectives have been invaluable: Jeff Swers, Dave Colby, and Andy Rakestraw. OK, and yes, you too, Jordi Mata-Fink.

I certainly owe a special debt of gratitude to Eugene Antipov and Dasa Lipovsek, both of whom, in different ways, have been extremely important to me throughout grad school. I'm not sure if Eugene has quite paid down the debt of time spent in my early graduate years listening to him discuss love and life, but if he hasn't, he's certainly come close. I'm also not sure if I could ever pay down the debt of gratitude that I owe Dasa for her friendship and her interest in my success, but I hope to.

I had the fortune of spending four months at Genentech during my third year of grad school, through an internship in the Biotechnology Training Program, and I would like to thank Dev Sidhu for giving so much of his time and energy to an intern, as well as the rest of the Sidhu lab, and in particular Yingnan Zhang, for helping to make it such a great experience.

I'd also like to thank my thesis committee members Doug Lauffenburger and Forest White, for helpful discussions about my project, and my UROP, Xindi Song, for her work on improving antibody secretion from yeast (Chapter 2). In addition, part of the work in this thesis was accomplished through collaboration, and while individual contributions are acknowledged at the end of each chapter, in particular I'd like acknowledge Andy Rakestraw, who engineered leader peptides that allow for the improved secretion of IgGs from yeast (Chapter 2); Rene Ott, in Jeff Ravetch's lab at Rockefeller, who performed some of the characterization of the aglycosylated IgG variants (Chapter 3); and Nate Silver, in Bruce Tidor's lab at MIT, who modeled the interaction of aglycosylated Fc with FcγR (Chapter 3).

I would also like to thank my friends in Boston, and in particular: my common-law roommate Seenu Susarla; Brian Chow, who has quite literally known me since when I first started breaking test tubes in high school chemistry class; and Dave Lendler and Marc Gershow.

Finally, last only in order, I would especially like to thank my family. I know that I don't say it often enough, but I am extremely grateful, and thankful, for all that you've done for me. It's certainly an understatement to say that I'm a product of my environment, and I am exceedingly fortunate for it.

## Table of Contents

# Chapter 1. Introduction

Over the past two decades, monoclonal antibodies (mAbs) have emerged as a promising class of therapeutics for the treatment of human disease, and in particular cancer (1-3). To date there are 21 FDA-approved antibodies, nine for the treatment of cancer. In addition, there are over 150 mAbs in various stages of clinical trial, primarily against oncology targets, a number which has increased steadily in recent years (2). In cancer treatment, mAbs have been approved for the treatment of breast cancer (trastuzumab/herceptin), colorectal cancer (bevacizumab/avastin; cetuximab/erbitux; panitumumab/vectibix), non-Hodgkin's lymphoma (rituximab/rituxan; ibritumomab tiuxetan/zevalin; tositumomab/bexxar); and acute myelogenous leukemia (gemtuzumab ozogamicin/mylotarg) and chronic lymphocytic leukemia (alemtuzumab/campath). These mAbs target a number of cell surface proteins, such as the ErbB family receptor tyrosine kinases, the EGF receptor (erbitux, vectibix) and ErbB2/Her2 (herceptin); immune cell associated markers, such as the B-cell expressed CD20 (rituxan, zevalin, bexxar), the myeloid-expressed CD33 (mylotarg) and lymphocyte-expressed CD52 (campath); as well as the soluble angiogenic factor VEGF (avastin).

Monoclonal antibodies contribute to improved therapeutic outcomes through several mechanisms, some of which may occur simultaneously during treatment (4). In one strategy, mAbs can be used to directly alter the signaling properties of a target cell by interfering with an essential event that triggers aberrant cellular behavior, such as the binding of a growth factor to a receptor. Here, the competitive binding of a mAb to the ligand binding site of a receptor (erbitux) or the sequestration of ligand (avastin) serves to block the signaling event. mAbs have also been used to deliver cytotoxic agents – such as toxins, radionucleotides, and DNA damaging agents – to tumor cells. Here, the specificity of mAbs for a tumor-specific antigen is used to distinguish cancerous cells from healthy cells, in turn delivering an antibody-conjugated cytotoxic payload to the tumor (zevalin, bexxar, mylotarg). Alternatively, unconjugated ("naked") mAbs have been used to target tumor-specific antigens and trigger activation of the immune system's native effector functions – those at work during the body's response to infection in the

antibody-mediated adaptive immune response – to initiate immune cell mediated tumor clearance (rituxan).

While all of the above mechanisms contribute to therapeutic efficacy, immune cell activation has been shown to play a critical role, in particular through an mAb's engagement of Fc gamma receptors (FcγRs) (5). The FcγRs, differentially expressed on immune cells, bind to the conserved Fc region of immunoglobulin G (IgG) – the most abundant immunoglobulin (Ig) isotype in serum and the Ig of choice in mAb therapy – and in immunity act to sense the presence of opsonized antigen. Here, the antibody acts as a flexible adaptor molecule, marking an antigen of interest (such as, in the case of mAb therapy, a tumor associated antigen) through the interactions of a diverse set of antibody variable regions that allow for the recognition of a wide array of targets; and in a second step, allow for the recruitment of common immune effector pathways through the recognition of the conserved Fc domain. Of particular interest is antibody-dependent cellular cytotoxicity (ADCC), which leads to phagocytosis of the bound pathogen and release of inflammatory mediators (5), and in therapeutic antibodies directed against tumor-specific antigens, the immune cell mediated killing of antibody-bound tumor cells.

The role of antibodies in immunity, the FcγR family that in part mediates antibody function, and the physical interaction of the two are discussed in more detail below, as well as previous efforts at the engineering of this interaction for improved therapeutic properties.

**The role of IgG in immunity**

Antibodies play a critical role in the adaptive immune response as soluble mediators for marking the destruction of specific pathogens, and comprise a key part of the mechanism in which immunological memory against specific pathogens is achieved. During infection, engagement of B cell receptors (BCRs) with non-self antigen derived from a pathogen – together with a co-stimulatory signal initiated during the innate immune response to infection – leads to the propagation of activated, antigen-binding B cells. Ultimately, further selection and expansion of activated B cells leads to their differentiation into memory cells (which allow for long-term immunological memory for the recognition of a specific antigen) and plasma cells (which produce antibodies, the

soluble form of the BCR). Antibodies circulate and mark the infecting pathogen by binding to the specific antigen recognized by the activated B cell. These antibody-coated pathogens are then cleared through one of several mechanisms: direct neutralization, such as through sequestration of soluble toxins or inhibiting the infection mechanism of a virus; pathogen opsonization – which occurs when several antibodies bind to multiple antigens (or multiple copies of a single antigen) expressed on a cell surface such as that of a bacterium – which leads to phagocytosis and destruction of the pathogen by recognition of the antibody by immune cells; and activation of the complement cascade, present during innate immunity, which leads to lysis of the antibody-bound infecting cell.

B cells respond to a wide set of antigens through molecular diversity in their BCRs, which is generated by the combinatorial rearrangement of multiple gene segments present in the genome, and further diversity is generated after B cell activation through somatic hypermutation, leading to BCRs with higher affinity for antigen. Together, these segments comprise the variable, or V, region of the antibody. While antibodies are unique in their variable regions, they share common effector pathways that are mediated by a small set of framework constant regions. These functions are spatially distant in the "Y-shaped" antibody structure, as one end of the antibody molecule, comprising the two variable-domain containing Fab arms, binds antigen, while the opposite end, comprising the Fc domain, which is connected to the two Fab arms by a flexible hinge, interacts with the immune system.

During activation and maturation, B cells switch the constant regions associated with the antigen-binding variable regions. There are five different Ig heavy chain constant region isotypes – IgG, IgM, IgA, IgD, and IgE – and over the course of an immune response a B cell will typically irreversibly switch to the production of IgG. In addition, within the IgG isotype there are four subclasses ($IgG_{1, 2, 3, \text{and } 4}$), which reflect the order of their serum abundance. Most therapeutic mAbs are of human, murine, or chimeric IgG origin, with the human $IgG_1$ subclass most commonly used in therapy.

**The human FcγR family**

The human FcγR family, differentially expressed on immune cells, recognizes IgG primarily in the context of antibody:antigen complexes. The hFcγR family consists

of the activating receptors FcγRI, FcγRIIA, and FcγRIIIA, as well as the inhibitory receptor FcγRIIB. FcγRI binds Fc with high affinity, and is thought to be occupied by monomeric IgG, and is thus incapable of binding antibody-bound antigen. Deletion of FcγRI in murine models has no effect on therapeutic antibody activity, and it is thought that this FcγR is dispensible for therapeutic efficacy (5). In contrast, FcγRIIA, FcγRIIB, and FcγRIIIA (the "low affinity FcγRs") bind Fc with weak affinity (micromolar binding constants), approximately two to three orders of magnitude weaker than FcγRI. These FcγRs become activated only through multivalent interactions between immune cells and antibody-coated target cells, and engagement of these receptors is thought to be critical to therapeutic response.

The extracellular domains of the low-affinity FcγRs share similar two-domain topologies, folding into highly similar three-dimensional structures. The signaling properties of the FcγRs are controlled by the presence of cytoplasmic immunoreceptor tyrosine-based activation motifs (ITAMs) or inhibitory motifs (ITIMs) associated with the FcγR, either directly linked through the transmembrane domain, in FcγRIIA and FcγRIIB, or through the association of a common gamma chain, in FcγRIIIA and FcγRI. The FcγRs become activated through receptor crosslinking, a result of the simultaneous engagement of multiple IgGs bound to a target antigen. The extracellular domains of FcγRIIA and FcγRIIB are highly identical (sharing greater than 90% sequence identity), and intracellularly differ in the presence of an ITIM in FcγRIIB, the lone inhibitory receptor. In addition, allelic variation exists within both FcγRIIA (which can contain an Arg or a His at position 131) and FcγRIIIA (which can contain a Val or Phe at position 176) – these variations, located near sites of contact between IgG Fc and FcγR, impact binding affinity, and in some cases, biological response.

**Interactions between IgG and FcγRs**

The FcγRs bind to a cleft in the antibody Fc formed by the antibody hinge and the loops of the CH2 domain (6, 7), making asymmetric contacts with the homodimeric Fc. In addition to the lower hinge region, three CH2 loops make direct contacts with receptor: the B/C loop, the C'/E loop, and the F/G loop. The C'/E loop, in addition to mediating protein-protein interactions, encodes information for an essential post-

translation modification – the addition of a glycan to an asparagine residue (in human $IgG_1$, at position asparagine 297) – which is thought to allow the Fc to adopt an open conformation capable of being bound by FcγR (8). Loss of Fc N-linked glycosylation – either through enzymatic truncation, point mutation, expression in the presence of N-linked glycosylation inhibitors, or prokaryotic expression – has been shown to ablate FcγR binding and immune cell activation, leading to the view that N-linked glycosylation of the IgG Fc is strictly required for activation of immune effector functions. In addition, the binding of FcγRs, and subsequent biological response, is sensitive to the types of sugar residues comprising the glycan. For example, the absence of a fucose residue increases the affinity of FcγRIIIA for Fc, promoting a more potent activating response (9), while the presence of terminal sialic residues switches the IgG to an anti-inflammatory mode (10).

The differential engagement of the low-affinity FcγRs – in particular the lone inhibitory receptor FcγRIIB and the activating receptor FcγRIIIA, the only FcγR expressed on natural killer cells – has been shown to be important to therapeutic response. Murine models have shown that lack of the inhibitory signal, or a large preference for engaging activating receptor over inhibitory receptor, lead to greatly enhanced therapeutic responses (11, 12), suggesting that the balance of signals coming from the engagement of activating and inhibitory FcγRs on a given immune cell is a key factor in antibody potency. In addition to the inhibitory signal, the strength of activating signals also appears to be important to antibody efficacy. Clinical data of patients treated with the FDA-approved antibodies rituxan and herceptin have shown a significant correlation between objective response rate and allelic variation within FcγRIIIA, with patients homozygous for a valine at position 176 of the receptor, instead of a phenylalanine, having significantly better outcomes (13-16). The FcγRIIIA 176V allele ($FcγRIIIA^{176V}$) binds Fc several-fold more tightly than $FcγRIIIA^{176F}$, suggesting that the persistence of engagement of this activating receptor is a key factor in therapeutic outcome. To this end, numerous approaches have been taken to engineer the interaction of antibody Fc with FcγR for improved immunotherapy (17).

**Implications of antibody N-linked glycosylation to biotechnology**

N-linked glycosylation, critical for the recognition of IgG by FcγR, occurs at asparagine residues within the polypeptide motif Asn-Xaa-Ser/Thr (where Xaa can be any amino acid except Pro), and is a common feature of the eukaryotic protein folding and secretory pathway. While the initiation of this post-translational processing is conserved across eukaryotic organisms, through the attachment of a common core oligosaccharide to the asparagine residue, the downstream N-linked glycosylation pathways and processing of the glycan vary widely among eukaryotes, resulting in widely divergent glycan structures. The human N-linked glycan (depicted in Figure 3.10), is a branched structure, resulting from the trimming of sugars from the core structure and subsequent differential addition of terminal galactose and sialic acid residues, as well as a fucose residue.

Other expression hosts commonly used in biotechnology for the production of recombinant proteins differ greatly in their glycan processing. The prokaryote *E. coli* lacks the N-linked glycosylation machinery, producing aglycosylated proteins; the yeast *S. cerevisiae* attaches multiple mannose residues to the core structure, resulting in hypermannosylation; and the yeast *P. pastoris* likewise attaches terminal mannose residues, although without hypermannosylation. In addition to these microbial expression systems, other expression systems, such as filamentous fungi (terminal mannose residues), plants (attachment of non-human sugar residues), and insect cells, all have non-human N-linked glycosylation patterns. In the context of therapeutic antibody biomanufacture, such variation in the composition of the N-linked glycan – in addition to altering FcγR binding affinity – can lead to the presence of sugars that are rapidly cleared and/or immunogenic, greatly decreasing the serum half-life of the mAb. As a result, production of therapeutic antibodies has largely been limited to mammalian cell lines capable of attaching human glycans, or more recently, to yeast strains engineered to allow for humanized glycosylation patterns (18).

**Previous approaches to engineering antibody Fc domains**

Numerous approaches have been taken to engineer the properties of the antibody Fc and its interaction with FcγR, in particular with FcγRIIIA, which has been strongly

correlated with objective response. These approaches fall into two classes: altering the composition of the N-linked glycan attached to the Fc, or altering the characteristics of the polypeptide chain itself (17). In the glyco-engineering front, human cell lines have been developed to preferentially express proteins with defucosylated N-linked glycans (19), which allow for higher affinity binding to FcγRIIIA and more potent receptor activation; in addition, *P. pastoris* strains engineered to attach homogeneous populations of humanized glycoforms to IgG are also capable of eliciting enhanced FcγRIIIA binding and immune cell activation (18).

Similarly, most efforts to engineer the polypeptide itself have focused on increasing the binding affinity to FcγRIIIA, and have employed a variety of protein engineering methods. In one approach, *in silico* prediction and experimental validation was used to construct an Fc variant that binds FcγRIIIA with approximately 100-fold increased affinity (20). Separate approaches have also aimed to selectively increase the binding affinity to the activating FcγRIIIA compared to inhibitory FcγRIIB (21, 22), or to the activating FcγRIIA compared to FcγRIIB (23). In one approach, alanine scanning point mutagenesis was used to comprehensively define Fc positions that contribute to FcγR specificity, and alanine point mutants combined to generate an Fc variant with enhanced specificity (21). In a second approach, yeast display of randomly mutated Fc libraries was used to identify point mutations that both improve binding to FcγRIIIA, as well as those that impart FcγRIIIA-specific binding, and then mutations combined to generate a variant Fc that binds FcγRIIIA with approximately 10-fold increased affinity but imparts little change in binding affinity to FcγRIIB (22).

**Summary of thesis work**

In the following chapters, I describe the production and engineering of antibodies and antibody constant domains in the yeast *S. cerevisiae*. Chapter 2 describes a microbial system for the production of full-length antibodies in *S. cerevisiae*, achieving yields of secreted antibody approximately 200-fold greater than those previously reported for this yeast. In addition to enabling the laboratory-scale production of IgGs in low milligram per liter titers, this system also serves as a platform for the engineering of antibody Fc

domains with defined properties, outlined in Chapters 3 through 5. A shortcoming of our yeast expression system, and in general any microbial or non-human therapeutic antibody expression system, is the inability of the host organism to place native N-linked glycans on the Fc of the IgG. The presence of the N-linked glycan, as well as the specific composition of the glycoforms comprising it, is critical to the binding of the Fc to FcγRs on immune cells and subsequent immune cell activation. Thus, decoupling this binding event from the post-translational processing of the antibody should allow for the production of therapeutic antibodies in expression systems not currently accessible for antibody biomanufacture. In Chapter 3, I describe the identification of aglycosylated antibody variants that bind a subset of the human low-affinity FcγRs, FcγRIIA and FcγRIIB, with approximately wild-type binding affinity and activate immune effector functions *in vivo*. Building upon this work, Chapter 4 describes the engineering of aglycosylated Fc variants that bind all of the low-affinity FcγRs with approximately wild-type binding affinity. Finally, Chapter 5 addresses another challenge in antibody Fc engineering, the engineering of binding specificity between activating and inhibitory receptors, which has been hypothesized to lead to more potent antibody therapeutics.

# Chapter 2. Secretion of full-length IgG from *S. cerevisiae* [1]

## Introduction

The expression of heterologous proteins in microorganisms has long facilitated the detailed characterization as well as biotechnological use of many proteins of interest. Expression in hosts such as the bacterium *Escherichia coli* and the yeast *Saccharomyces cerevisiae* offer several advantages, such as fast doubling times, high cell densities, inexpensive cell culture and fermentation requirements, and well-characterized and easily manipulatable genomes, making them highly accessible and productive systems. Eukaryotic expression hosts offer the advantages of the eukaryotic protein folding machinery, oxidative folding environment, and ability to attach N-linked glycans, a common post-translational modification of eukaryotic proteins; *S. cerevisiae* in particular is an extremely well characterized model organism, with much known about its genetics and biochemistry.

Of particular interest to the biotechnology community is the expression of immunoglobulins, a class of molecules utilized in immunity for the recognition and subsequent clearance of pathogens. The advent of hybridoma technology (24) enabled the production and characterization of monoclonal antibodies, a modality that has rapidly become a platform of choice to specifically recognize myriad therapeutic targets, and in particular oncology targets (2). In addition, the specific recognition of proteins of interest conferred by antibodies has led to their widespread use as all-purpose reagents in laboratory settings, enabling an array of immunoassays.

While antibody fragments such as scFvs and Fabs have been efficiently produced in microbial expression systems, the expression of fully-assembled immunoglobulins in microbial expression systems has met with more modest success. In *E. coli*, Simmons and coworkers achieved ~ 100 mg/L titers under fermentation conditions, by developing a dual cistron system for controlling the mRNA levels of heavy and light chain transcripts, which was found to greatly affect the yield of fully-assembled antibody (25). More

[1] Portions of this chapter are adapted from a manuscript under review, "Directed Evoluiton of a Secretory Leader for the Improved Expression of Heterologous Proteins and Full-Length Antibodies in *S. cerevisiae*", J. Andy Rakestraw*, Stephen L. Sazinsky*, Andrea Piatesi, Eugene Antipov, and K. Dane Wittrup.

recently, Mazor and coworkers reported a dicistronic system that allows for ~ 0.2 – 1 mg/L expression in shake flask culture (26)

Less progress has been made in the secretion of fully-assembled immunoglobulins from *S. cerevisiae*, which has not been shown to secrete full-length IgG in titers sufficient for use as an expression host (27). Wood and coworkers reported the intracellular accumulation of low levels of IgM (28), and later, Horwitz and coworkers reported the secretion and purification of fully-assembled human IgG, at yields of approximately 50 μg/L in 5 mL shake flask culture (29). Other yeasts, such as *Pichia pastoris* (30) and filamentous fungi (31) have met with more success, with yields up to 30 mg/L reported for *P. pastoris* and 900 mg/L for *Aspergillus niger*.

Such reports suggest that there is further capacity for IgG expression from *S. cerevisiae*, and here we ask whether IgG secretion from *S. cerevisiae* can be improved by altering the properties of the signal sequence that directs the movement of the IgG heavy and light chains as they transit through the secretory pathway. Mutant signal sequences, based upon the wild-type alpha mating factor 1 leader peptide (MFα1pp) commonly used to direct the secretion of heterologous proteins from yeast (32, 33) were previously identified using a directed evolution approach, utilizing a cell surface secretion assay (CeSSA) that allows for the quantitative enrichment of surface captured target protein reflective of the true secretion properties of an individual variant (34). The screen identified several MFα1pp variants that improve the secretion of a model scFv, 4m5.3, in some cases up to 16-fold (35). These leaders direct the improved secretion of additional scFvs and the structurally unrelated proteins HRP and an IL-2 variant, from two- to five-fold (35).

Below, we show that the combination of leader sequence evolution as well as engineering of the host strain leads to the secretion of fully-assembled IgG in low mg/L titers, an approximately 200-fold improvement over previously reported yields (29). In the process, we characterize the IgG secreted from *S. cerevisiae*, highlighting some of the challenges in using this expression host.

## Results

**Construction of *S. cerevisiae* hIgG$_1$ secretion vectors.** The yeast IgG secretion vectors, created by Andy Rakestraw, are detailed in his thesis (35). Briefly, the human IgG$_1$ heavy chain and human kappa light chain were cloned out of the vector 6-23 IgG (36), a derivative of the mammalian hIgG$_1$ secretion vector pPNL501 (generous gift of Michael Feldhaus, formerly of Pacific Northwest National Labs), and placed in front of the galactose inducible GAL10 promoter and alpha terminator on the auxotrophic shuttle vectors, pRS316 and pRS314 (37), respectively. To direct the secretion of the polypeptide, the wild-type alpha-factor pre-pro signal sequence (MFα1pp), as well as the evolved versions αpp8 and αppS4 (35), were placed in front of the heavy and light chains. The heavy chain secretion vector contains unique MluI and NheI restriction sites for variable domain cloning; the light chain secretion vector contains unique NheI and BsiWI sites for variable domain cloning, as well an N-terminal FLAG epitope tag following the secretion signal and Kex2 Lys-Arg cleavage site, for characterization and purification.

**Initial secretion of IgG from *S. cerevisiae*.** As an initial model system for hIgG$_1$ secretion from *S. cerevisiae*, the 4m5.3 variable domains (38) were cloned into the yeast secretion vectors, co-transformed into BJ5464α and the PDI-overexpressing derivative YVH10 (39), and assayed for their ability to direct IgG secretion. Yeast cell culture supernatants of αpp8- and αppS4-led 4m5.3 IgG displayed large (low mg/L) secretion yields by fluorescein quench titration assay (Andy Rakestraw, unpublished results), yet sequential Protein A and FLAG purification yielded little purified IgG (Andy Rakestraw, unpublished results), suggesting the presence of relatively large amounts of antibody, but not in a purifiable format.

The data suggest the presence of functional antibody variable domains, yet non-functional or non-assembled constant domains. Western blots of yeast culture supernatants confirm this hypothesis (**Figure 2.1**). Anti-Fc (polyclonal) blotting under reducing conditions reveals distinct heavy chain bands, with two bands displaying mobility approximately that of a hIgG$_1$ kappa control, and two additional bands present with much faster mobility, at approximately 30 kDa (fragment 1) and 10 kDa (fragment

2). The presence of these smaller, anti-Fc reactive bands suggests that the heavy chain is proteolyzed during the secretion process.

To confirm heavy chain proteolysis, as well as characterize the fragments present during secretion, 4m5.3 IgG was freshly secreted and purified with an anti-Fc polyclonal antibody, and bands present from the purified protein subjected to N-terminal sequencing. N-terminal sequencing of the two lower molecular weight bands revealed the following mixture of N-termini:

Fragment #1: KVEPKS
Fragment #2: TISKAKG, AKGQPRE

When mapped to the $hIgG_1$ sequence, these fragments suggest proteolysis after lysine residues at positions K213, K334, and K338 (**Figure 2.2**), and give expected fragment molecular weights of 26.3 kDa (234 amino acids), 12.7 kDa (113 a.a.), and 12.3 kDa (109 a.a.). K213 is located at the C-terminal end of the heavy chain CH1 domain, adjacent to the hinge region; K334 and K338 are located in the CH2 domain, near the CH2-CH3 domain interface (**Figure 2.2**). Given their location near relatively flexible regions of the IgG structure, it's possible that these sites represent protease accessible regions of the heavy chain.

**Approaches to limiting heavy chain proteolysis.** Experiments using control $hIgG_1$, treated with or without reduction with DTT and/or with and without boiling to denature the polypeptide, reveal that proteolysis likely does not occur after secretion of IgG into the cell culture supernatant, but intracellularly, as no heavy chain degradation products are present during the secretion of an irrelevant control protein (data not shown). To limit or eliminate proteolysis during the secretion process, as well as test the hypothesis of site-specific, enzymatic proteolysis, a series of lysine to alanine point mutants were constructed and analyzed by anti-Fc Western blotting (**Figure 2.3**). K334A alone does not eliminate the ~10 kDa molecular weight band, as well as an ~40 kDa band that likely represents heavy chain residues 1-333 and 1-337, yet K334A/K338A appears to remove both of these bands (**Figure 2.3b**), consistent with the N-terminal sequencing data.

Interestingly, K213A/K214A alone does not limit proteolysis, but the quadruple mutant K205A/K210A/K213A/K214A does, suggesting that other nearby sites contribute to cleavage (**Figure 2.3a**). Given the presence of multiple lysine residues flanking K213, we asked which combinations of alanine mutations would block proteolysis. The minimal mutant, K210A/K213A, limits the presence of the ~ 30 kDa band, suggesting that this double mutant could alter protease recognition (**Figure 2.3b**). Secretion of the quadruple mutant K210A/K213A/K334A/K338A, which combines the minimal motifs at both protease sites, yields full-length IgG under non-reducing conditions (**Figure 2.3c**). Thus, removal of specific lysines limits proteolysis, although in the process appears to reduce secretion yields, as evidenced by the faint bands present (compare **Figure 2.3c** to **Figure 2.6**, left, with equivalent loading standards).

As an orthogonal approach, a search of known *S. cerevisiae* endoproteases pointed to a family of enzymes, the yapsins, which cleave after mono- and dibasic residues (40, 41). Much precedent exists for the unintended action of yapsin proteases in the secretion of heterologous proteins from yeast, in particular implicating the enzymes yps1 and yps2 (42-45). To probe the hypothesized role of the yapsins in proteolysis, as well as potentially create an improved strain for the secretion of full-length IgG, the single yapsin deletions ΔYPS1, ΔYPS2, and ΔYPS3 were constructed in the parent YVH10 strain, through homologous recombination of a kanmx cassette into the native YPS genes, and assessed for the extent of heavy chain proteolysis during 4m5.3 IgG secretion (**Figure 2.4**). IgG secretion from all deletion strains does not vary significantly than that from the wild-type strain, as similar, lower molecular weight anti-Fc reactive bands are present for secretion from all strains.

In addition to altering the characteristics of the polypeptide and the strain, the effect of induction temperature upon proteolysis was assessed (**Figure 2.5**). Interestingly, and fortuitously, there is a strong correlation between induction temperature and proteolysis, with almost complete proteolysis occurring at 37 °C induction, substantial proteolysis occurring at 30 °C induction (the standard induction temperature used in the above experiments), and limited proteolysis at 20 °C. At 20 °C induction, reducing and non-reducing anti-Fc and anti-FLAG Western blots show the presence of fully-assembled $hIgG_1$ with limited proteolysis (**Figure 2.6**). Interestingly, for 4m5.3, the light chain is

secreted in vast excess over the heavy chain, as evidenced by a faint high molecular weight band of fully-assembled IgG present in the anti-FLAG blot, compared to the intense lower molecular weight band (free light chain monomer) and the ~ 50 kDa band (light chain dimer) (**Figure 2.6**, right). This is perhaps a feature of microbial expression of antibody chains, as a vast excess of light chain was also observed during *E. coli* expression (25).

**Characterization of *S. cerevisiae* secreted IgG.** To characterize the yeast-secreted IgG, 4m5.3 $hIgG_1$ was expressed in 1 L shake flask culture and purified. Protein gels of protein A and FLAG-purified supernatant show a band consistent in size with a full-length human $IgG_1$ (**Figure 2.7**). Additional, smaller molecular weight bands consisting of partially assembled IgG are also purified. When reduced with DTT, the IgG bands collapse into a 30 kDa light chain band and two Fc-containing bands at approximately 50 kDa. Treating the IgG with the N-glycosidase EndoH results in a slight increase in the mobility of both heavy chain bands. The new mobility is consistent with that of the DTT-reduced, non-N-glycosylated 4m5.3 N297Q mutant, which removes the lone N-linked glycosylation site in $hIgG_1$, demonstrating that the fully assembled IgG contains N-linked Fc glycosylation. Further treatment of the IgG with mannosidase causes the upper heavy chain band to collapse into the lower band, suggesting that a subpopulation of the secreted heavy chain has some O-linked glycosylation in addition to the typical N-linked Fc glycosylation. N-terminal sequencing of the upper and lower heavy chain bands were both consistent with proper signal sequence cleavage (data not shown), eliminating this as a possible explanation for the differences in mobility. It also appears that some higher molecular weight N-linked glycosylated protein is present (lanes 6 and 8), likely indicative of uncleaved, glycosylated, leader peptide.

4m5.3 IgG secretion was further enhanced through manipulation of the host strain. IgG secretion directed by the αpp8 and αppS4 leaders was compared to the wild-type leader with and without the overexpression of protein disulfide isomerase (PDI), a chaperone previously shown to be beneficial to scFv expression (**Figure 2.8**) (39, 46). The improved leaders, in combination with PDI, enhanced IgG secretion 50-fold over the wild-type leader alone, with about 25-fold of that improvement due to the mutant leaders.

In previous studies, it has been shown that heterologous protein expression can put significant negative selection pressure on low-copy plasmid retention resulting in a substantial subpopulation of cells to be plasmid negative (47, 48). To compensate for expression instability caused by the dual plasmid system, chromosomal integrations of the two genes were made resulting in an additional four-fold improvement in secretion. The total yield of 4m5.3 IgG secreted from the enhanced expression strain in five mL culture was determined to be approximately 9 mg/L by fluorescein quench assay and quantitative Western blotting. The total yield of a one-liter shake flask culture after protein A and FLAG purification was determined to be approximately 1.5 mg/L. Combined, these strategies impart a 200-fold improvement in IgG secretion over the native leader alone making *S. cerevisiae* a productive host for the expression of full-length IgG.

To test IgG functionality and specificity, the heavy and light chains of the 4m5.3 IgG were reformatted to express the anti-EGFR antibody 225 as well as the anti-CEA antibody sm3E as $hIgG_1$ chimeras (**Figure 2.9**). Antibody titers for 225 and sm3E in 1 L cultures were similar to or better than the yields derived for 4m5.3 expression. The 4m5.3 IgG binds strongly and specifically to yeast cells labeled with fluorescein. The yeast-produced 225 IgG binds to the EGFR expressing A431 cell line and is competed off when cells are pre-incubated with murine 225 or when the IgG is pre-incubated with soluble 404SG, a yeast produced version of the extracellular domain of EGFR, demonstrating antigen specificity. Similarly, the sm3E IgG labels the CEA-expressing LS174T cell line and can be competed off with sm3E scFv. Functional expression of these three antibodies, derived from different mouse variable genes, and in some cases further altered by humanization and affinity maturation, suggests that this system can robustly express full-length antibodies regardless of their family or origin.

## Discussion

Through a combination of leader sequence engineering and secretion optimization, we demonstrate that *S. cerevisiae* can be used as a host for the expression of fully-assembled IgG in milligram per liter titers, making it an accessible laboratory-scale tool for antibody production. Such a system may enable the rapid production of reagents, the engineering and characterization of antibodies of interest, or, as described in subsequent chapters, serve as a platform for the high-throughput engineering of antibody Fc domains with desired properties.

The yields we see represent an approximately 200-fold improvement over previously reported IgG secretion yields from *S. cerevisiae* (29), and come from a variety of sources. By far the greatest source of improvement is imparted by the mutant leaders themselves, which account for an approximately 25-fold improvement. Over-expression of protein disulfide isomerase, which has previously been shown to improve the expression of disulfide-containing proteins (39) and immunoglobulin-derived scFvs (46), contributes about a two-fold increase. Finally, chromosomal integration of the heavy chain and light chain open reading frames (ORFs) accounts for an additional four-fold increase. The contribution of signal sequence engineering alone highlights the success of this approach, and points to its potential as a tool that can be used alongside, or in the case of our work, in conjunction with traditional approaches to protein expression improvement, which typically consist of host strain manipulation.

While we have achieved vast improvements in the secretion of fully-assembled IgG from *S. cerevisiae* – in terms of yield, quantified at approximately two orders of magnitude – there is still substantial room for improvement in this system. In particular, proteolysis of the antibody heavy chain, while dramatically reduced, still greatly reduces yield. Purification of yeast-secreted IgG from 1 L shake flask culture has shown that only approximately 25% of the Protein A purified protein can also be FLAG purified (data not shown), likely due to both proteolysis and the presence of unassembled heavy and light chains. While constructing alanine point mutants at likely protease sites limits proteolysis, it also appears to have generated mutations that reduce secretion, likely offsetting the gains in yield due to improved processing. A better strategy will likely be

through strain manipulation, through identifying and deleting candidate proteases, which also has the advantage of maintaining the native IgG polypeptide sequence. Our initial look at the yapsin family did not identify any single gene deletions that limited proteolysis, although it's possible that yapsin family members could still be the proteolytic agent(s), as members of this family have overlapping substrate specificities (41, 43), and thus a strain with multiple yapsin deletions could allow for non-proteolyzed heavy chain secretion. Another possibility is that IgG secretion leads to elevated stress in *S. cerevisiae*, and finding expression conditions that limit stress may solve the dual problems of heavy chain proteolysis and O-linked mannosylation.

As constructed, our system is most suitable as a laboratory scale tool for the production or engineering of IgGs. In addition to proteolysis and overall yield, the largest hurdle in becoming a viable alternative for therapeutic antibody production is glycosylation. The binding of antibody Fc domains to Fcγ receptors (FcγRs) is highly sensitive to the presence of a single N-linked glycan on the antibody Fc, and while eukaryotes share a core glycan structure, the nature of the sugars attached to this core structure varies widely across organisms. *S. cerevisiae* hypermannosylates N-linked glycans (49, 50), producing a highly variable structure that almost certainly has different FcγR binding properties. In addition, terminal mannose residues, such as those present in typical yeast N-linked glycans, as well the O-linked glycans present on a sub-population of the heavy chains we see, are recognized by mannose receptors and rapidly cleared, and would dramatically reduce the circulation half-time of a yeast-secreted therapeutic antibody. To this end, major efforts have been undertaken to glyco-engineer the yeast *P. pastoris*, resulting in strains with humanized glycosylation patterns (51-54), and in particular for IgG (18). An alternative approach, described in Chapters 3 and 4, would be to develop aglycosylated variants of the IgG Fc in which the function of the Fc (to elicit immune effector functions) is decoupled from its post-translation processing.

## Materials and Methods

**hIgG$_1$ yeast secretion vector construction (35).** The human IgG$_1$ constant heavy chain was PCR amplified from vector 6-23 IgG (55), a derivative of the human IgG$_1$ kappa expression vector pPNL501 (generous gift of Michael Feldhaus) introducing MluI and XhoI sites on the 5' and 3' ends respectively. The heavy chain was then subcloned into the vector WTappD1.3 using the MluI and XhoI subcloning sites. The 4m5.3 variable region was PCR amplified from WTappF4m5.3 with primers introducing MluI and NheI sites with which it was subcloned into the new heavy chain vector. The light chain was PCR amplified from 6-23 introducing 5' and 3' NheI and XhoI restriction sites respectively which were used for subcloning into the WTapp4m5.3 vector to make the 6-23 light chain yeast vector. The 4m5.3 variable light chain region was amplified from WTappF4m5.3 using primers introducing NheI and BsiWI sites used to subclone the $V_L$ behind the WT prepro. Mutant prepro leaders were inserted by amplifying the leaders introducing SphI and NheI sites and cloning them in front of the IgG heavy or light chain ORF.

**Small-scale secretion of IgG for characterization of cell culture supernatants.** 4m5.3 containing heavy and light chain vectors were transformed into YVH10 and selected for growth on SD-CAA plates (2% glucose, 0.67% yeast nitrogen base, 0.54% $Na_2HPO_4$, 0.86% $NaH_2PO_4 \cdot H_2O$, 0.5% casein amino acids, plus 1.5% agar). A single colony was inoculated into 5 ml SD-CAA, pH 6.0 and grown overnight at 30°C until saturation ($OD_{600} \sim 5$). Upon saturation ($OD_{600} \sim 5$), cells were pelleted and resuspended in 5 mL of phosphate buffered YPG, pH 6.0 (2% galactose, 2% peptone, 1% yeast extract, 0.54% $Na_2HPO_4$, 0.86% $NaH_2PO_4 \cdot H_2O$) and allowed to secrete for 72 hrs at a given induction temperature. Cell culture supernatants were harvested by centrifugation, and either directly assayed or stored at 4 °C until assayed.

For integration strains, the heavy and light chain ORFs were subcloned into pRS304 and pRS306, respectively, with KpnI and SacI digests. Five micrograms of vector were linearized by restriction digest and transformed into BJ5464α or YVH10 using electroporation, and selected for growth on SD-CAA plates.

**Western blotting.** For a given analysis, equal volumes of cell culture supernatant were loaded onto 12% bis-tris gels (Invitrogen) and resolved by SDS-PAGE in MOPS running buffer (Invitrogen). Proteins were transferred to nitrocellulose (BioRad), blocked with 5% dried milk in TBS plus 0.1% Tween 20 (TBST), and probed with a 1:2000 dilution of anti-Fc HRP (Pierce) or 1:3000 anti-FLAG HRP (Sigma). Blots were incubated with the Pierce West Dura luminescent substrate (Pierce) and imaged on a FluorS Imager (BioRad).

**N-terminal sequencing.** Wild-type 4m5.3 $hIgG_1$ was secreted from YVH10 in 1 L shake flask culture, under similar conditions as described above, and allowed to secrete for 72 hrs at 30°C. Cell culture supernatant was clarified by centrifugation followed by vacuum filtration, then concentrated and exchanged into PBS, pH 7.4. IgG was purified from concentrated supernatant by an anti-Fc polyclonal antibody conjugated to agarose (Sigma).

5 μg of total purified protein was resolved by SDS-PAGE (described above) and transferred to PVDF (BioRad). PVDF was incubated for 5 min with Coomassie dye, destained with three exchanges of Coomassie destain solution for 60 min each, then washed five times with $ddH_2O$. Upon drying, individual bands were excised from the PVDF blot and submitted for seven cycles of N-terminal sequencing analysis (Tufts University Core Facility).

**Construction of $hIgG_1$ point mutants.** Site-directed mutagenesis was performed by PCR amplifying the entire mutant plasmid using complementary primers containing the desired point mutations in a 50 μl reaction, using Pfu Turbo polymerase (Stratagene). The amplification was digested with one microliter of DpnI (New England Biolabs), and two microliters were transformed into 50 microliters XL-1 Blue Supercompetent *E. coli* (Stratagene), and selected for growth on LB plates supplemented with 100 μg/ml ampicillin. The transformants were then sequenced to confirm the desired mutations.

***YPS* Chromosomal Deletions.** The deletion strategy is an antibiotic cassette disruption technique based on previously described protocols (56). The KanMX gene conferring G418 resistance to yeast was amplified from the appropriate *S. cerevisiae* deletion strain (Open Biosystems) by PCR with intergenic primers that allow for greater than 200 bases of homology to the target gene on the 5' and 3' ends. The PCR product was then transformed into YVH10 by electroporation, where the cassette inserts itself into the target site on the chromosome by homologous recombination. Transformants were then selected by growth on YPD plates containing G418 (Gibco). The location of the integration was confirmed by colony PCR using one primer with homology to sequence just outside of the insertion site and one primer with homology to the KanMX insertion cassette, as well as by the absence of a PCR product using one primer with homology to sequence just outside the insertion site and one primer with homology to the native gene.

**Expression and purification of 4m5.3 hIgG$_1$.** Wild-type 4m5.3 or 4m5.3 N297Q containing heavy and light chain vectors were transformed into either YVH10 or the PDI and BiP over-expressing strain HBiPPDI (57) (generous gift of Anne Robinson, University of Delaware) and selected for growth on SD-CAA plates. A single colony was inoculated into 5 ml SD-CAA and grown overnight at 30 °C until saturation ($OD_{600}$ ~ 5), and then used to inoculate 1 L of SD-CAA in a shake flask at 30 °C for ~ 24 hrs. Upon saturation ($OD_{600}$ ~ 5), cells were pelleted and resuspended in 1 L of phosphate buffered YPG and allowed to secrete for 72 hrs at 20 °C. Cell culture supernatant was clarified by centrifugation followed by vacuum filtration, then concentrated and exchanged into PBS, pH 7.4. IgG was purified from concentrated supernatant by Protein A (Pierce) followed by anti-FLAG (Sigma) affinity chromatography.

For characterization of IgG glycosylation, 50 μg of purified IgG was treated with EndoH (New England Biolabs) and/or jack bean mannosidase (Prozyme), then re-purified with Protein A agarose (Pierce).

**Cloning of 225 and sm3E as hIgG$_1$ chimeras.** The 225 variable regions were PCR-amplified from the yeast surface display vector pCT-225, expressing 225 as a scFv (225 scFv DNA generously provided by Winfried Wels). The oligos 5-

agtcacacgcgtcaggtacaactgaagcagtcagg and 5'-tcatacgctagcagcggaaacggtgaccagggtcccttgg were used to amplify the 225 Vh with 5' and 3' MluI and NheI sites for ligation into the $hIgG_1$ heavy chain backbone; the oligos 5'-caacgtgctagcgacatcctgctgacccagtctccag and 5'-atgtaccgtacgtttgagctccagcttggtcccagc were used to amplify the 225 Vl with 5' and 3' NheI and BsiWI sites for ligation into the light chain backbone. Similarly, the sm3E variable regions were PCR-amplified from the yeast secretion vector sm3E-His, expressing a $His_6$-tag fusion of the sm3E scFv.

**Flow cytometric analysis of IgG labeling.** 1 x $10^7$ YVH10 cells were washed three times with 500 µl carbonate buffer (4.2% $NaHCO_3$ and 0.034% $NaCO_3$, pH 8.4), incubated for 30 min with either 4 µg/µl NHS-PEG-fluorescein or NHS-PEG-biotin (Nektar), and then washed three times with 1000 µl PBS/BSA. Fluorescein-labeled yeast were then incubated with 10 µg/ml 4m5.3 $hIgG_1$ or a $hIgG_1$ kappa polyclonal control antibody (Sigma) for 60 min at room temperature, washed, and then labeled with a 1:100 dilution of goat anti-human phycoerythrin conjugate (Rockland) for 30 min on ice. For competition experiments, 10 µg/ml 4m5.3 $hIgG_1$ was pre-incubated with 10 µM fluorescein (Pierce) for 60 min at room temperature, and the mixture then incubated with fluorescein-labeled yeast.

Prior to labeling, A431NS cells (ATCC; kind gift of Jennifer Cochran), a derivative of the EGFR-overexpressing epidermoid carcinoma cell line A431 (58) were maintained in DMEM plus 10% FBS. At approximately 80% confluency, cells were trypsinized, washed three times with ice cold PBS/BSA, and counted on a hemocytometer. 2 x $10^5$ cells were incubated with 5 µg/ml yeast-produced 225 $hIgG_1$ or $hIgG_1$ kappa control antibody for 60 min on ice, washed, and then labeled with a 1:100 dilution of goat anti-human PE for 30 min on ice. For competition experiments, 5 µg/ml yeast-produced 225 $hIgG_1$ was pre-incubated with either 1 µM EGFR ectodomain (404SG) (59) for 60 min on ice, and the mixture then incubated with A431NS cells; or, A431NS cells were pre-incubated with 50 µg/ml commercial murine 225 IgG (Lab Vision) for 60 min on ice, and then the yeast-produced 225 IgG added to a final concentration of 5 µg/ml and 25 µg/ml murine 225 IgG.

Prior to labeling, LS174T cells (ATCC), a CEA-overexpressing colorectal adenocarcinoma cell line, were maintained in MEM supplemented with 10% fetal bovine serum and 1% penicillin/streptomycin. At approximately 80% confluency, cells were trypsinized, washed three times with ice cold PBS/BSA, and counted on a hemocytometer. $2 \times 10^5$ cells were incubated with 10 nM yeast-produced sm3E $hIgG_1$ or $hIgG_1$ kappa control antibody for 60 min on ice, washed, and then labeled with a 1:100 dilution of goat anti-human PE for 30 min on ice. For competition experiments, 200 nM sm3E scFv was pre-incubated with LS174T cells for 60 min on ice, then sm3E IgG added to a final concentration of 10 nM and 100 nM scFv.

**Acknowledgements**

Andy Rakestraw, for leader sequence engineering, fluorescein quench titration analysis (Figure 2.8), and analysis of flow cytometry data (Figure 2.9), as well as for helpful discussions and suggestions; Mike Schmidt for assistance with LS174T cell culture and providing the sm3E scFv; Ginger Chao for assistance with A431NS cell culture; the MIT Biopolymers Core Facility; the Tufts University Core Facility, for N-terminal sequencing.

**Figure 2.1**

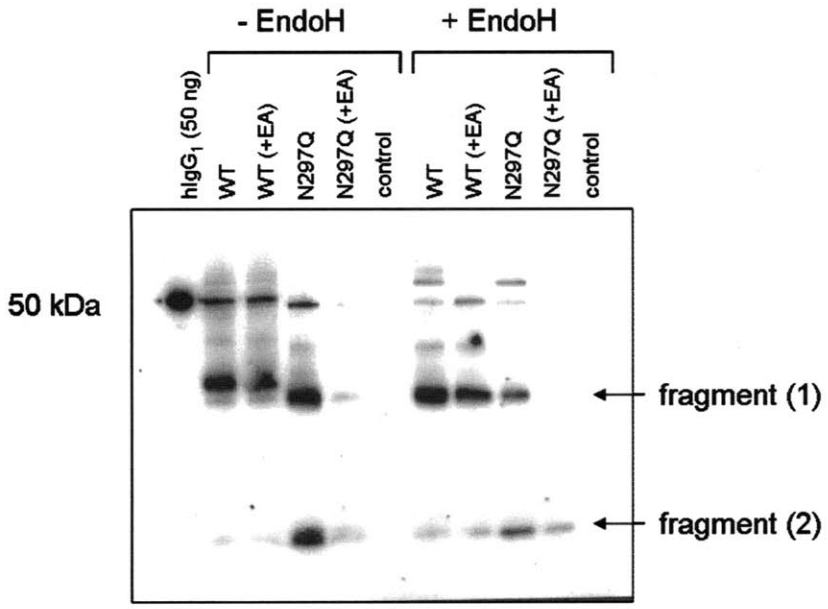


**Anti-Fc Western blot of yeast-secreted 4m5.3 IgG.** Yeast cell culture supernatants of app8-led 4m5.3 IgG were analyzed by anti-Fc Western blotting under reducing conditions, with and without the addition of the N-linked glycosidase EndoH. Abbreviations: $hIgG_1$ (human $IgG_1$ standard), WT (wild-type 4m5.3 IgG), +EA (addition of a Glu-Ala spacer following the Lys-Arg Kex2 cleavage site at the C-terminus of the signal sequence), N297Q (non-N-glycosylated 4m5.3 N297Q point mutant), control (irrelevant protein secreted under similar conditions).

**Figure 2.2**

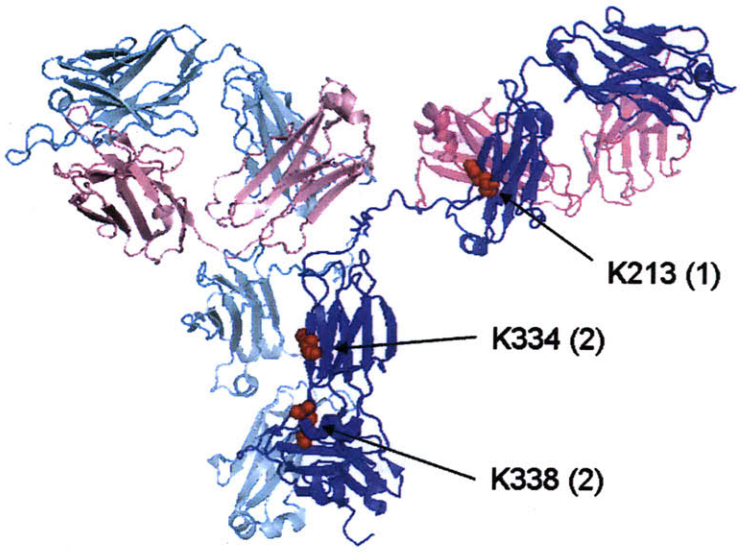


**N-terminal sequence data mapped to IgG structure.** Location of the hypothesized protease sites within $hIgG_1$ secreted from *S. cerevisiae*. Lysine residues (red spheres) identified in the structure directly precede fragments identified by N-terminal sequencing, and are mapped onto a crystal structure of full-length $hIgG_1$ (PDB ID: 1HZH). Numbers in parentheses next to amino acids represent the corresponding fragment submitted for N-terminal sequencing (Figure 2.1).

**Figure 2.3**

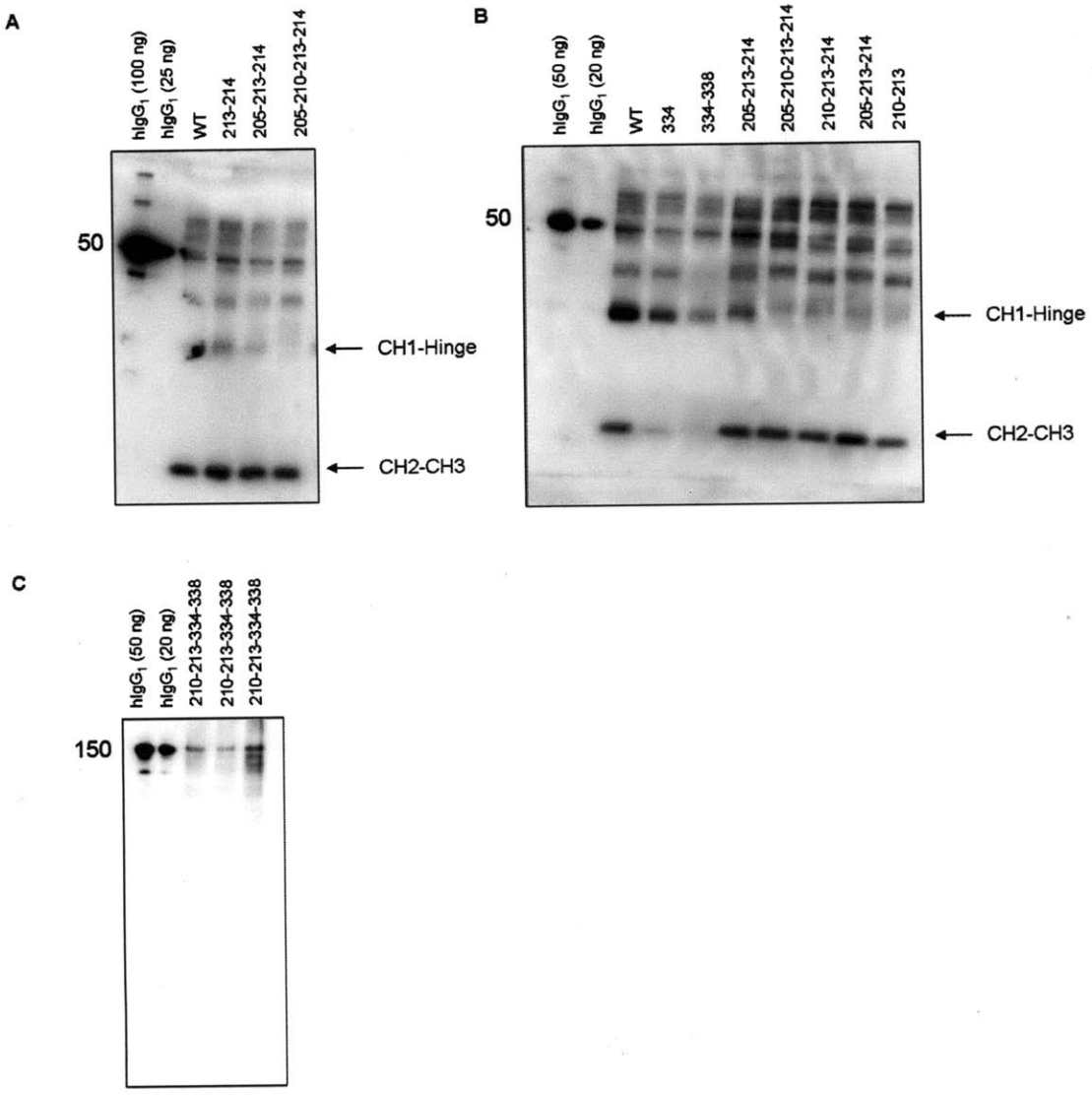


**Effect of lysine to alanine point mutants upon heavy chain proteolysis.** Anti-Fc Western blotting of wild-type (WT) and lysine to alanine point mutants (designated by residue number) of yeast-secreted, αpp8-led 4m5.3 IgG, under reducing **(A, B)** and non-reducing **(C)** conditions. Abbreviations: $hIgG_1$ (human $IgG_1$ standard), CH1-Hinge (fragment corresponding to proteolysis at the CH1-Hinge interface, at residue K213 in Figure 2.2), CH2-CH3 (fragment corresponding to proteolysis at the CH2-CH3 interface, at residues K334 and K338 in Figure 2.2).

**Figure 2.4**

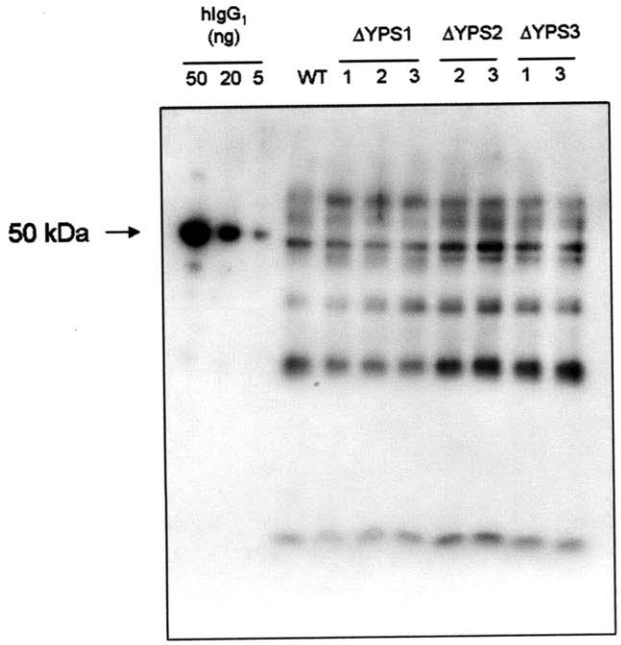


**Yapsin deletion strains.** Reducing anti-Fc Western blotting of wild-type, αpp8-led 4m5.3 IgG secreted from YVH10 (WT) and a series of YVH10-derived deletion strains of the yapsin family genes yps1, yps2, and yps3. Numbers below the yapsin gene indicate strains confirmed to have the correct deletion, and subsequently transformed with the IgG secretion vectors. Abbreviations: $hIgG_1$ (human $IgG_1$ standard).

**Figure 2.5**

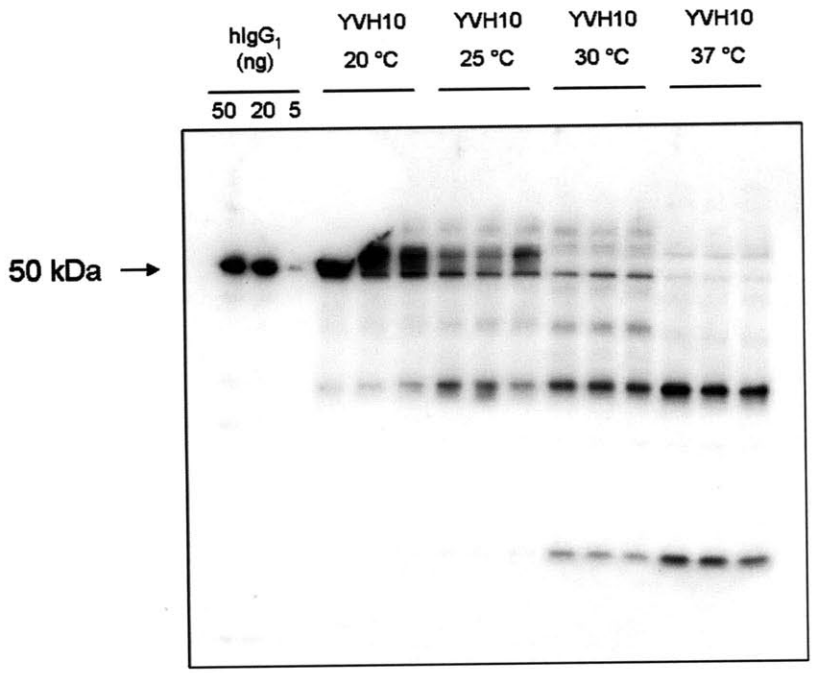


**Effect of induction temperature on IgG secretion.** Reducing anti-Fc Western blotting of wild-type, αpp8-led 4m5.3 IgG secreted from YVH10 at a series of induction temperatures, as indicated. Abbreviations: $hIgG_1$ (human $IgG_1$ standard).

**Figure 2.6**

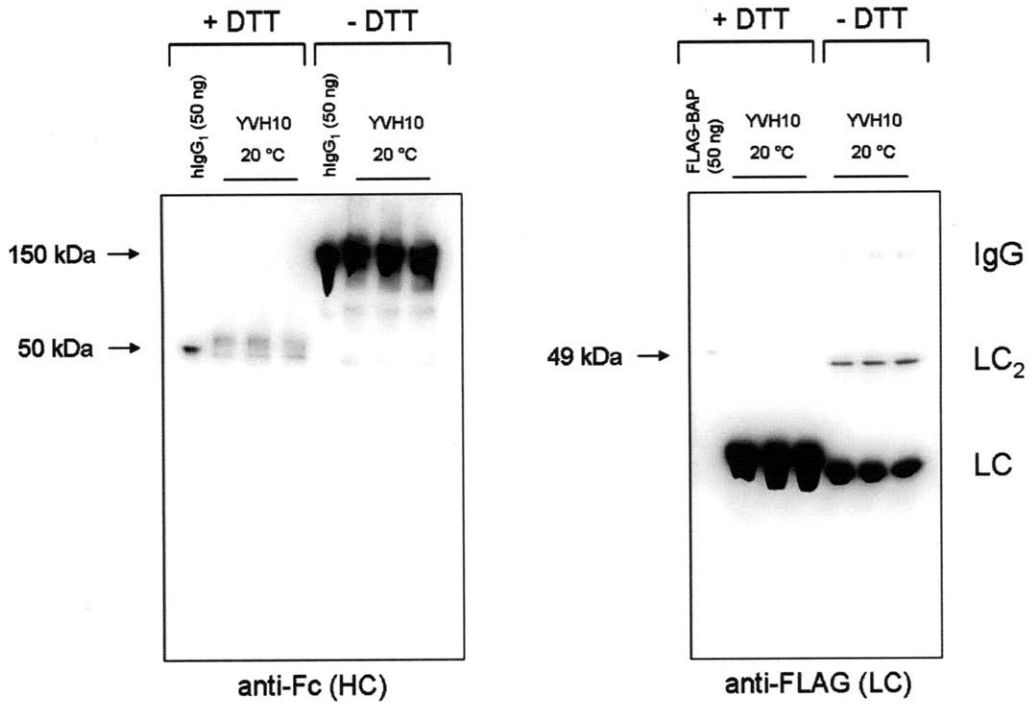


**Analysis of IgG secretion at 20 °C.** (Left) anti-Fc Western blotting of yeast-secreted, αpp8-led 4m5.3 IgG under reducing (+ DTT) and non-reducing (- DTT) conditions. (Right) anti-FLAG Western blotting of yeast-secreted, αpp8-led 4m5.3 IgG under reducing (+ DTT) and non-reducing (- DTT) conditions. Abbreviations: $hIgG_1$ (human $IgG_1$ standard), HC (heavy chain), LC (light chain), $LC_2$ (light chain dimer), FLAG-BAP (FLAG tagged standard).

**Figure 2.7**

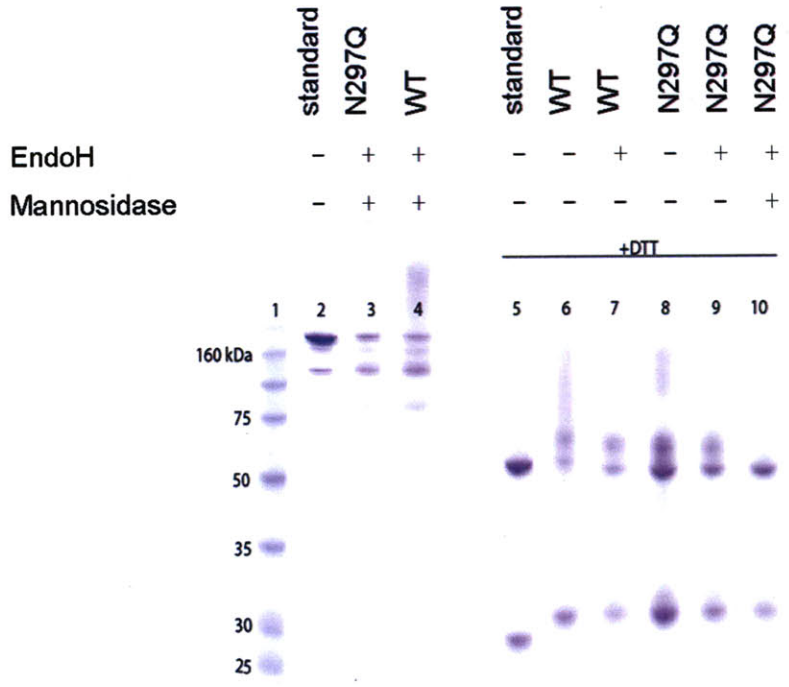


**SDS-PAGE of Protein A and FLAG purified 4m5.3 $IgG_1$.** Purified IgG was analyzed under non-reducing (lanes 2-4) and reducing (lanes 5-10) conditions, with and without treatment of the glycosidases EndoH and mannosidase. Abbreviations: standard (control human $IgG_1$ standard), WT (wild-type, yeast-secreted 4m5.3 IgG with app8 leader), N297Q (yeast-secreted 4m5.3 N297Q non N-glycosylated mutant with app8 leader).

**Figure 2.8**

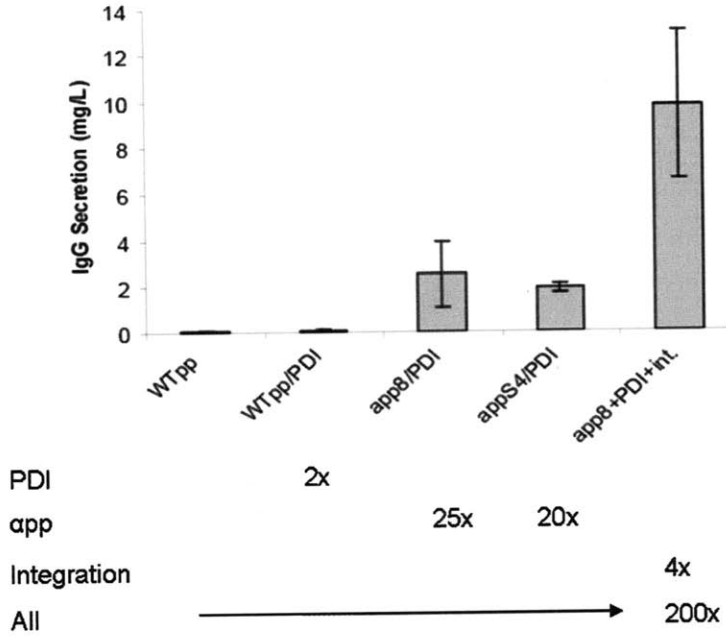


**Sources of improvement in antibody secretion.** The effects of the leader sequence and strain manipulation upon the secretion of a 4m5.3 $IgG_1$ mouse/human chimera was quantified by fluorescein quench titration assay. The $V_H$ and $V_L$ genes were expressed separately on two CEN plasmids, under the control of the WTαpp (WTpp), and transformed into BJ5464α cells or YVH10 cells, which carry an additional copy of PDI (WTpp/PDI). Effects of the mutant leaders app8 and appS4 were also assayed in YVH10 (app8/PDI and appS4/PDI). For the app8 leader, these genes were also integrated (int.) into the chromosomes of YVH10 cells in place of CEN plasmid expression (app8+PDI+int.).

**Figure 2.9**

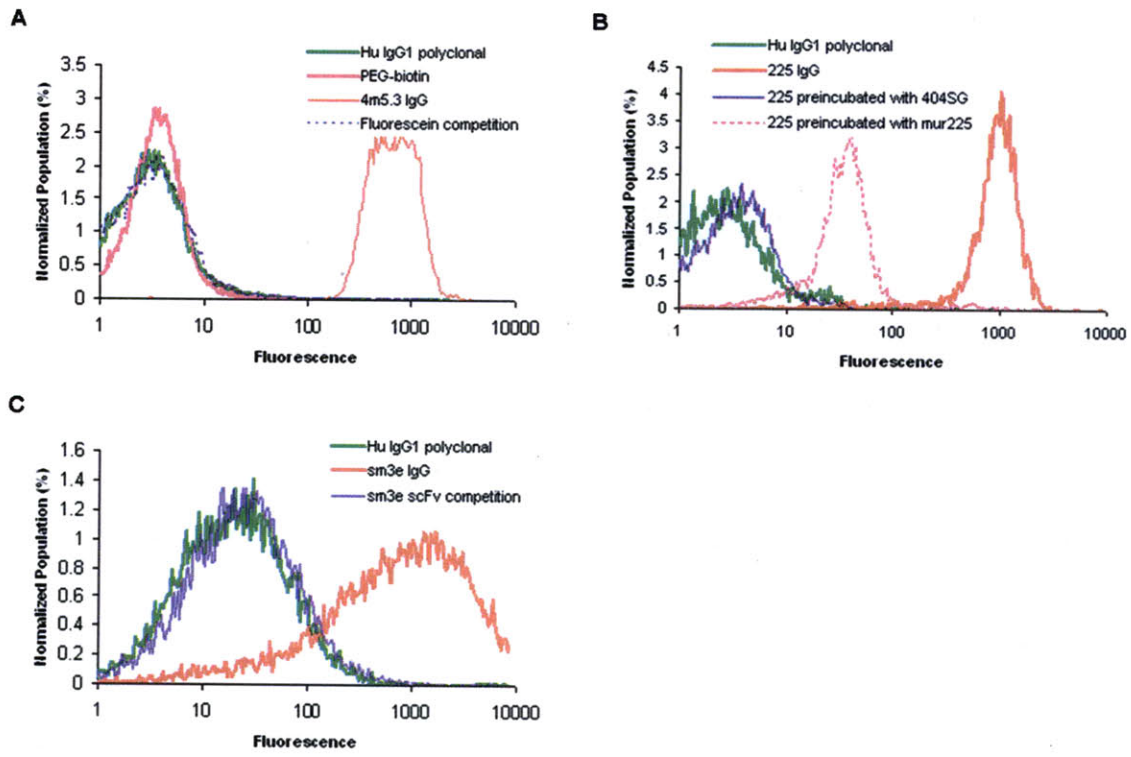


**Cell labeling of yeast-secreted IgGs. (A)** Labeling of fluorescein-conjugated yeast with purified 4m5.3 IgG followed by an anti-human PE-conjugated antibody and analysis by flow cytometry. A type-matched, non-specific, human $IgG_1$ kappa polyclonal antibody (Hu $IgG_1$ polyclonal) and cells labeled with biotin (PEG-biotin) instead of fluorescein were used as negative controls. Pre-incubation of the 4m5.3 IgG with 10 μM fluorescein was also done to demonstrate specificity. **(B)** Labeling of the EGFR expressing cell line A431NS with yeast-produced 225 IgG. Specificity was determined through competition assays: yeast 225 IgG was pre-incubated with yeast-produced EGFR ectodomain, 404SG, or the EGFR-expressing cells were pre-labeled with murine 225 IgG. **(C)** Labeling of the CEA presenting cell line LS174T with sm3E IgG. Specificity was demonstrated by pre-incubating the cells with the sm3E scFv.

# Chapter 3. Engineering Aglycosylated IgG variants that Productively Engage Fc gamma Receptors [2]

## Introduction

Fcγ receptor (FcγR) engagement is essential to the function of immunologlobulin G (IgG) in both immunity (60) and in antibody-based therapy (5, 17). IgGs act as the adaptor between a pathogen and the immune response by simultaneously binding antigen through their variable regions and activating an immune response through interaction of conserved Fc regions with FcγRs on cells of the immune system. The human FcγR (hFcγR) family consists of the activating receptors FcγRI, FcγRIIA, and FcγRIIIA, and the inhibitory receptor FcγRIIB. While FcγRI binds IgG with high affinity (nanomolar binding constants), FcγRIIA, FcγRIIB, and FcγRIIIA bind IgG with micromolar affinity, becoming activated only via avid multivalent interactions with opsonized antigen (60). The binding of IgG to FcγR is highly sensitive to the presence of glycosylation at a single N-linked glycosylation site at asparagine 297 (N297) in its CH2 domain (8, 61), with a loss of binding to the low-affinity FcγRs observed in N297 point mutants (21, 62), enzymatic Fc deglycosylation (63), recombinant IgG expression in the presence of the N-linked glycosylation inhibitor tunicamycin (64), or expression in bacteria (26, 65). In addition, the nature of the carbohydrate attached to N297 modulates the affinity of the FcγR interaction (9, 10). The sensitivity of FcγR binding to specific glycoforms has limited therapeutic antibody biomanufacture to mammalian expression systems, and has led to the development of glycosylation-engineered mammalian cell lines (9, 19) and microbial strains with humanized glycosylation (66) as methods of enhancing antibody cytotoxicity.

In crystal structures of the complex, FcγR/Fc contact is mediated not only by protein-protein contacts, but also by specific interactions with the glycan on the Fc that are proposed to contribute to binding affinity (6, 7). Additional intramolecular contacts are made between the Fc-linked glycan and residues on the IgG CH2 domain, and it is

[2] This chapter has been adapted from: Sazinsky SL, *et al.* (2008) Aglycosylated Immunoglobulin $G_1$ Variants Productively Engage Activating Fc Receptors. *Proc Natl Acad Sci U S A.* Copyright 2008 National Academy of Sciences, U.S.A.

thought that these interactions stabilize an open Fc conformation capable of being engaged by FcγR (8). Successive truncation of an $IgG_1$ glycan results in an incremental loss of binding affinity (63) and concomitant incremental collapse of the open Fc conformation (67). However, glycosylation is not strictly required for engagement of all immunoglobulin receptors with their corresponding Fc ligands, notably in the binding of IgE Fc to IgεR (68). Interestingly, the IgE Fc adopts a similar mode of binding to FcR as the $IgG_1$ Fc in the $IgG_1$ Fc:FcγRIII complex and both receptors and Fcs share structural similarity (69). In the $IgG_1$ Fc:FcγRIII complex, extensive contacts are made by both chains of the $IgG_1$ hinge region, with additional receptor contacts made by the B/C loop, F/G loop, and both sidechains and glycosylation of the C'/E loop of the CH2 domain (6, 7) (**Figure 3.1**). It is particularly striking that this loop plays a part in receptor recognition through both direct side chain contacts as well as in encoding information for a critical post-translational modification.

In the present study, we reasoned that by optimizing the protein-protein interactions about the C'/E loop:FcγR interface at the expense of glycosylation, we could identify aglycosylated $IgG_1$ variants that maintain engagement to FcγRs. Here, we demonstrate that a small subset of substitutions at both N297 and T299 of the glycosylation motif lead to aglycosylated Fcs that maintain engagement of FcγRs, and in a particular example are active *in vivo*. Such aglycosylated antibodies would be facile templates for further efforts to engineer Fc effector functions and potentially enable a far wider range of options for therapeutic antibody biomanufacture.

## Results

**Screening for aglycosylated Fc variants that bind FcγRIIA.** To determine if glycosylation of the Fc was an absolute requirement for FcγR engagement by $hIgG_1$, we constructed saturation mutagenesis libraries at the Fc C'/E loop and screened them by displaying the full-length IgG variants on the yeast cell surface (**Figure 3.2**). In this display system, the femtomolar affinity fluorescein-binding 4m5.3 single-chain antibody (38) was reformatted as a $hIgG_1$, allowing 4m5.3 $hIgG_1$ library variants to be captured on fluorescein-labeled yeast from which they are secreted, by using a cell surface secretion capture assay (34) in conjunction with an engineered leader sequence that allows for the improved secretion of fully-assembled $hIgG_1$ from *S. cerevisiae* [(35); Chapter 2; and Rakestraw JA, SLS, Piatesi A, Antipov E, & KDW, *submitted*). Three saturation libraries centered about the C'/E loop – theoretically encoding all amino acid combinations at residues 296-299, 297-299, and 297-300 – were pooled and screened for binding to fluorophore labeled tetramers of a soluble form of the $Fc\gamma RIIA^{131R}$ allele by multiple rounds of fluorescence activated cell sorting (FACS).

Using this screening strategy, in addition to glycosylated variants and the wild type clone, mutants lacking the canonical Asn-X-Ser/Thr N-linked glycosylation motif were enriched from the C'/E loop libraries for binding to FcγRIIA (**Figure 3.3a**). After two rounds of screening three aglycosylated motifs were identified: the double mutants S298G/T299A, S298G/T299G, and the single mutant T299A. After a third round of screening at increased stringency, the sublibrary was dominated by the S298G/T299A variant, suggesting it as the highest-affinity FcγRIIA binding motif in the library (**Figure 3.3b**).

To study the contributions of the S298G and T299A mutations to receptor binding, a series of point mutants were constructed, secreted from yeast, and assayed for their ability to bind to $Fc\gamma RIIA^{131R}$ (**Figure 3.3c**). Both the S298G and T299A mutations alone retain binding to FcγRIIA at comparable or increased levels to wild-type $IgG_1$, and the S298G mutation in the aglycosylated T299A background yields a variant capable of binding FcγRIIA to a much greater extent. The S298G/T299A double mutant is incapable of rescuing binding in the N297Q, N297D, and N297A backgrounds, suggesting there is

a strong requirement for asparagine at position 297 for FcγRIIA binding even in the absence of conjugated carbohydrate, a finding consistent with its conservation in the initial library screen.

**S298G/T299A is aglycosylated and binds to FcγRs.** To confirm that the potential aglycosylated motifs identified from the yeast-based screen indeed lacked the N-linked glycan and were capable of engaging FcγRs, wild-type, S298G/T299A, and the non-receptor binding N297Q aglycosylated control were expressed and purified from HEK 293 cells. Both N297Q and S298G/T299A exhibit increased mobility by reducing SDS-PAGE (**Figure 3.4a**) and critically, are not recognized by the mannose-specific lectin LCA (**Figure 3.4b**), consistent with the expected absence of N-linked glycosylation. Surface Plasmon Resonance (SPR) measurements show that S298G/T299A binds to both FcγRIIA alleles, FcγRIIA$^{131R}$ and FcγRIIA$^{131H}$, and to FcγRIIB; however, this mutant does not bind to FcγRIIIA nor the complement component C1q and binding to FcγRI was weakened by 10-fold. (**Figure 3.4c**). S298G/T299A binds FcγRIIA$^{131R}$ with a dissociation constant ($K_d$) of 1.7 μM, approximately three-fold stronger than wild-type Fc, and binds FcγRIIA$^{131H}$ with a $K_d$ of 7.0 μM, slightly weaker than wild type. A small increase in affinity compared to wild type for FcγRIIB was also observed, suggesting a preferential binding of FcγR with an arginine at position 131 (**Figure 3.5**).

To determine whether S298G/T299A can engage native FcγRs as expressed on the cell surface, CHO cell lines stably transfected with FcγRIIA$^{131R}$, FcγRIIA$^{131H}$, and FcγRIIB were labeled with 4m5.3 hIgG$_1$ immune complexes (ICs) (**Figure 3.4d**, and data not shown). Both wild-type and S298G/T299A IgG ICs label all receptor-expressing CHO cells in a concentration dependent manner, demonstrating that S298G/T299A binds FcγRs in this context as well. Consistent with the soluble binding measurements, S298G/T299A IgG ICs label FcγRIIA$^{131R}$ and FcγRIIB expressing CHO cells at similar levels as wild type; however, S298G/T299A shows only intermediate labeling of the FcγRIIA$^{131H}$ allele compared to wild type and the aglycosylated control.

**S298G/T299A activates FcγRIIA *in vivo*.** To determine whether this aglycosylated IgG is functional *in vivo*, a murine platelet clearance model was used to test the extent of

S298G/T299A activity. The platelet integrin antigen-binding antibody 6A6 was reformatted as a mouse-human $IgG_1$ chimera and the S298G/T299A mutations subsequently introduced into the human Fc domain. The antibody was tested in a transgenic mouse model, in which the endogenous murine FcγRs have been deleted by gene targeting and the human activation FcγR, hFcγRIIA$^{131R}$, is expressed as a transgene, thus maintaining cell type expression appropriate for the human transgene (70). Mice with this genotype were treated with wild-type, N297A, and S298G/T299A 6A6 $hIgG_1$ purified from HEK 293 cells and the extent of platelet clearance measured over time (**Figure 3.6**). After four hours, S298G/T299A-6A6 treated mice (n=3) showed a statistically significant drop in platelet count when compared to those treated with N297A-6A6 or PBS, exhibiting a response that was comparable to wild-type-6A6 and demonstrating the ability of S298G/T299A to productively engage FcγRIIA *in vivo* and result in platelet clearance.

**Model of S298G/T299A-FcγRIIA interaction.** To explore the structural basis for FcγR binding of this aglycosylated Fc domain variant, we constructed homology models of Fc:FcγRIIA complexes based on the previously solved structures of the $IgG_1$ Fc, the FcγRIIA structure (71) and the Fc:FcγRIII complex (7) (**Figure 3.7**). Three features emerge from this modeling. First, in the model of the wild-type interaction, there is only limited interaction between the two N-linked glycans and FcγRIIA (**Figure 3.7a**). The asymmetric nature of the $IgG_1$ Fc: FcγRIIA interaction predicts that the glycan attached to the B chain of the Fc dimer may interact with residues K117, T119, F121, S126, and F129 of the receptor, whereas the glycan attached to the other chain (the A chain) does not make contact with FcγRIIA. These glycan:FcγR contacts provide negligible calculated screened electrostatic intermolecular interactions (approximately zero kcal/mol), compared to the much larger intramolecular ones between glycan and Fc [roughly –1.3 kcal/mol, with a dominant contribution from N297/glycan(B)–D265(B)] and suggest that both oligosaccharides are primarily interacting with their respective Fc chains. Second, N297 is important for the Fc: FcγRIIA interaction. Aglycosylated N297 has the potential to make hydrogen bond interactions across the interface with S126 of the receptor (**Figure 3.7b**). These interactions may be mediated by a bridging water

molecule that can be observed nearby in an unbound FcγRIIA crystal structure (71). Replacement of N297 with glutamine or alanine disrupts this interaction (and fails to make similar, stabilizing ones) and is consistent with the observed absence of binding for such mutants (**Figure 3.3c, Figure 3.8a**). Interestingly, replacement with aspartic acid may be able to make a similar interaction, however the greater desolvation penalty of the charged side chain upon FcγR binding likely results in the reduced binding of this variant.

Finally, the intermolecular interaction between the aglycosylated S298G/T299A mutant and FcγRIIA includes a salt bridge formed between D265 on the B chain of the Fc dimer and K117 on the FcγR. In the wild-type structure, this interaction is shielded from solvent by the oligosaccharide chain (**Figure 3.7c**). In the aglycosylated S298G/T299A mutant this salt bridge is exposed to the solvent (**Figure 3.7d**), which nearly halves the screened electrostatic interaction energy compared to wild type (-5 kcal/mol vs. -10 kcal/mol). However, this effect is more than compensated in the S298G/T299A mutant by a reduced desolvation penalty (72), a measure of the loss of electrostatic interactions with solvent upon binding, resulting in an overall stabilized structure. This effect is illustrated (**Figures 3.7e,f**) by a reduction in the residual electrostatic potential present on D265(B) in the mutant compared to the wild-type; similarly, the Figure also shows the S298G mutation results in a reduced desolvation penalty that contributes to the stability of the mutant complex. Thus, the predictions made by this homology model provide a hypothetical mechanism for the stability of the aglycosylated Fc:FcγR complex, resulting from hydrogen bonding and electrostatic interactions altered in the aglycosylated mutant.

**Aglycosylated Fc variants that bind FcγRIIIA.** To evaluate the contribution of individual sidechains in the C'/E loop to FcγR engagement, as well as the nature of the specificity between FcγRIIA and FcγRIIIA seen in S298G/T299A, we constructed the full set of single point mutations at positions 297, 298, and 299, and assayed yeast-secreted IgG variants for binding to both FcγIIA and FcγIIIA (**Figure 3.8**). Side chain scanning of 297 and 299 revealed additional mutations that remove the glycosylation motif but retain residual weak receptor binding: T299H to FcγIIA, and N297D and N297H to FcγIIIA$^{176V}$ (**Figures 3.8a,c-e**). T299A is the only aglycosylated mutant identified that displays dual specificity, exhibiting improved binding to FcγIIA while

retaining moderate binding to the FcγIIIA$^{176V}$ allele. Interestingly, the nature of the sidechains at position 299, and not just glycosylation, greatly impacts receptor binding, as the yeast-expressed glycosylated T299S mutant binds all receptors to a much lesser extent than the wild-type Fc.

In contrast to positions 297 and 299, where mutations largely disrupt the N-linked glycosylation motif Asn-X-Ser/Thr, multiple substitutions in a glycosylated Fc background are tolerated at position 298 (**Figure 3.8b**). FcγRIIA binding is much more sensitive to substitution at position 298, with only glycine (S298G) maintaining a level of binding that is comparable to wild type. In contrast, FcγRIIIA tolerates an array of substitutions at position 298, and the data highlight potential mutations for engineering FcγRIIIA vs. FcγRIIA/IIB specificity, such as the previously identified S298A and S298N mutations (21, 22). Only S298G maintained engagement to both FcγRIIA and FcγRIIIA in our assay, a finding that taken together with a preference for threonine at 299 (T299) suggests an explanation for the conservation of the motif N-S/G-T in IgG CH2 domains across virtually all species (data not shown).

While our initial efforts focused on FcγRIIA resulted in specificity for FcγRIIA and FcγRIIB at the expense of FcγRIIIA binding (**Figure 3.4c**), the sidechain scanning data suggested that aglycosylated Fcs that bind FcγRIIIA with comparable affinity to wild type could also be identified. Within the C'/E loop, rational design of double mutants based upon the weakly FcγRIIIA-binding N297D and N297H substitutions yielded variants that bound FcγRIIIA$^{176V}$ at levels 10 to 40% of wild type and with specificity for FcγRIIIA (**Figure 3.9**), a desired property in engineering Fcs with enhanced immune effector functions (17). In a separate strategy, the consensus mutations K326E, K290E, and K290N – identified in a separate screen for improved FcγRIIA binding (data not shown) as well as through the efforts of previous groups (22, 73) – were introduced into the T299A background. Incorporation of the K326E mutation, located at the base of the F/G loop, led to enhanced binding for FcγRIIIA, approaching wild type levels for FcγRIIIA$^{176V}$ and weakly binding FcγRIIIA$^{176F}$ (**Figure 3.9**). This result suggests that additional second-site mutations at contact interfaces other than the C'/E loop can lead to aglycosylated FcγRIIIA- and FcγRIIA-binding Fcs with a range of affinities and specificities.

## Discussion

Until this study the general knowledge of the binding interaction between IgG and FcγRs indicates a dependence on the N-linked glycan attached to asparagine 297 on the IgG heavy chain. The Fc variants described here clearly demonstrate that glycosylation is not a strict requirement for FcγR engagement, either *in vitro* or *in vivo*. In an initial strategy, by generating aglycosylated Fc variants that bind to FcγRIIA and FcγRIIB we could demonstrate that the set of mutations necessary to switch from a wild-type glycosylated binder to a functionally aglycosylated binder is fairly small – in our case it involved the introduction of only two point mutations. In a second more directed screening strategy, we could further demonstrate that by introducing additional modifications into our aglycosylated mutants we can combine features from single mutants discovered from different screenings, thereby modulating the overall affinity features of the IgG variant. This combinatorial behavior of the contribution of single mutations is of special interest for the engineering of IgG variants with very well defined binding properties.

In addition to the enhanced FcγRIIA$^{131R}$ binding observed in the aglycosylated S298G/T299A variant, we were able to restore binding to FcγRIIIA$^{176V}$ to near wild-type levels, suggesting that further engineering can also lead to aglycosylated variants with wild-type or improved binding to FcγRIIIA. In particular, we anticipate that introducing mutations into the T299A background, which weakly binds both FcγRIIA and FcγRIIIA, will lead to fully FcγR competent aglycosylated antibody variants. Building upon these aglycosylated FcγRIIIA-binding variants will be essential for their potential use as cytotoxic antibodies, which have emerged as a promising class of therapeutics for treatment of human cancer in recent years (3). Support for a critical role for FcγR engagement in the mechanism of anti-tumor activity, and specifically for FcγRIIIA, has come from three independent studies which found a strong positive correlation between patient response and the presence of specific alleles of the activating FcγR FcγRIIIA that conferred enhanced binding for the IgG1 Fc domain of the antibody (13, 15, 16). While the S298G/T299A variant does not bind complement, the above studies, as well as murine models that demonstrate a dominant role for FcγR engagement in therapeutic

antibody activity (5), suggest that restoration of complement binding would be unnecessary for engineered Fc variants. In addition to their ability to bind FcγR, it will also be important to assess the stability of these variants, as previously characterized Fc variants (74) and deglycosylated wild-type Fc (75) have displayed reduced thermal stability.

Given the small number of mutations required to achieve N-linked glycosylation-independent FcγR binding, it is striking that all naturally occurring IgGs utilize this post-translational modification nevertheless. Among different antibodies there is variation in the fucose and galactose-sialic acid attached to the core glycan structure (**Figure 3.10**), and it has been reported that these variations dramatically influence the antibody activity. The absence of fucose in the glycan was reported to enhance the affinity of FcγRIIIA for IgG up to 50-fold (9) and thereby switching the antibody into an inflammatory mode. This is required, for example, for cytotoxic antibodies, but also occurs when autoantibodies generate pathogenic immune complexes and activate autoimmune cascades. In contrast to fucose, the presence of terminal sialic acid was demonstrated to be the critical factor for the anti-inflammatory action of high dose IVIG (10, 76). Sialic acid reduces the affinity of FcγRs to IgG by 5-10 fold (10) and, in addition, marks IgGs and subsequently allows them to bind to non-FcR lectins (76) and mediate downstream actions through these novel interactions, resulting in anti-inflammatory responses, including the upregulation of FcγRIIB on effector macrophages (77). The conservation of the N-S/G-T glycosylation motif among different species at the expense of this post-translational variability supports the view that the glycan, although not necessarily required for FcγR binding, serves as a platform for further modulation of the IgG's activity, enabling post-translational switching or tuning of the IgG function between an anti-inflammatory or inflammatory mode.

Finally, our demonstration that IgG variants can be generated that have uncoupled FcγR binding from N-linked glycosylation opens up new possibilities for protein engineering and biomanufacture. Our results suggest that receptor binding affinity and specificity can be engineered on the simpler template of an unmodified polypeptide chain, and these properties selected for by yeast surface display of aglycosylated Fc mutant

libraries. Such mutants could then be produced in essentially any recombinant expression system without loss of the desired altered effector functions.

## Materials and Methods

**Library construction.** Libraries were constructed by homologous recombination of a mutated heavy chain constant region insert into the 4m5.3 heavy chain yeast secretion vector template according to previously published methods (78). The 4m5.3 heavy chain secretion vector was previously constructed from the pRS316 shuttle vector by insertion of the GAL10 promoter and alpha terminator, signal peptide, and 4m5.3 variable heavy chain domain upstream of the $hIgG_1$ CH1 to CH3 constant domains [(35); Chapter 2; and Rakestraw JA, SLS, Piatesi A, Antipov E, & KDW, *submitted*).

4m5.3 heavy chain template vector was prepared by digestion with NheI (New England Biolabs) and XhoI (New England Biolabs), which flank the 5' region of the $hIgG_1$ CH1 domain (NheI) and 3' region of the CH3 domain (XhoI). Saturation mutagenesis of the C'/E loop was performed by gene reconstruction with the oligonucleotides 297-299NNK (all oligos from Integrated DNA Technologies), 296-299NNK, and 297-300NNK for each of the three libraries, respectively. In a first PCR step the mutagenic oligo and reverse primer 4m-CH3-epPCR-rev were used to amplify the region 5' of the C'/E loop through the 3' region of the CH3 domain, using the wild type vector as a template. In a second PCR step, this PCR product was used along with the forward primer 4m-CH1-epPCR-for to amplify the 3' region of the 4m5.3 variable heavy chain to the 3' end of the CH3 domain, reconstructing the heavy chain CH1 to CH3 gene insert with ~50 base pairs of overlap with the digested template vector for efficient yeast homologous recombination.

Gene inserts were transformed with digested template vector by electroporation into the yeast strain YVH10/LC, a derivative of the yeast strain YVH10, containing a chromosomally integrated copy of the 4m5.3 light chain yeast secretion vector. The 296-299 and 297-300 saturation libraries had ~$6x10^7$ transformants, 60-fold greater than their theoretical diversity at the DNA level ($32^4$ ~ $1.0x10^6$); the 297-299 library had ~$4x10^7$ transformants.

**Oligonucleotides.**

297-299NNK (5'-AGCCGCGGGAGGAGCAGTACNNKNNKNNKTACCGTGTGGTCAGCGTCCT)

296-299NNK (5'-CAAAGCCGCGGGAGGAGCAGNNKNNKNNKNNKTACCGTGTGGTCAGCGTCCT)

297-300NNK (5'-AGCCGCGGGAGGAGCAGTACNNKNNKNNKNNKCGTGTGGTCAGCGTCCTCAC)
4m-CH1-epPCR-for (5'-ATGGAATACTTGGGTCAAGGAACCTCAGTCACCGTCTCCGCTAGC)
4m-CH3-epPCR-rev (5'-ATTTTGTTACATCTACACTGTTGTTATCAGATTTCGCTCGAGTCA)
297NNK (5'-CCGCGGGAGGAGCAGTACNNKAGCACGTACCGTGTGGTCAG)
298NNK (5'- GCGGGAGGAGCAGTACAACNNKACGTACCGTGTGGTCAGCG)
299NNK (5'- GGAGGAGCAGTACAACAGCNNKTACCGTGTGGTCAGCGTC)
297NHC (5'- CCGCGGGAGGAGCAGTACNHCAGCACGTACCGTGTGGTCAG)
298NHC (5'- GCGGGAGGAGCAGTACAACNHCACGTACCGTGTGGTCAGCG)
299NHC (5'- GGAGGAGCAGTACAACAGCNHCTACCGTGTGGTCAGCGTC)

N, H, and K encode the following groups of nucleotide bases: N encodes all four nucleotides; K encodes G and T; H encodes A, C, and T.

**Library screening.** Library screening was performed using the cell surface secretion assay (CeSSA) (34). Briefly, libraries were grown in SD-CAA (2% glucose, 0.67% yeast nitrogen base, 0.54% $Na_2HPO_4$, 0.86% $NaH_2PO_4 \cdot H_2O$, 0.5% casein amino acids) at 30 °C to an $OD_{600}$ of ~ 5, and then induced in YPG (2% galactose, 2% peptone, 1% yeast extract, 0.54% $Na_2HPO_4$, 0.86% $NaH_2PO_4 \cdot H_2O$) for 12 hrs at 20 °C. Following this pre-induction phase, yeast were labeled with fluorescein-PEG-NHS (Nektar) and re-induced in YPG containing 15% PEG (w/v) at 20 °C for 36 hrs. Cells were washed with PBS containing 0.1% (w/v) BSA (PBS/BSA) and labeled with biotinylated hFcγRIIA$^{131R}$ preloaded onto streptavidin-Alexa 647 (Invitrogen). The library was sorted on a BD FACSAria (Becton Dickinson) and collected cells grown in SD-CAA supplemented with penicillin/streptomycin (Invitrogen), for a total of three rounds of screening. Library populations were labeled at increasingly stringent concentrations of FcγRIIA tetramer as follows: round one (50 nM FcγRIIA tetramer), round two (2 nM FcγRIIA tetramer), and round three (80 pM FcγRIIA tetramer). All clones isolated from screening were re-transformed into YVH10/LC and individually assayed for FcγRIIA binding.

**Site Directed Mutagenesis.** For sidechain scanning of positions 297, 298, and 299, mutagenesis of the 4m5.3 heavy chain yeast secretion vector was performed using the Quikchange Multi Site-Directed Mutagenesis Kit (Stratagene) and the degenerate oligos 297NNK, 298NNK, 299NNK, 297NHC, 298NHC, and 299NHC. Clones were identified

and confirmed by subsequent sequencing and re-sequencing. All other point mutants were constructed by PCR-amplification of the entire vector using complementary primers containing the desired point mutations.

**Characterization of yeast-secreted Fc mutants.** Fc mutants freshly transformed into YVH10/LC were grown in 5 ml SD-CAA at 30 °C until an $OD_{600}$ ~ 5, then induced in 5 ml YPG at 20 °C for 72 hrs. Cell culture supernatants were loaded onto fluorescein-conjugated yeast overnight at 4 °C; yeast were then washed with PBS/BSA, labeled with 10 nM of biotinylated FcγR preloaded onto streptavidin-Alexa 647 at 4 °C for > 2 hrs, and analyzed by flow cytometry. Labeling with 10 μg/ml Protein A-Alexa 647 (Invitrogen) was performed as a separate IgG loading control for all samples.

**Mice.** $\gamma^{-/-}$ FcγRIIB$^{-/-}$ mice were generated in the Ravetch laboratory, backcrossed for 12 generations to the C57BL/6 background and crossed to hFcγRIIA$^{tg}$ mice (The Jackson Laboratory, Bar Harbor, ME). Female mice at 2 to 4 months of age were used for the experiments and maintained at the Rockefeller University animal facility. All experiments were performed in compliance with federal laws and institutional guidelines and have been approved by the Rockefeller University (New York).

**Cell culture.** CHO cells were cultured according to the ATCC guidelines. CHO-hFcγRIIA$^{131H}$, CHO-hFcγRIIA$^{131R}$ and hFcγRIIB were obtained by transfection of the pCMV-Script-hFcγRIIA$^{131H}$, CHO-hFcγRIIA$^{131R}$ and hFcγRIIB plasmids and subsequent selection with 1 mg/ml geneticin (Invitrogen).

**Antibodies and recombinant proteins.** The 6A6-human Fc chimeric variants and soluble hFcγ-receptors were produced by transient transfection of 293T cells and subsequent purification from culture supernatants. For protein production, cells were cultured in DMEM medium supplemented with 1% Nutridoma SP (Roche). Cell culture supernatants were harvested 6 days after transfection, and protein was precipitated by ammonium sulfate precipitation. The 4m5.3-human Fc chimeric variants were produced by transient transfection of 293F cells (Invitrogen) and subsequent purification from cell

culture supernatants. For protein production, cells were cultured in Freestyle 293F Expression Medium (Invitrogen). Recombinant receptors were purified with Ni-NTA (Qiagen) and recombinant antibodies were purified with protein G sepharose (GE Healthcare) or immobilized protein A (Pierce) by affinity chromatography. All proteins were dialyzed against PBS. Purity was assessed by SDS-PAGE followed by Coomassie Blue staining.

**Immune complex binding assay.** For studying immune complex binding to surface FcγRs, ICs were generated by incubating 10 μg of the respective 4m5.3 (anti-FITC) chimera with 10 μg of BSA-FITC (Sigma) in 1 ml PBS for 2 hours at 37 °C while shaking gently. CHO cells were stained for 2 hours at 4 °C with 1 μg, 0.5 μg, 0.2 μg or 0.1 μg of ICs, washed with PBS and analyzed by FACS analysis.

**Surface Plasmon Resonance analysis.** To determine the interaction between soluble hFcγ-receptors RIa (R&D Systems), $RIIA^{131H}$, $RIIA^{131R}$, RIIB, RIIIA, CIq (Calbiochem) and 4m5.3 antibody chimera, steady state affinity measurements on a Biacore T100 biosensor were performed. Antibodies were immobilized at high densities to CM5 sensor chips (Biacore) by standard amine coupling. Soluble hFcγ-receptors were injected in 5 different concentrations through flow cells at room temperature in HBS-EP running buffer (Biacore) for 3 min at a flow rate of 30 μl/min and dissociation was observed for 10 min. $K_d$ values were calculated after subtraction of background binding to a control flow cell using Biacore T100 Evaluation software.

**Lectin blot.** 10 μg of 4m5.3 wt, N297Q, and S298G/T299A antibody chimera were resolved by SDS-PAGE using a polyacrylamide gel (NuPAGE, Invitrogen) under non-reducing conditions. Proteins were transferred to a polyvinylidene difluoride (PVDF) membrane (Millipore), blocked with Western Blocking Reagent (Roche), and followed by incubation with biotinylated LCA lectin (2 μg/ml, Vector Laboratories) and alkaline phosphatase-conjugated goat anti-biotin antibody (Sigma). Bound antibody was visualized with 4-nitro blue tetrazolium chloride/5-bromo-4-chloro-3-indolyl phosphate (Roche).

***In vivo* model systems.** Mice were injected intravenously with 50 μg 6A6-hFc1 wt, N297A, or S298G/T299A in 100 μl PBS. Platelet counts were determined before injection and at 4, 24, and 72 hours after injection by blood collection of 50 μl from the retro-orbital plexus and measuring platelet counts of a 1:10 dilution in PBS/5% BSA in an Advia 120 hematology system (Bayer). Platelet clearance for mice treated with each 6A6-hIg$G_1$ variant was analyzed 4 h post-injection by a one-way ANOVA test using SIGMASTAT. Error bars represent the standard deviation of three mice per group.

**Computational modeling.** Beginning from the crystal structure of the extracellular portion of the FcγRIIIB receptor bound to the Fc region of the human Ig$G_1$ immunoglobulin (PDB ID 1E4K) (7), structures were prepared using methods from Lippow et al. (79). Hydrogen atoms were placed and the sidechains of H116(C) and H131(C) on the receptor were flipped by 180° around $\chi_2$ and treated in their neutral, ε-protonated form. In the Fc fragment, all histidine sidechains were neutral and protonated as indicated, to maximize hydrogen bonding potential: 268(A)-δ, 268(B)-ε, 285(A)-δ, 285(B)-δ, 310(A)-δ, 310(B)-ε, 429(A)-δ, 429(B)-δ, 433(A)-δ, 433(B)-δ, 435(A)-δ, and 435(B)-δ. A preliminary homology model of the corresponding FcγRIIA complex was constructed on this backbone as follows. All non-alanine, non-glycine residues further than 4.75 Å from an interface residue were replaced by alanine. Both glycosylated and aglycosylated forms of the structure were prepared, and in the glycosylated structure, a sliding, restrained harmonic minimization was performed on the sidechain of the N-glycosylated N297(B). Partial atomic charges for the N-glycosylated N297(C) residues were derived by fitting to the electrostatic potential using the restrained fitting methods of Bayly et al. (80) for each monosaccharide. The charges associated with hydrogens missing in the polysaccharide were added to their parent atoms to ensure charge conservation. To generate the FcγRIIA receptor structure, all FcγRIIIB interfacial residues were mutated to their FcγRIIA$^{R131}$ counterparts using the dead-end elimination and A* protocol described by Lippow et al. (79) in the presence of wild-type or mutant Fc region. For each mutant sequence, the global minimum energy conformation, as well as a collection of progressively higher energy conformations, was identified in the

context of discrete rotameric conformational freedom of all placed sidechains except the glycosylated form of N297. All of the Fc mutants examined were generated in the presence of the receptor during this conformational search. Note that one interfacial residue in the linker region of the FcγR structure (E86 in the FcγRIIA sequence) was left as a glycine, as all glutamate rotamers searched had a van der Waals clash with the receptor backbone. In the unbound FcγRIIA crystal structure (71), the two domains of the receptor separate slightly to accommodate this larger residue. The solvent screened electrostatic interactions and the residual electrostatic potential upon binding for these structural models were computed by solving the linearized Poisson–Boltzmann equation as described by Lee and Tidor (72). PARSE radii and charges were used for all examined complexes (81).

**Acknowledgements**

Rene Ott for performing lectin blotting, CHO cell immune complex labeling, SPR, and the murine platelet clearance experiment; Nate Silver for constructing the Fc:FcγR homology models; Vladimir Voynov for assistance with HEK cell culture; Andy Rakestraw for helpful discussions and suggestions; and the MIT Flow Cytometry and Biopolymers Core Facilities.

**Figure 3.1**

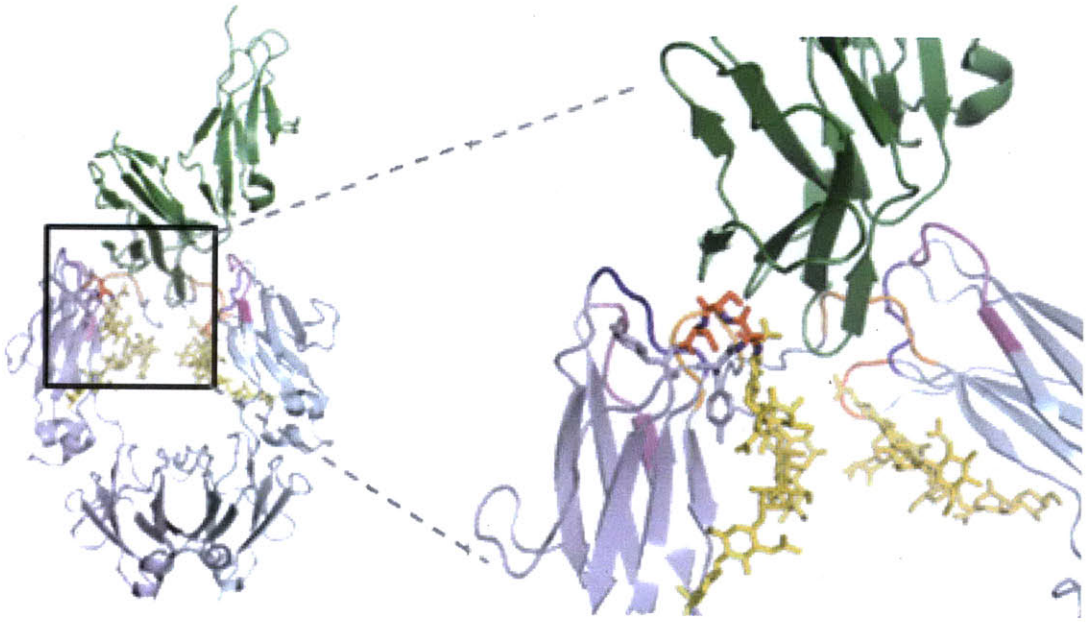

Cartoon representation of the crystal structure of the $hIgG_1$ Fc complex with hFcγRIII (PDB ID 1E4K). FcγRIII is shown in green, and both chains of the Fc in pale blue. Fc contact surfaces are colored: lower hinge (orange), B/C loop (blue), C'/E loop (red), and F/G loop (purple). Fc glycosylation is shown in yellow. The highlighted area shows an enlarged view of the C'/E loop interaction with FcγRIII. Fc residues 296-300 are shown as sticks.

**Figure 3.2**

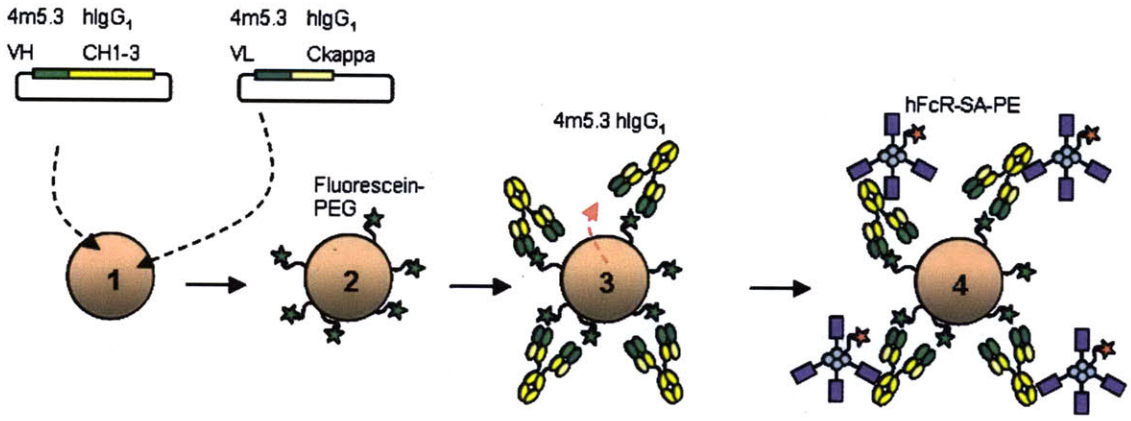


**Full-length $hIgG_1$ Fc display on the yeast cell surface.** Yeast transformed with 4m5.3 heavy chain and light chain secretion vectors are conjugated with NHS-PEG-fluorescein, then induced for secretion in PEG-containing medium. IgG variants are preferentially captured on the fluorescein-labeled yeast cell from which they were secreted (34). The displayed library is subsequently screened with preformed tetramers consisting of biotinylated soluble hFcγRs and fluorophore conjugated streptavidin (SA).

**Figure 3.3**

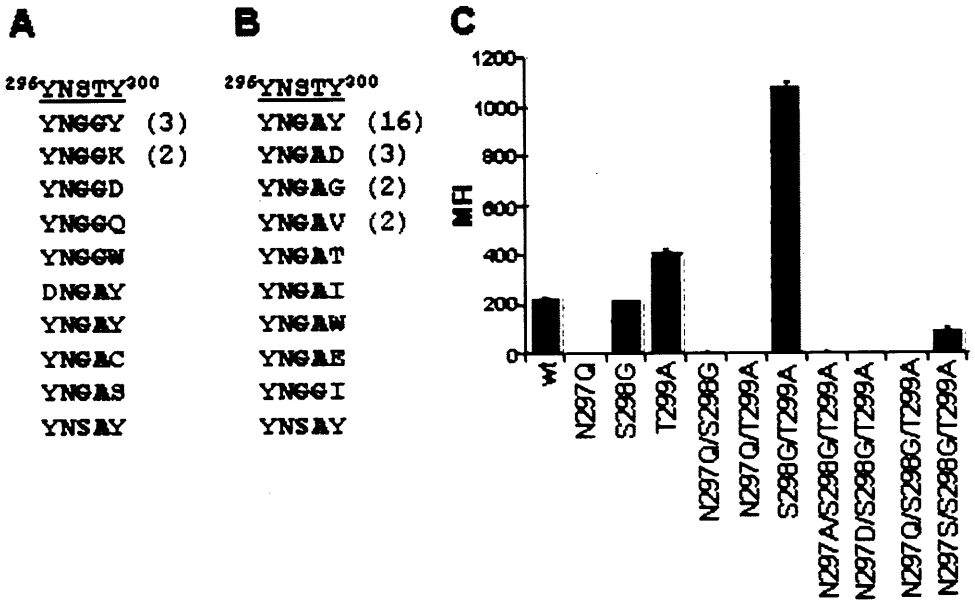


**Aglycosylated C'/E loop variants with FcγRIIA binding.**
**(A)** Unique sequences of aglycosylated Fc variants isolated for FcγRIIA binding after two rounds of FACS. Displayed sequences represent the residues randomized in the saturation libraries, positions 296-300, with the wild-type sequence underlined. Numbers in parentheses denote number of times a particular mutant was isolated; in some cases, identical protein sequences were isolated from multiple unique clones at the DNA level. Sequences of glycosylated variants enriched from the screen have been omitted.
**(B)** Unique sequences of aglycosylated Fc variants isolated for FcγRIIA binding after a third round of FACS, using a more stringent screening strategy.
**(C)** Binding of yeast-produced 4m5.3 $hIgG_1$ variants to 10 nM $Fc\gamma RIIA^{131R}$ streptavidin-Alexa 647 tetramers. IgG from yeast culture supernatants was loaded onto fluorescein-conjugated yeast and median fluorescence intensity (MFI) of receptor labeling was measured by flow cytometry. Protein A Alexa 647 labeling of all samples was assessed to determine similar IgG loading (data not shown). All data represent the average of two trials.

**Figure 3.4**

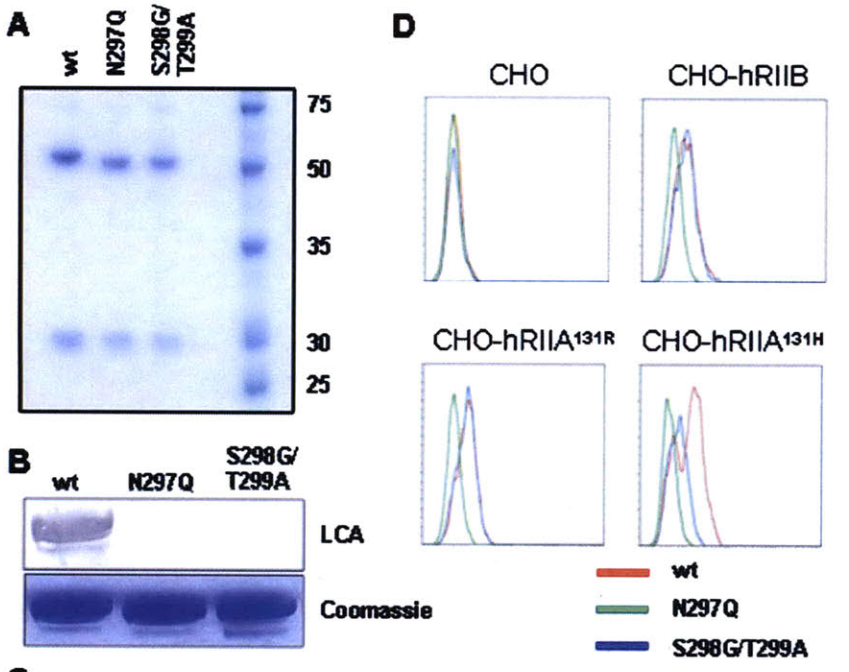


**C**

**Affinity: $K_D$ (x$10^{-6}$ M)**

| Variant | RIa | RIIA$^{131H}$ | RIIA$^{131R}$ | RIIB | RIIIA$^{176F}$ | RIIIA$^{176V}$ | C1q |
|---|---|---|---|---|---|---|---|
| wt | 0.04 | 5.5 | 5.0 | 9.8 | 13 | 4.6 | 0.3 |
| N297Q | 0.4 | n.b. | n.b. | n.b. | n.b. | n.b. | n.b. |
| S298G/ T299A | 0.3 | 7.0 | 1.7 | 5.7 | n.b. | n.b. | n.b. |

**S298G/T299A binds to soluble and cell surface FcγRIIA and FcγRIIB.**
**(A)** Reducing SDS-PAGE of HEK-produced wild-type 4m5.3 $hIgG_1$ and the aglycosylated variants S298G/T299A and N297Q.
**(B)** Glycan blotting with the mannose-specific lectin LCA (upper panel). Coomassie staining of SDS-PAGE was assessed to demonstrate similar protein loading (lower panel).
**(C)** Dissociation constants ($K_d$) for binding of FcγRs and C1q to wild-type 4m5.3 $hIgG_1$ and aglycosylated variants; n.b. indicates no binding detected.
**(D)** Labeling of CHO cell lines stably transfected with FcγRs with 4m5.3 IgG immune complexes. Cells were incubated with 1 μg of ICs and analyzed by flow cytometry.

**Figure 3.5**

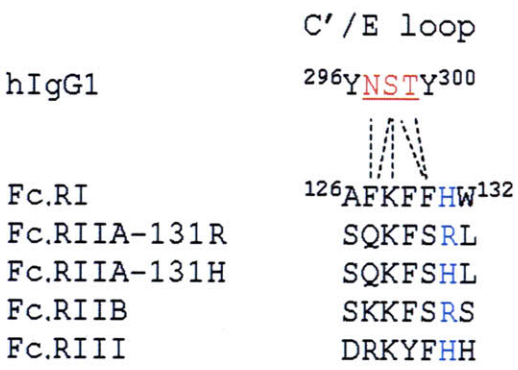


**C'/E loop contacts with FcγRs.** hFcγR family sequence alignment near predicted contacts with the $hIgG_1$ C'/E loop. Asn-Ser-Thr glycosylation motif shown in red. Position 131 of the aligned FcγRs is shown in blue. Dotted lines represent predicted contacts between residues on the Fc and FcγR (82).

**Figure 3.6**

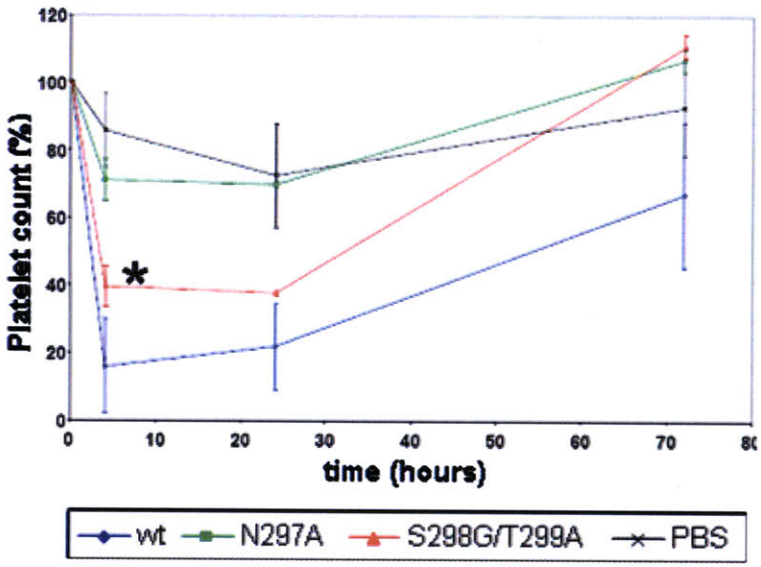


Platelet clearance in murine FcγR knockout, hFcγRIIA$^{131R}$ transgenic mice treated with chimeric anti-platelet antibody 6A6 hIgG$_1$ or the aglycosylated variants N297A and S298G/T299A. Mice (n=3) were injected with either antibody or PBS control and bled at 4, 24, and 72 h post-injection. Normalized to platelet counts prior to injection, counts 4 h following injection of the 6A6 antibodies were 15.8 ± 13.9 % for wt, 39.5 ± 5% for S298G/T299A, 71.0 ± 6.1% for N297A and 85.7 ± 11.0% for those treated with PBS only. S298G/T299A treated mice displayed a statistically significant difference in platelet reduction compared to N297A ($P$ = 0.017) and PBS ($P$ = 0.002), but not a statistically significant difference compared to wt ($P$ = 0.068).

**Figure 3.7**

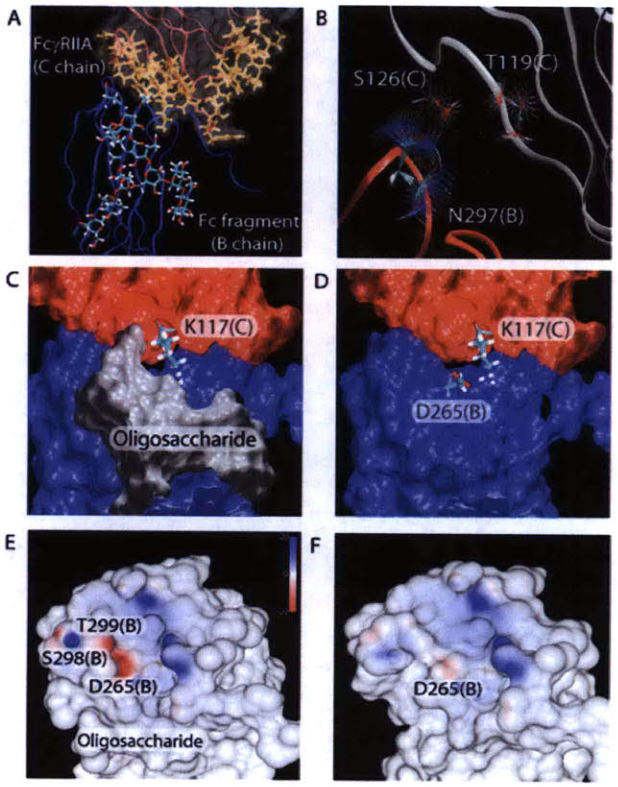


**Homology model of wild-type and S298G/T299A Fc interactions with FcγRIIA.**
**(A)** Structure of the wild-type B chain Fc fragment bound to the constructed FcγRIIA$^{131R}$ homology model. The highlighted portion of the B chain shows the large N-glycosylated residue making primarily intramolecular interactions. The portion of FcγRIIA (chain C) highlighted as orange sticks shows those side chains that were conformationally relaxed, through rotamerization, during model construction.
**(B)** Structure of the aglycosylated N297(B) interactions with a superposition of the possible discrete side chain conformations (rotameric states) of N297(B), T119(C), and S126(C) in the S298G/T299A mutant form of the Fc fragment.
**(C,D)** Structure of the K117(C)-D265(B) salt bridge in the wild-type structure (panel C) enclosed within the binding cavity in the presence of the oligosaccharide, and the same salt bridge as seen in the aglycosylated S298G/T299A mutant (panel D).
**(E,F)** Residual potential after binding mapped onto the interaction face of the B chain of the Fc fragment in the wild-type (panel E) and S298G/T299A mutant (panel F) structures. White regions indicate areas of ideal complementarity between the Fc fragment and FcγRIIA$^{131R}$, while deep red or blue regions indicate areas of poor complementarity due to ligand desolvation costs uncompensated by interactions made upon binding. Red corresponds to negative residual potentials and blue to positive residual potentials. The coloring scale, identical in both panels, is indicated in units of *kT/e*.

**Figure 3.8**

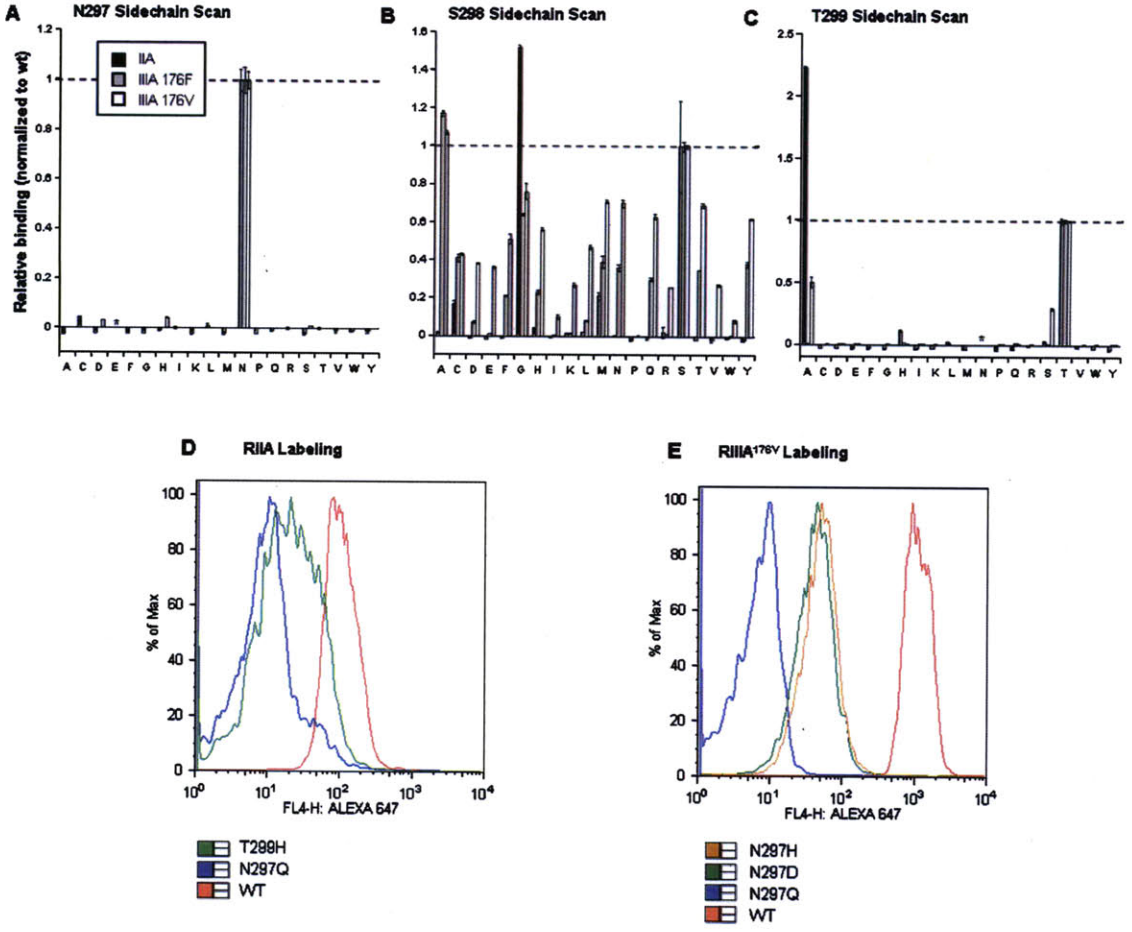


**Sidechain scanning of Fc positions 297, 298, and 299.**
**(A-C)** Yeast-secreted 4m5.3 $hIgG_1$ point mutants were loaded on fluorescein-conjugated yeast and assayed for binding to 10 nM $Fc\gamma RIIA^{131R}$, $Fc\gamma RIIIA^{176V}$, and $Fc\gamma RIIIA^{176F}$ streptavidin-Alexa 647 tetramers by flow cytometry. All data represent the average of two trials and are normalized to the wild-type signal; * indicates binding to variant not determined.
**(D,E)** Histograms of $Fc\gamma RIIA^{131R}$ streptavidin-Alexa 647 and $Fc\gamma RIIIA^{176V}$ streptavidin-Alexa 647 tetramer labeling of weakly binding aglycosylated clones.

**Figure 3.9**

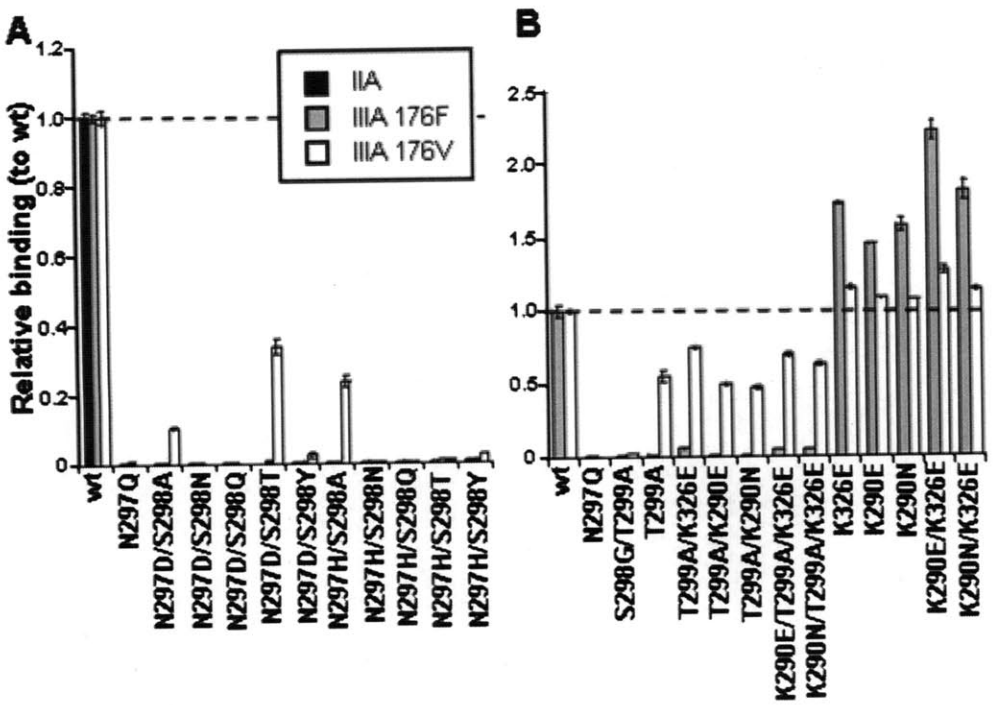


**Designed aglycosylated Fc mutants with FcγRIIIA binding.**
Yeast-secreted 4m5.3 $hIgG_1$ C'/E loop double point mutants **(A)** or T299A point mutants with the 'second-site' mutations K326E and K290E/N **(B)** were loaded on fluorescein-conjugated yeast and assayed for binding to 10 nM $Fc\gamma RIIIA^{176V}$, $Fc\gamma RIIIA^{176F}$, and $Fc\gamma RIIA^{131R}$ (for panel A only) streptavidin-Alexa 647 tetramers by flow cytometry. All data represent the average of two trials and are normalized to the wild-type signal.

**Figure 3.10**

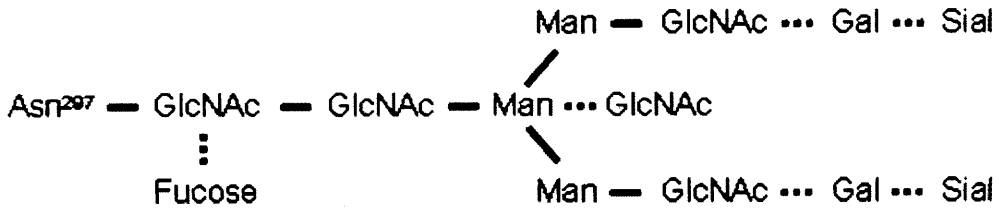


**Composition of the N-linked glycan attached to Asn297.** GlcNAc, N-acetylglucosamine; Man, mannose; Gal, galactose; Sial, sialic acid. Dark lines represent core glycosylation, dotted lines represent glycoforms variably attached to the core structure.

# Chapter 4. Engineering Aglycosylated Fc variants with FcγRIIIA binding

## Introduction

Over the past several decades, antibody-based therapy has emerged as a promising mode of treatment of human disease, and in particular in the treatment of human cancer (1, 2). While multiple mechanisms contribute to the efficacy of therapeutic antibodies (1, 4), activation of immune effector functions has been shown to play a critical role in the efficacy of several therapeutic antibodies, in particular through an antibody's engagement of the Fcγ receptors (FcγRs) of immune cells (5). Here, as in immunity, IgGs act as the adaptor between a target cell or pathogen and the immune response by simultaneously binding antigen through their variable regions and activating an immune response through interaction of their conserved Fc regions with FcγRs on immune cells.

The human FcγR (hFcγR) family consists of the activating receptors FcγRI, FcγRIIA, and FcγRIIIA, and the inhibitory receptor FcγRIIB. While FcγRI binds IgG with high affinity (nanomolar binding constants), FcγRIIA, FcγRIIB, and FcγRIIIA bind IgG with micromolar affinity, becoming activated only via avid multivalent interactions with opsonized antigen (60). In particular, the efficacy of therapeutic antibodies is strongly correlated to the allelic forms of FcγRIIIA possessed by a given individual. Populations homozygous for a valine at position 176 of FcγRIIIA (FcγRIIIA$^{176V}$), as opposed to a phenylalanine (FcγRIIIA$^{176F}$), have dramatically improved objective response rates (13-16), likely due to a several-fold stronger binding of wild-type hIgG$_1$ for the FcγRIIIA$^{176V}$ allele.

Recently we demonstrated that aglycosylated human IgG$_1$ Fc variants are capable of engaging a subset of the low-affinity FcγRs with approximately wild-type binding affinity and activating immune effector cells *in vivo*, demonstrating that N-linked glycosylation of the Fc is not a strict requirement for FcγR engagement. Numerous previous studies have shown that the binding of IgG to FcγR is highly sensitive to the presence of a single N-linked glycosylation site at asparagine 297 (N297) of the Fc, with

deglycosylation resulting in a complete loss of FcγR binding (8, 21, 25, 62-64). Thus, aglycosylated variants that maintain engagement to FcγRs have the potential to open up therapeutic antibody production to virtually any expression system, removing the post-translational variation in N-glycan synthesis that occurs across organisms, or in the case of the common prokaryotic expression host *E. coli*, the complete absence of N-linked glycosylation. Such variation in the nature of the N-linked glycan imparts substantial changes in the affinity to FcγR and subsequent biological response (9, 10), and additionally can lead to the presence of sugars that are rapidly cleared and/or immunogenic.

Our initial screening methodology focused on engineering the Fc C'/E loop, which contains the N-linked glycosylation site ($Asn^{297}$-$Ser^{298}$-$Thr^{299}$) as well as makes direct contacts with FcγR (**Figure 3.1**). A library screen of all possible C'/E loop variants yielded a variant (S298G/T299A) that binds FcγRIIA and FcγRIIB with approximately wild-type affinity, but not FcγRIIIA. A second approach, based on screening each single point mutation within the C'/E loop, then combining candidate mutations, identified variants that weakly bind $FcγRIIIA^{176V}$ – T299A, N297D, N297H, and the double mutants N297D/S298T, N297D/S298A, and N297H/S298A – demonstrating that aglycosylated Fcs can engage this FcγR as well. However, given the importance of FcγRIIIA to therapeutic outcome, it is likely that these variants would have limited therapeutic utility.

Building upon our previous work, we report here aglycosylated $hIgG_1$ variants that can engage all of the low-affinity hFcγRs with approximately wild-type or improved binding affinity, thus identifying variants that might effectively substitute for the wild-type, glycosylated $hIgG_1$. In doing so, we have focused on engineering additional loops of the Fc domain that make contact with FcγR, screening libraries that encode all possible amino acid diversity within segments of these loops to enrich variants with improved $FcγRIIIA^{176F}$ binding. Such variants, when placed in the previously identified aglycosylated backgrounds that allow for weak $FcγRIIIA^{176V}$ binding, yield fully FcγR competent aglyco Fcs with a range of affinities. In addition, we find that our approach of searching sequence space at contact loops in a focused manner, which allows us to theoretically screen all possible amino acid diversity at these sites in short segments,

uncovered variants with mutations that act cooperatively, and thus not easily predicted by combining the properties of single point mutations identifiable through other protein engineering strategies.

## Results

**Engineering approach and screening methodology**. Previously, we showed that the binding affinity of aglycosylated Fcs can be modulated by placing 'second-site' mutations selected for improved binding to FcγRs in a glycosylated background into an aglycosylated background. Here, combining a mutation located near a contact interface (K326E) with the mutation T299A improved FcγRIIIA binding relative to T299A alone, while second-site mutations at a site distant from the contact interface (K290E/N) had no effect upon aglycosylated Fc binding (**Figure 3.9**). This result suggested that modulating the interactions about the Fc contact loops with FcγR, in a glycosylated background, could likewise translate into improved binding affinity in an aglycosylated background. To accomplish this, we set out to systematically ask which combinations of mutations at Fc contact loops yield improved FcγRIIIA binding.

Here, we constructed saturation libraries about three contact sites within the Fc – the lower hinge, the B/C loop, and F/G loop (**Figure 4.1**) – and screened them by displaying these full-length $hIgG_1$ variants on the surface of yeast. In this display system, the femtomolar affinity scFv 4m5.3 (38) has been reformatted as a $hIgG_1$, allowing 4m5.3 $hIgG_1$ Fc library variants to be captured on fluorescein-labeled yeast from which they are secreted (**Figure 3.2**) by adapting features of a cell surface secretion capture assay (34) and the improved secretion of full-length $hIgG_1$ from *S. cerevisiae* (Chapter 2). Contact interface libraries were constructed by fully-randomizing four amino acid stretches using degenerate NNK codons (N=ATCG, K=GT), which encode all 20 possible amino acids in 32 codons. This design approach allows for over-sampling the codon diversity ($32^4$ ~ $1x10^6$), and thus amino acid diversity, in these yeast-based libraries, which often have a transformation efficiency on the order of $1x10^7$. The following libraries were constructed and pooled by contact region: lower hinge (234-237, 236-239), B/C loop (265-268, 267-270), and F/G loop (326-329, 327-330, 329-332, 331-334). As a target we chose the $FcγRIIIA^{176F}$ allele, which, given its weaker binding for wild-type Fc, likely represents a more stringent, as well as therapeutically relevant, barrier for improved FcγRIIIA binding. Libraries were pooled by loop and individually screened by two rounds of enrichment on

FcγRIIIA$^{176F}$ coated magnetic beads followed by three rounds of fluorescence activated cell sorting (FACS) at increasing stringency.

**B/C and F/G loop variants enriched for improved FcγRIIIA binding**. The sequences of variants enriched for FcγRIIIA$^{176F}$ binding after the second and third rounds of FACS (rounds four and five in total) for the B/C and F/G loop libraries are shown in **Figure 4.2**. Enrichment of only wild-type clones was observed from the lower hinge libraries. Clones enriched from the B/C loop libraries (**Figures 4.2a,b**) show an absolute preference for D265, consistent with the importance of this residue in binding FcγR (21, 83). The majority of clones enriched from the screen have substitutions at positions 266-268, indicating that variation within the 265-268 sublibrary more strongly contributed to FcγRIIIA$^{176F}$ binding. Enriched variants show a strong preference for mutation of H268 to Glu, and to a lesser extent a likewise negatively charged Asp. At position 266 there is a strong preference for either Leu or the wild-type Val, while position 267 appears to be more promiscuous to substitution, with enrichment of the wild type Ser, as well as more frequently Ala, Glu, and Asp. Of the clones enriched from the 267-270 sublibrary (i.e. those clones with mutations at positions 269 and/or 270), there is a strong preference for retaining negative charge at E269 and D270, either as the wild-type residue or as E269D or D270E.

Clones enriched from the F/G loop libraries (**Figures 4.2c,d**) fall into two broad classes of loop diversity – those enriched from the 326-329 sublibrary and those with substitutions at the opposite end of the loop, primarily at position 332 and to a lesser extent at 334, both of which have been previously identified as modulating FcγRIIIA binding affinity (20-22). Substitution of I332 with Glu dominates the screen, and has been previously shown to greatly enhance binding to all FcγRs, including FcγRIIIA$^{176V}$ and FcγRIIIA$^{176F}$ (20). Virtually all clones potentially enriched from the 331-334 sublibrary (i.e. those with mutations at positions 333 and/or 334, or those lacking mutations at positions 329 and 330 found in the 329-332 sublibrary) also contain a substitution at position 334, with a preference for Val and Ala, and to a lesser extent Ser, Glu, and Gln. These data are consistent with previous studies, in which K334A, K334E, K334Q, and K334V were shown to strengthen binding FcγRIIIA (21), and the frequent

enrichment of K334E and K334N from a random mutagenesis library for improved binding to FcγRIIIA (22).

Within the clones enriched from the 331-334 sublibrary there is a strong preference for either the wild-type Pro at position 331 or Ser or Ala. P331A alone has been shown to have no effect on FcγRIIIA$^{176V}$ binding affinity, and P331S alone to reduce FcγRIIIA$^{176V}$ binding (21). Interestingly, when P331 is mutated, it is almost always derived from the 331-334 sublibrary and not the 329-332 sublibrary, suggesting that the context of flanking residues is important to binding. Clones enriched from the 329-332 sublibrary have a strong preference for substitution at position 330, and thus mutation of the wild-type Pro at position 331, within the background of I332E and A330x may be disfavored. Previous studies have shown that A330V alone slightly improves FcγRIIIA$^{176F}$ binding (22) and A330L in the context of I332E imparts improved FcγRIIIA$^{176F}$ binding (20).

In contrast, relatively little is known about how diversity at positions 326-328, and in particular positions 327 and 328, impact FcγR binding. The variants enriched for improved FcγRIIIA$^{176F}$ binding from our screen from the 326-329 sublibrary show a strong preference for substitution of K326 with the hydrophobes Ile, Leu, and Val. K326A has previously been shown to increase binding to all FcγRs (21), while K326E, and to a lesser extent K326I and K326Q, were frequently enriched in a screen for improved binding to FcγRIIIA$^{176V}$ (22). In addition, multiple substitutions at position 326 impart improved binding to the complement component C1q (73). In our screen A327 has a strong preference for Asp, although tolerates additional residues as well, with the similarly negatively charged Glu, the wild-type Ala, and Gly appearing multiple times; similarly, L328 has a strong preference for Ala and appears to tolerate multiple substitutions, with Gly appearing multiple times. Within the clones enriched from this sublibrary, P329 is absolutely conserved, consistent with its substitution being disfavored within the 329-332 library. P329A alone has been shown to reduce binding to all FcγRs (21).

**Binding of HEK secreted B/C and F/G loop variants**. To determine whether variants enriched from this yeast-based screen impart improved FcγRIIIA binding when expressed

from a more standard host, a subset of variants were subcloned into mammalian expression vectors, secreted from HEK 293 cells, and assayed for their relative ability to bind FcγRIIIA$^{176F}$. Most B/C loop variants tested displayed a slight increase in binding affinity to FcγRIIIA$^{176F}$ compared to wild-type Fc (**Figure 4.3a**). Within the S267A/H268E background, there is a slight preference Leu at position 266 compared to the wild-type Val at position 266, suggesting that either of these residues can mediate FcγRIIIA$^{176F}$ binding. Within the V266L/H268E background, there is a slight preference for Ala or Asp over the wild-type Ser at position 267, although substitution to Thr results in a variant with reduced FcγRIIIA$^{176F}$ binding. Interestingly, the addition of D270E in the S267A/H268E background results in decreased binding to FcγRIIIA. The D270E mutation alone has been shown to impart slightly improved binding to FcγIIIA but weakened binding to FcγRIIA$^{131R}$ and FcγRIIB (21, 22) – FcγRs with Arg at position 131 of the receptor – suggesting that multiple mutations within this loop may not act in an additive fashion.

Since the consensus mutations from our screen at positions I332 and K334 have been extensively characterized, we chose to look in more depth at the contributions of positions 326, 327, and 328 of the Fc to FcγRIIIA binding (**Figure 4.3b**). As a whole, these F/G loop variants bind FcγRIIIA$^{176F}$ to a greater extent than the sampled B/C loop variants, with two F/G loop variants, K326I/A327Y/L328G (IYG) and K326I/A327E/L328E (IEA), binding FcγRIIIA$^{176F}$ to a much greater extent than wild-type Fc. Interestingly, the presence of a Tyr at position 327 in the K326I/L328G background imparts a large increase in binding affinity, as K326I/L328G alone binds at near wild-type levels.

To assess the contribution of the individual mutations within these clones, as well as ask whether additional improved variants exist – such as those that could be present if, for example 10-fold more clones were sequenced and analyzed – we performed a detailed point mutant analysis of both the IYG and IEA variants (**Figure 4.4**). K326I alone imparts an increase in binding affinity to FcγRIIIA$^{176F}$, suggesting that part of the large increase in binding affinity of the IYG and IEA variants compared to wild-type is due to the presence of this mutation. Interestingly, no other combination of mutations other than the triple mutant imparts improved binding in the IYG variant (and in most cases

dramatically weakens binding), suggesting that for this variant substitution at A327 and L328, in the K326I background, act cooperatively to impart improved receptor binding. Similarly, substitutions at A327 and L328 in the IEA variant also act in a coordinated way with K326I. L328A by itself weakens receptor binding, but when placed alongside K326I results in a double mutant with strengthened binding compared to K326I alone. Likewise, A327E alone and A327E/L328A weaken receptor binding, yet in the context of the IEA variant yield substantially improved FcγRIIIA$^{176F}$ binding.

**Binding of aglycosylated F/G loop variants**. To assess whether enriched variants from our screens could lead to aglycosylated Fcs with improved FcγRIIIA binding, the T299A mutation was placed in the F/G loop variants described above, secreted from HEK cells, and as a stringent test of binding affinity, assayed for their ability to bind FcγRIIIA$^{176F}$ (**Figure 4.5**). Only T299A/K326I/A327Y/L328G (T299A/IYG) and T299A/K326I/A327E/L328E (T299A/IEA) bound FcγRIIIA$^{176F}$ with detectible affinity, consistent with these mutations imparting the largest improvements in binding affinity in the glycosylated background. In this assay, T299A/IYG binds FcγRIIIA$^{176F}$ to a slightly greater degree than wild type hIgG$_1$, and T299A/IEA to a slightly lesser degree. In addition, both of these aglycosylated variants bind FcγRIIIA$^{176V}$, FcγRIIA$^{131R}$, and FcγRIIB at approximately wild-type or improved levels (**Figure 4.6**), demonstrating not only that aglycosylated Fc variants can be engineered that bind FcγRIIIA, but that such variants can be engineered to bind the panel of human low-affinity FcγRs as well. In particular, the binding to FcγRIIB (**Figure 4.6b**) appears to be greatly strengthened compared to wild-type Fc for the T299A/IYG and T299A/IEA variants, and given the high sequence identity between receptors, likely greatly strengthened for FcγRIIA (**Figure 4.6a**) as well (the similar signals in this panel likely represent saturation of binding, as there is little reduction in signal with a 10-fold decrease in receptor labeling concentration).

**Modulating FcγRIIA and FcγRIIB binding of aglycosylated variants**. Given the large increase in binding to FcγRIIA and FcγRIIB imparted by using the T299A mutation to place the F/G loop variants in an aglycosylated background, we next sought to reduce

the binding of the aglycosylated variant Fcs to these two receptors by placing the K326I/A327Y/L328G (IYG) F/G loop variant in alternative aglycosylated C'/E loop backgrounds. Previously, we identified the aglycosylated double mutants N297D/S298T (DTT), N297D/S298A (DAT), and N297H/S298A (HAT), which weakly bind FcγRIIIA$^{176V}$, but have no detectible binding to FcγRIIA$^{131R}$ (**Figure 3.9a**), suggesting that these variants preferentially bind FcγRIIIA. The variants T299A/IYG, DTT/IYG, DAT/IYG, and HAT/IYG all display varied FcγR-binding profiles (**Figure 4.7**), with the DTT/IYG, DAT/IYG, and HAT/IYG variants having greatly reducing FcγRIIA and FcγRIIB binding compared to T299A/IYG (**Figures 4.7a,b**), consistent with the binding properties of T299A, DTT, DAT, and HAT alone. All variants appear to bind the FcγRIIIA$^{176V}$ allele equally as well as wild-type Fc (**Figure 4.7c**), and most (DTT/IYG, T299A/IYG, and DAT/IYG) display similar, if not slightly improved binding for the FcγRIIIA$^{176F}$ allele (**Figure 4.7d**). Interestingly, HAT/IYG has greatly reduced binding for both FcγRIIA and FcγRIIB, and is thus essentially FcγRIIIA specific. The DTT/IYG and DAT/IYG variants come closest, in this assay, to displaying near wild-type binding for all low affinity FcγRs – DAT/IYG has similar binding as wild-type Fc for FcγRIIA and increased binding for FcγRIIB; DTT/IYG has reduced binding for FcγRIIA and similar binding as wild-type for FcγRIIB. Taken together with the T299A/IYG variant, these variants clearly demonstrate that aglycosylated IgG variants can be engineered to bind all of the low-affinity FcγRs, and with a range of affinities and specificities.

## Discussion

In the present study, we demonstrate that aglycosylated IgG variants can be engineered to engage FcγRIIIA at wild-type or improved levels, and that these variants can bind to all of the human low-affinity FcγRs. Such variants represent a further step towards the development of fully-functional aglycosylated IgGs and the potential production of therapeutic antibodies in virtually any expression system without regard to post-translational processing.

In engineering these aglycosylated variants, we chose a modular design strategy, based upon the hypothesis that properties imparted by altered contact loops will be additive. In our previous work, we identified a series of C'/E loop mutations that impart a range of aglycosylated FcγR binding properties. By combining these mutant aglycosylated C'/E loops with an altered F/G loop isolated for improved FcγRIIIA$^{176F}$ binding, we have generated a series of aglycosylated Fc variants capable of binding FcγRIIIA whose relative receptor binding properties mirror those of the C'/E loop variants alone.

In addition, in screening for variants with improved FcγRIIIA binding, we chose a directed evolution approach that allowed us to experimentally explore the sequence space at the sites of Fc:FcγR interaction in a vastly more comprehensive manner than previously reported approaches, which have included alanine scanning point mutagenesis (21), screening random mutagenesis libraries of the entire Fc region (22), and *in silico* prediction and experimental validation of variants (20). While it's likely that combining previously described point mutations present in the literature would have also led to variants with the properties we describe here, it was our hope that the approach we took would allow us to add further insight to the current knowledge of Fc:FcγR interactions, and in particular the engineering of these interactions.

The strength of this approach is highlighted in the variants enriched with substitutions at positions 326-328. While many groups have identified substitutions at position 326 that strengthen FcγR binding affinity (21, 22, 73), there has been no demonstration that substitutions at positions 327 and 328 can also lead to improved variants. In the context of the two best variants from our screen, IYG and IEA, our data

show that mutations at positions 327 and 328 are not additive, yet act in a cooperative fashion to improve binding affinity. Such variants would not be found by combining single point mutations identified for improved binding, and are extremely unlikely to be found in screens of random mutagenesis libraries.

Our yeast display system allows for the rapid screening of millions of variants, and for the most part enriches variants with properties that translate to improved binding when secreted from mammalian cells. It is not without artifacts, however, and this is particularly apparent in the clones enriched from the B/C loop libraries. While there is a clear preference for several similar variants from these libraries, our screening assay suggests that these variants as a whole do not substantially improve receptor binding. This may reflect a limit to the degree to which this loop is capable of improving FcγRIIIA binding (i.e. it has reached its near optimized level), and/or potentially reflect variations in the affinity that these mutations impart in yeast-secreted antibodies (containing yeast N-linked glycoforms) compared to HEK-secreted antibodies (containing human glycosylation patterns).

Having shown that aglycosylated variants with these receptor binding properties can be identified, it will be important to quantitatively describe their binding affinity to the panel of human FcγRs, as well as test their activity in *in vitro* and *in vivo* models. Murine models and clinical data suggest a strong correlation between therapeutic activity and the presence of the low-affinity FcγRs (5) – FcγRIIA, FcγRIIB, FcγRIIIA – and thus the variants described here may effectively substitute in these models for wild-type Fc. It will also be important to assess the biophysical properties and serum half-life of these IgGs, as previous work has shown reduced stability of deglycosylated wild-type $hIgG_1$ (75) as well as the reduced stability of a glycosylated Fc variant engineered for improved FcγR binding (74). Previous studies have shown that lack of glycosylation does not affect serum half-life (25), and that most substitutions within these contact loops have little effect upon FcRn binding (21).

## Materials and Methods

**Loop saturation mutagenesis library construction.** Libraries were constructed by homologous recombination of a mutated heavy chain constant region insert into the 4m5.3 heavy chain yeast secretion vector template according to previously published methods (78). The 4m5.3 heavy chain secretion vector was previously constructed from the pRS316 shuttle vector by insertion of the GAL10 promoter and alpha terminator, signal peptide, and 4m5.3 variable heavy chain domain upstream of the $hIgG_1$ CH1 to CH3 constant domains (35). The 4m5.3 heavy chain template vector was prepared by digestion with NheI (New England Biolabs) and XhoI (New England Biolabs), which flank the $hIgG_1$ constant domains.

Saturation mutagenesis of the lower hinge was performed by gene reconstruction with the degenerate oligonucleotides 234-237NNK (all oligos from Integrated DNA Technologies) and 236-239NNK; the B/C loop with 265-268NNK and 267-270NNK; and the F/G loop with 326-329NNK, 327-330NNK, 329-332NNK, and 331-334NNK (see Oligonucleotides below for sequences of all oligonucleotides used during library construction). Degenerate oligos were designed as 52-mers, with 20 bases of the wild type sequence flanking NNK codons (N=ATCG, K=GT) on both sides. Briefly, in a first PCR step a template for incorporation of the degenerate oligo was created by PCR amplifying the region directly 3' of the desired loop insertion site through the 3' region of the CH3 domain, using the wild type vector as a template. For a given library, this step used the forward primer ###-###flank-for (e.g. 265-268flank-for) and the reverse primer 4m-CH3-epPCR-rev; ###-###flank-for is a 20-mer consisting of the same 3' wild-type sequence in the degenerate oligo, which allows for incorporation of the degenerate oligo in a second PCR step. In this second step, the gel purified PCR product from step one was used as a template for the PCR incorporation and amplification of the degenerate sequence, using the forward primer ###-###NNK (e.g. 265-268NNK) and the reverse primer 4m-CH3-epPCR-rev.

Gene assembly was performed by PCR extension of the above, gel purified PCR product with a second PCR product, consisting of the 5' region of the gene with 20 bp of overlap with the 5' wild-type sequence of the degenerate oligo. This PCR product

was amplified from the wild-type vector using the forward primer 4m-CH1-epPCR-for and the reverse oligo ###-###flank-rev (e.g. 265-268flank-rev); ###-###flank-rev is a 20-mer consisting of the same 5' wild-type sequence in the degenerate oligo, allowing for extension of the two PCR products to re-construct the entire CH1-CH3 regions. In a final step, the gel purified extended PCR product was amplified with the oligos 4m-CH1-epPCR-for and 4m-CH3-epPCR-rev, which amplify the 3' region of the 4m5.3 variable heavy chain to the 3' end of the CH3 domain, reconstructing the heavy chain CH1 to CH3 gene insert with ~50 base pairs of overlap with the digested template vector for efficient yeast homologous recombination.

Gene inserts were then transformed with digested template vector by electroporation into the yeast strain YVH10/LC, a derivative of the yeast strain YVH10 (39), containing a chromosomally integrated copy of the 4m5.3 light chain yeast secretion vector. All saturation libraries had approximately 1-2x$10^7$ transformants, 10- to 20-fold greater than the theoretical diversity at the DNA level ($32^4$ ~ 1.0x$10^6$).

**Oligonucleotides.**

4m-CH1-epPCR-for (5'-ATGGAATACTTGGGTCAAGGAACCTCAGTCACCGTCTCCGCTAGC)
4m-CH3-epPCR-rev (5'-ATTTTGTTACATCTACACTGTTGTTATCAGATTTCGCTCGAGTCA)
234-237NNK (5'-CACCGTGCCCAGCACCTGAANNKNNKNNKNNKCCGTCAGTCTTCCTCTTCCC)
236-239NNK (5'-GCCCAGCACCTGAACTCCTGNNKNNKNNKNNKGTCTTCCTCTTCCCCCCAAA)
234-237flank-for (5'-CCGTCAGTCTTCCTCTTCCC)
234-237flank-rev (5'-TTCAGGTGCTGGGCACGGTG)
236-239flank-for (5'-GTCTTCCTCTTCCCCCCAAA)
236-239flank-rev (5'-CAGGAGTTCAGGTGCTGGGC)
265-268NNK (5'-AGGTCACATGCGTGGTGGTGNNKNNKNNKNNKGAAGACCCTGAGGTCAAGTT)
267-270NNK (5'-CATGCGTGGTGGTGGACGTGNNKNNKNNKNNKCCTGAGGTCAAGTTCAACTG)
265-268flank-for (5'-GAAGACCCTGAGGTCAAGTT)
265-268flank-rev (5'-CACCACCACGCATGTGACCT)
267-270flank-for (5'-CCTGAGGTCAAGTTCAACTG)
267-270flank-rev (5'-CACGTCCACCACCACGCATG)
326-329NNK (5'-ACAAGTGCAAGGTCTCCAACNNKNNKNNKNNKGCCCCCATCGAGAAAACCAT)
327-330NNK (5'-AGTGCAAGGTCTCCAACAAANNKNNKNNKNNKCCCATCGAGAAAACCATCTC)
329-332NNK (5'-AGGTCTCCAACAAAGCCCTCNNKNNKNNKNNKGAGAAAACCATCTCCAAAGC)
331-334NNK (5'-CCAACAAAGCCCTCCCAGCCNNKNNKNNKNNKACCATCTCCAAAGCCAAAGG)
326-329flank-for (5'-GCCCCCATCGAGAAAACCAT)
326-329flank-rev (5'-GTTGGAGACCTTGCACTTGT)

| | |
|---|---|
| 327-330flank-for | (5'-CCCATCGAGAAAACCATCTC) |
| 327-330flank-rev | (5'-TTTGTTGGAGACCTTGCACT) |
| 329-332flank-for | (5'-GAGAAAACCATCTCCAAAGC) |
| 329-332flank-rev | (5'-GAGGGCTTTGTTGGAGACCT) |
| 331-334flank-for | (5'-ACCATCTCCAAAGCCAAAGG) |
| 331-334flank-rev | (5'-GGCTGGGAGGGCTTTGTTGG) |

**Library screening.** Library screening was performed using the cell surface secretion assay (CeSSA) (34). Briefly, pooled loop libraries were grown in SD-CAA (2% glucose, 0.67% yeast nitrogen base, 0.54% $Na_2HPO_4$, 0.86% $NaH_2PO_4 \cdot H_2O$, 0.5% casein amino acids) to an $OD_{600}$ of ~ 5, and then induced in YPG (2% galactose, 2% peptone, 1% yeast extract, 0.54% $Na_2HPO_4$, 0.86% $NaH_2PO_4 \cdot H_2O$) for 12 hrs at 20 °C. Following this pre-induction phase, yeast were labeled with fluorescein-PEG-NHS (Laysan Bio) and re-induced in YPG containing 15% PEG (w/v) at 20 °C for 36 hrs. Cells were then washed with PBS containing 0.1% (w/v) BSA (PBS/BSA).

For the first two rounds of screening, libraries were incubated with biotinylated hFcγRIIIA$^{176F}$ preloaded onto streptavidin magnetic beads (Invitrogen), and enriched variants captured by magnetic separation, with non-bound yeast discarded (Margaret Ackerman, *manuscript submitted*). Beads were washed with PBS/BSA, then placed in SD-CAA supplemented with penicillin/streptomycin (Invitrogen) to amplify captured yeast cells. Starting with the third round of screening, yeast were labeled with biotinylated hFcγRIIIA$^{176F}$ preloaded onto streptavidin-Alexa 647 (Invitrogen). The subpopulations were sorted on either a BD FACSAria (Becton Dickinson) or a MoFlo Cell Sorter (Cytomation Inc) and collected cells grown in SD-CAA supplemented with penicillin/streptomycin (Invitrogen), for three additional rounds of screening (five rounds in total). Library populations were labeled for FACS sorting at increasingly stringent concentrations of FcγRIIIA$^{176F}$ tetramer as follows: round three (500 pM), round four (50 pM), and round five (50 pM).

**Cloning and Site Directed Mutagenesis.** Clones enriched from the yeast-based screen were cloned from the yeast secretion vectors into the gWIZ mammalian expression vector (Genlantis) by a variation of the Quikchange mutagenesis protocol (84). Fc domains

were PCR amplified from the pRS316 based heavy chain yeast secretion vector with the oligos:

gWIZ-Fc-for = (5'-GAGCCCAAATCTTGTGACAA)

gWIZ-SalI-rev = (5'-TCACACGTGTCGACTTATCATTTACCCGGAGACAGGGAGA)

which allow for ≥ 20 bp of homology to the wild-type segment in the gWIZ vector. PCR products were gel purified and used as oligos for PCR-amplification of the entire variant vector, incorporating the sequence of the Fc variant.

Point mutants were constructed by PCR-amplification of the entire vector using complementary primers containing the desired point mutations.

**Characterization of HEK-secreted Fc mutants.** Unless otherwise noted, Fc variants were transiently transfected into HEK 293F cells (Invitrogen) in a 6-well plate format. Cell culture supernatants were loaded onto fluorescein-conjugated yeast overnight at 4 °C; yeast were then washed with PBS/BSA, labeled with biotinylated FcγR preloaded onto streptavidin-Alexa 647 at 4 °C for > 2 hrs, and analyzed by flow cytometry. Labeling with 10 μg/ml Protein A-Alexa 647 (Invitrogen) was performed as a separate IgG loading control for all samples. FcγR labeling fluorescence for individual variants was normalized by the surface IgG loading of a variant relative to that of wild-type IgG, as determined by relative Protein A-Alexa 647 labeling. There was strong agreement (within 10% difference) between this approach to signal normalization and gating on a population of cells to give similar surface loading signals.

**Antibodies and recombinant proteins.** The 4m5.3-human Fc chimeric variants were produced by transient transfection of 293F cells (Invitrogen) and subsequent purification from cell culture supernatants. For protein production, cells were cultured in Freestyle 293F Expression Medium (Invitrogen). Recombinant antibodies were purified with immobilized protein A (Pierce) by affinity chromatography. All proteins were dialyzed against PBS. Purity was assessed by SDS-PAGE followed by Coomassie Blue staining.

**Acknowledgements**

Rene Ott, for providing biotinylated FcγRs; Margie Ackerman, for helpful discussions and suggestions about magnetic bead sorting; Ben Hackel, for helpful discussions and suggestions about saturation library creation; and the MIT Biopolymers and Flow Cytometry Core Facilities.

**Figure 4.1**

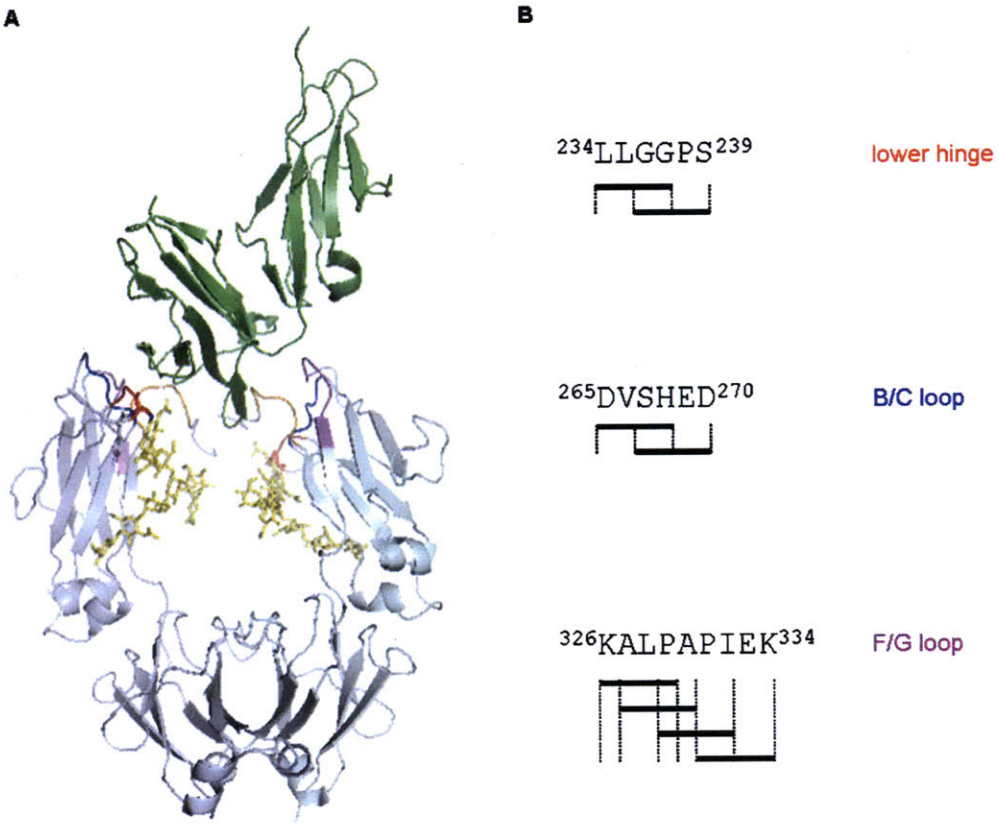


**Fc:FcγR contact interfaces. (A)** Cartoon representation of the crystal structure of the $hIgG_1$ Fc complex with hFcγRIII (PDB ID: 1E4K). FcγRIII is shown in green, and both chains of the Fc in pale blue. Fc contact surfaces are colored: lower hinge (orange), B/C loop (blue), C'/E loop (red), and F/G loop (purple). Fc glycosylation is shown in yellow. **(B)** Residues randomized in the Fc loop libraries used in the screen. Dark black bars represent four amino acid stretches that were completely randomized.

**Figure 4.2**

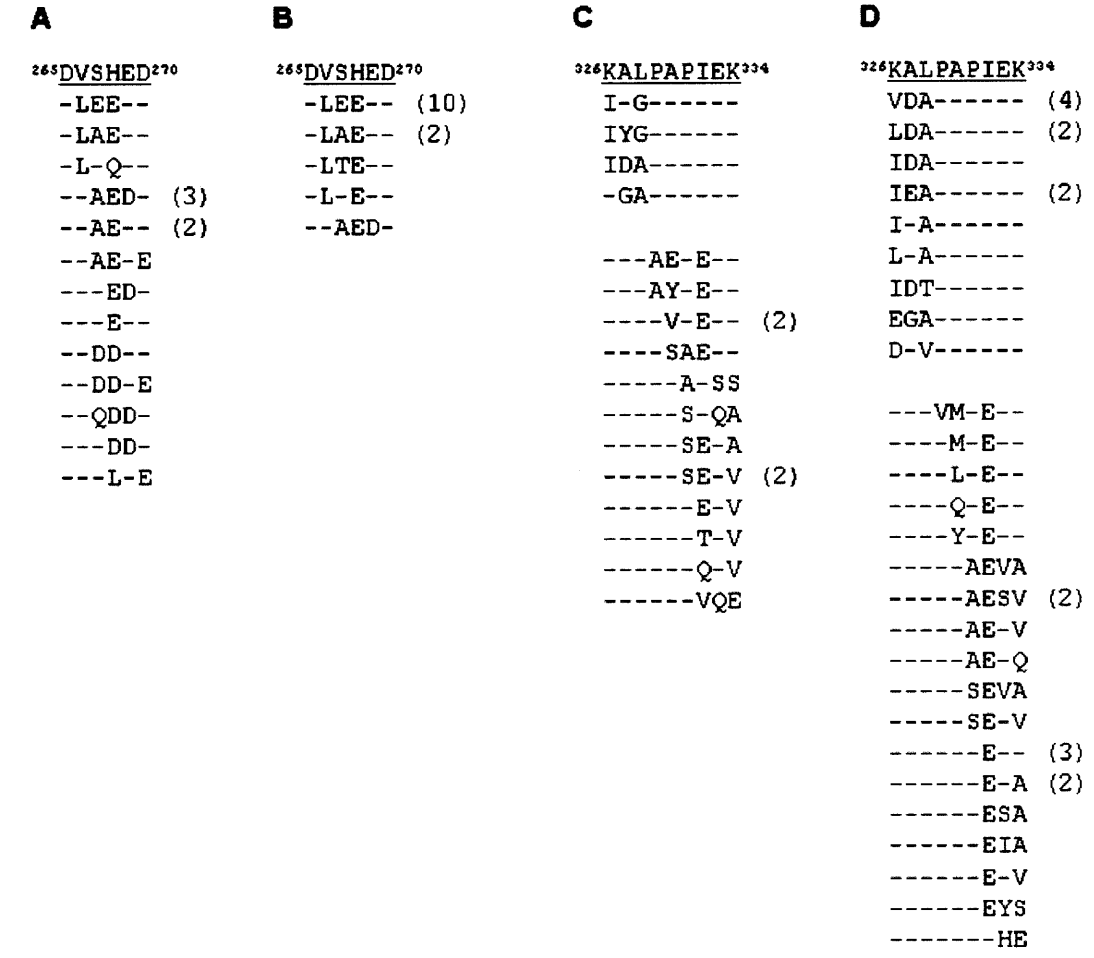


**Sequences of B/C and F/G loop variants enriched from the FcγRIIIA$^{176F}$ binding screen.** Sequences of B/C loop clones enriched after the fourth **(A)** and fifth **(B)** rounds of screening. Sequences of F/G loop clones enriched after the fourth **(C)** and fifth **(D)** rounds of screening. Dashes represent the same residue as the wild-type sequence. Numbers in parentheses represent the number of times a particular clone was present in the population sequenced.

**Figure 4.3**

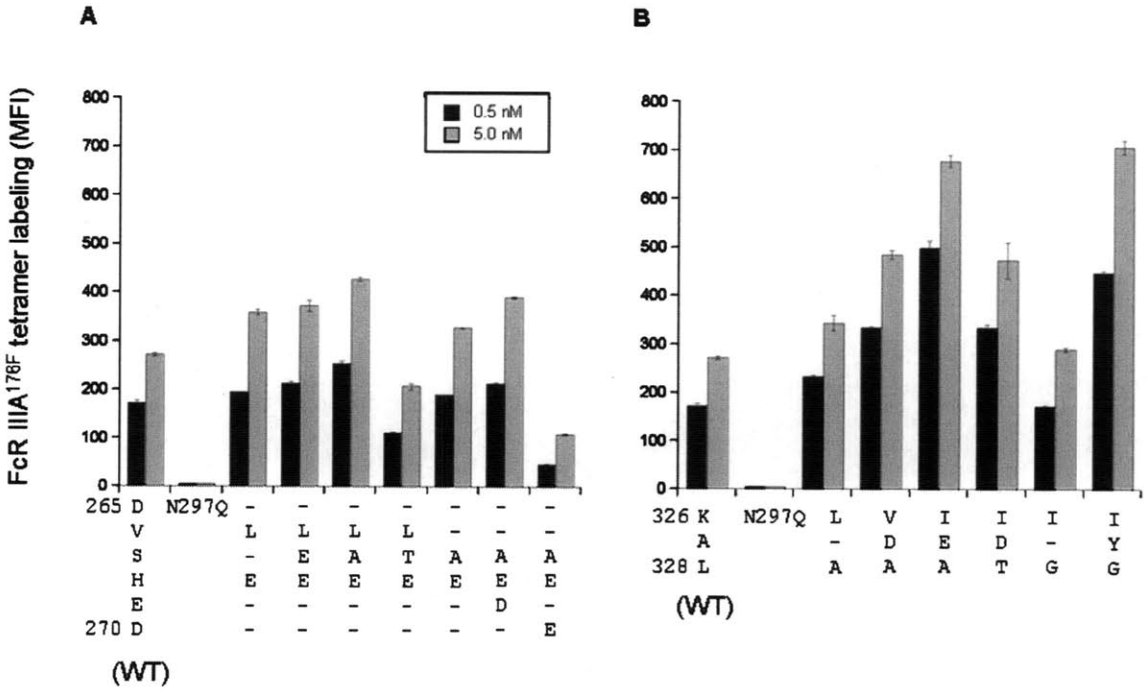


**Relative binding of clones enriched from screen.** B/C loop **(A)** and F/G loop **(B)** 4m5.3 Fc variants enriched for improved FcγRIIIA$^{176F}$ binding from the yeast-based screen were expressed from HEK cells and assayed for relative binding to FcγRIIIA$^{176F}$ compared to wild-type (WT). Fluorescein-labeled yeast were incubated with cell culture supernatants, then labeled with either 0.5 nM or 5.0 nM of streptavidin Alexa 647 FcγR tetramer, and then cells analyzed by flow cytometry. Data represent the average of two trials, normalized by the relative IgG surface loading of a given variant compared to wild-type, as determined by a separate Protein A 647 loading control. Dashes represent the same residue as the wild-type sequence.

**Figure 4.4**

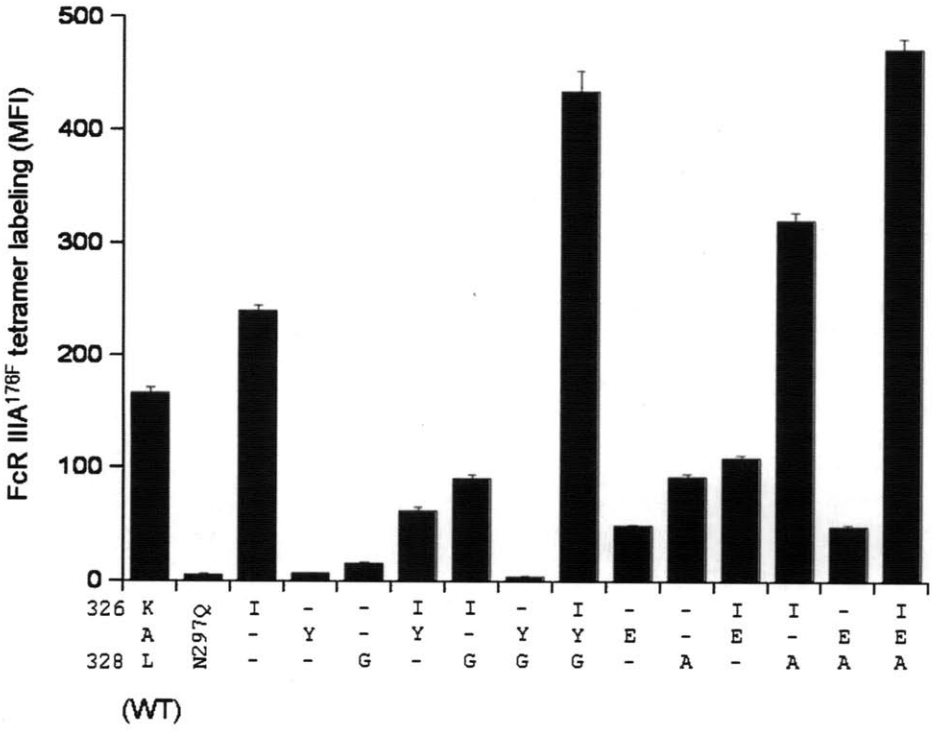


**Mutational analysis of IYG and IEA variants.** 4m5.3 Fc variants, comprising the ensemble of mutations present in the K326I/A327Y/L328G (IYG) and K326I/A327E/L328A (IEA) variants were assayed for binding to FcγRIIIA$^{176F}$. Fluorescein-labeled yeast were incubated with cell culture supernatants, labeled with 5 nM of streptavidin Alexa 647 FcγR tetramer, and then cells analyzed by flow cytometry. Data represent the average of two trials, normalized by the relative IgG surface loading of a given variant compared to wild-type (WT), as determined by a separate Protein A 647 loading control. Dashes represent the same residue as the wild-type sequence.

**Figure 4.5**

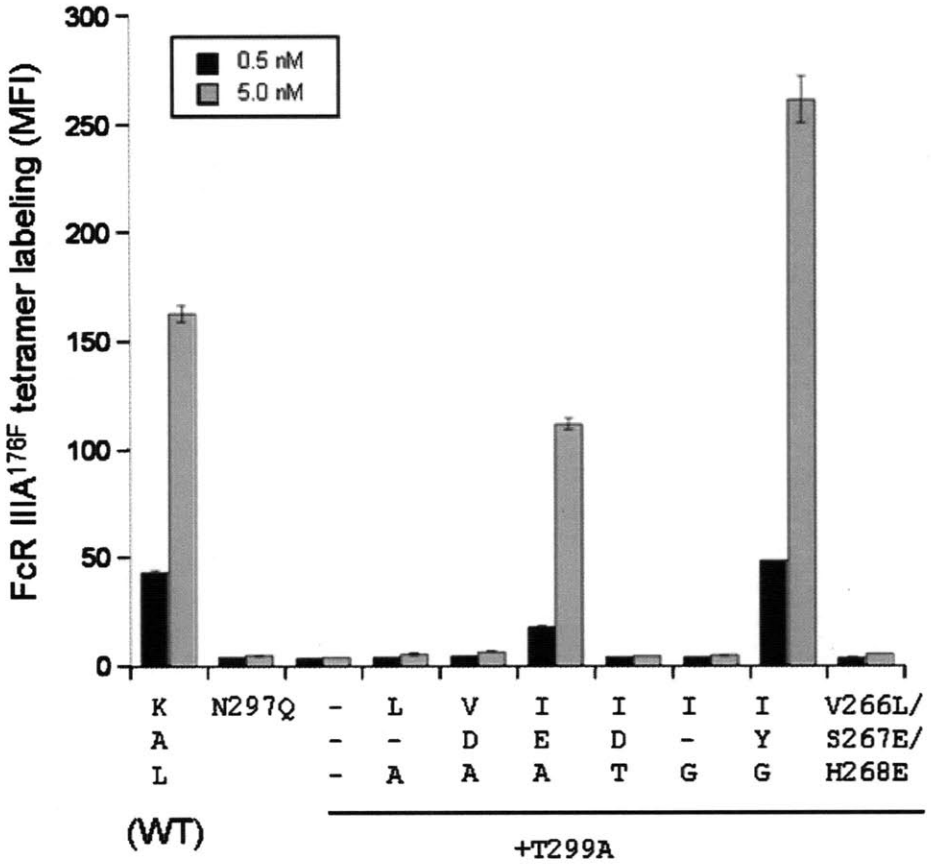


**FcγRIIIA binding of aglycosylated F/G loop variants.** Aglycosylated variants of the F/G loop clones enriched for improved FcγRIIIA$^{176F}$ binding, described in Figure 4.3, as well as the most frequently enriched B/C loop clone (V266L/S267E/H268E), were assayed for binding to FcγRIIIA$^{176F}$. The T299A mutation, which confers weak aglycosylated binding to FcγRIIIA$^{176V}$, was introduced into all clones. Fluorescein-labeled yeast were incubated with cell culture supernatants, labeled with either 0.5 nM or 5.0 nM of streptavidin Alexa 647 FcγR tetramer, and then cells analyzed by flow cytometry. Data represent the average of two trials, normalized by the relative IgG surface loading of a given variant compared to wild-type, as determined by a separate Protein A 647 loading control. Dashes represent the same residue as the wild-type sequence.

**Figure 4.6**

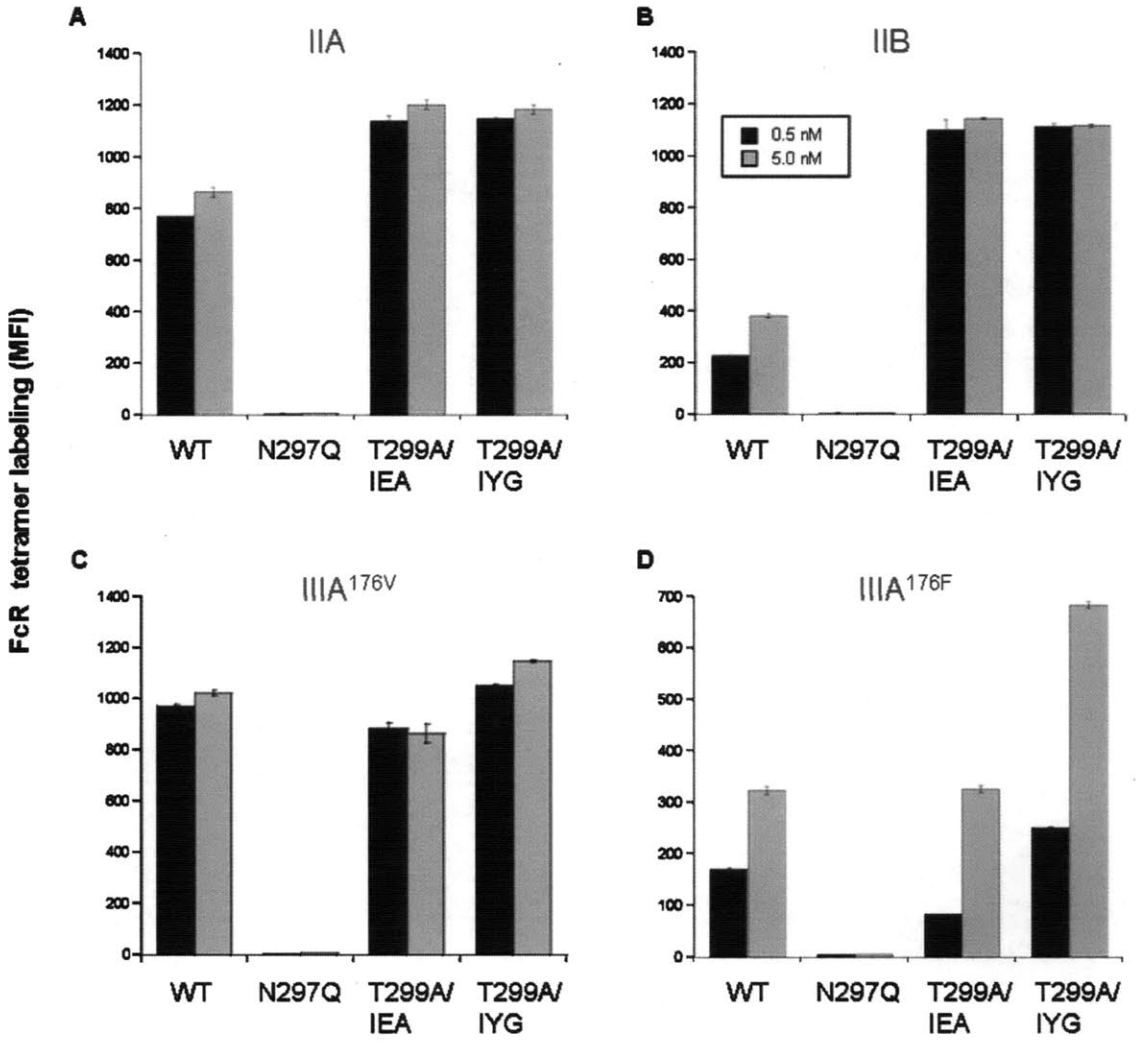


**FcγR binding of T299A/IEA and T299A/IYG variants.** T299A/IEA and T299A/IYG were assayed for relative binding to the panel of human FcγRs: **(A)** FcγRIIA$^{131R}$, **(B)** FcγRIIB, **(C)** FcγRIIIA$^{176V}$, and **(D)** FcγRIIIA$^{176F}$. Fluorescein-labeled yeast were incubated with cell culture supernatants, labeled with either 0.5 nM or 5.0 nM of streptavidin Alexa 647 FcγR tetramer, and then cells analyzed by flow cytometry. Data represent the average of two trials, normalized by the relative IgG surface loading of a given variant compared to wild-type, as determined by a separate Protein A 647 loading control.

**Figure 4.7 (a, b)**

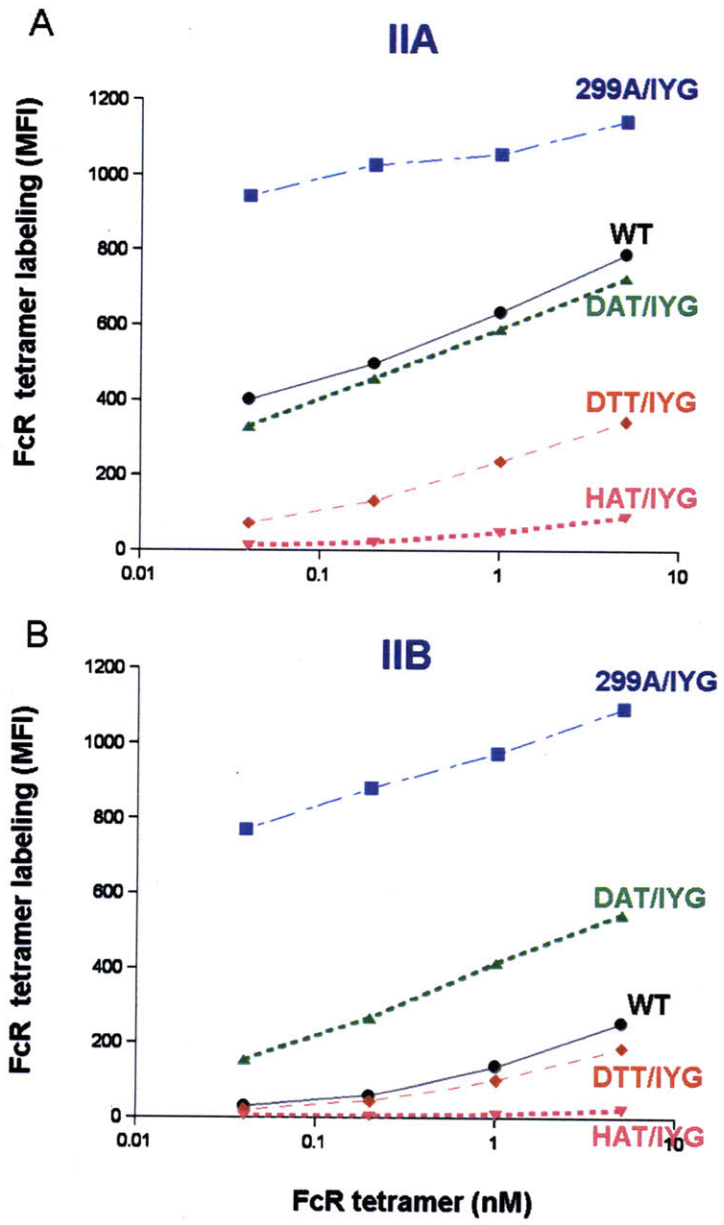
A
IIA
299A/IYG
WT
DAT/IYG
DTT/IYG
HAT/IYG
FcR tetramer labeling (MFI)
1200
1000
800
600
400
200
0
0.01
0.1
1
10
B
IIB
299A/IYG
DAT/IYG
WT
DTT/IYG
HAT/IYG
FcR tetramer labeling (MFI)
FcR tetramer (nM)

**Figure 4.7 (c, d)**

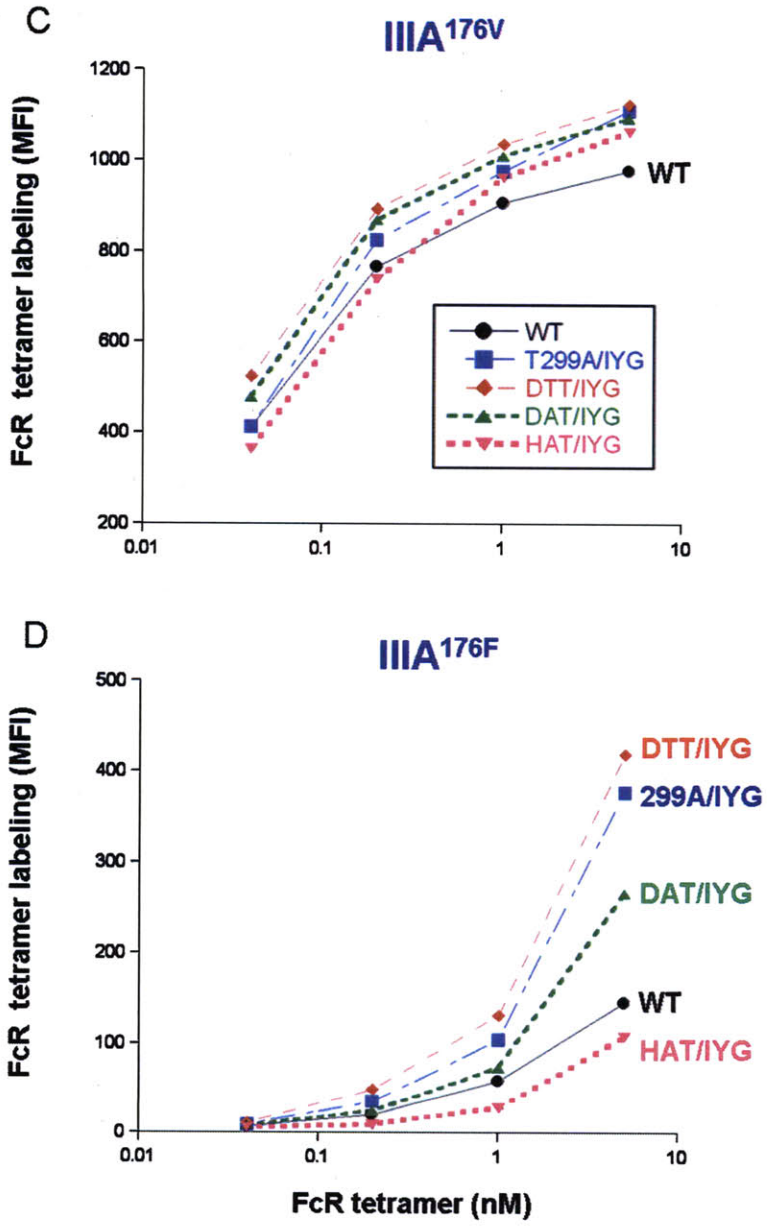


**FcγR binding of aglycosylated IYG variants.** T299A/K326I/A327Y/L328G (T299A/IYG), N297D/S298T/K326I/A327Y/L328G (DTT/IYG), N297D/S298A/K326I/A327Y/L328G (DAT/IYG), and N297H/S298A/K326I/A327Y/L328G (HAT/IYG) were assayed for relative binding to the panel of human FcγRs: **(A)** FcγRIIA$^{131R}$, **(B)** FcγRIIB, **(C)** FcγRIIIA$^{176V}$, and **(D)** FcγRIIIA$^{176F}$. Fluorescein-labeled yeast were incubated with 20 μg/ml purified IgG, labeled with streptavidin Alexa 647 FcγR tetramers at a range of concentrations, and then cells analyzed by flow cytometry. Data represent the average of two trials; MFI = median fluorescence intensity. Similar IgG surface loading of a given variant compared to wild-type was confirmed by a separate Protein A 647 loading control.

# Chapter 5. Engineering Fc variants with specificity for FcγRIIIA

## Introduction

The activation of immune effector functions, in particular through the engagement of cellular Fcγ receptors (FcγRs), is a critical mechanism in the efficacy of several therapeutic antibodies (5). In immunity, antibodies act as a bridge between a pathogen and immune effector cells, simultaneously binding antigen through their variable regions, while activating immune cells through interaction of their conserved Fc domains with the FcγRs of immune cells. This process, termed antibody-dependent cellular cytotoxicity (ADCC), leads to phagocytosis of the bound pathogen and release of inflammatory mediators (5), and in therapeutic antibodies directed against tumor-specific antigens, can lead to immune cell mediated killing of antibody-bound tumor cells.

The human FcγR (hFcγR) family consists of the activating receptors FcγRI, FcγRIIA, and FcγRIIIA, and the inhibitory receptor FcγRIIB. While FcγRI binds IgG with high affinity (nanomolar binding constants), FcγRIIA, FcγRIIB, and FcγRIIIA bind IgG with micromolar affinity, becoming activated only via avid multivalent interactions with opsonized antigen. Several studies point to the importance of the low affinity FcγRs in therapeutic efficacy (5) and have suggested ways in which modulating the properties of the IgG Fc and its interaction with FcγR may enhance therapeutic response (17).

Enhanced ADCC has been observed in mice lacking the lone inhibitory receptor FcγRIIB (11), and additional murine models suggest that the ratio of the binding affinity of a therapeutic IgG for an activating receptor compared to that of the inhibitory receptor (the activating to inhibitory, or A/I ratio) is predictive of therapeutic outcome (12). Other studies, including clinical data, point to the importance of allelic variation within human FcγRIIIA in therapeutic outcome (13-16). Populations homozygous for a valine at position 176 of FcγRIIIA (FcγRIIIA$^{176V}$), as opposed to a phenylalanine (FcγRIIIA$^{176F}$), have dramatically improved response rates, likely due to a several-fold stronger binding affinity of wild-type hIgG$_1$ for the FcγRIIIA$^{176V}$ allele.

Such observations have led to the development of Fc variants with improved, and more specific binding to FcγRIIIA, either through engineering the glycan attached to asparagine 297 (N297) of the Fc (9, 18, 19, 85), or through modifying the characteristics of the Fc polypeptide itself (20-22). The three most well characterized polypeptide variants, S239D/A330L/I332E (20), F243L/R292P/Y300L/V305I/P396L (22), and S298A/E333A/K334A (21), achieve improved FcγRIIIA binding with a range of FcγRIIB affinities. S239D/A330L/I332E confers an ~ 100-fold increase in FcγRIIIA binding as well as increased FcγRIIB binding; F243L/R292P/Y300L/V305I/P396L has an ~ 10-fold increase in FcγRIIIA binding and approximately wild-type FcγRIIB binding; and S298A/E333A/K334A has increased binding affinity for FcγRIIIA and dramatically reduced affinity for FcγRIIB. These Fc variants have been shown to have dramatically enhanced ADCC in *in vitro* models, as well as reduced tumor progression in xenograft models. Interestingly, a recent study using cell based assays showed a correlation between immune cell activation and binding affinity to activating receptors, but little correlation with FcγRIIB binding (23), raising the question of whether enhanced therapeutic outcome can be achieved by optimizing the activating receptor binding properties alone, or whether binding to the inhibitory receptor, FcγRIIB, also plays a role in therapeutic outcome.

In the present study, we have sought to, in a comprehensive manner, expand the window of specificity for the activating FcγRIIIA over the inhibitory FcγRIIB that can be engineered into the human $IgG_1$ Fc domain. Here, we have focused on screening for variants with enhanced $Fc\gamma RIIIA^{176F}$ binding but dramatically reduced FcγRIIB binding, simultaneously improving binding to the less-responsive low-affinity FcγRIIIA allele population while eliminating or reducing the inhibitory component to immune cell activation. We describe a screen that samples amino acid diversity at the loops of the Fc that make contact with FcγR, asking what combinations of mutations at these sites impart specificity in an experimentally much more comprehensive manner than previously reported. Our screen returns previously identified mutations within these loops that impart specificity, as well as additional mutations flanking these residues, not previously reported, that enhance specificity.

## Results

**Engineering approach and screening methodology**. Recently, our group developed and characterized a method for the improved enrichment (or depletion) of extremely weak binding proteins from yeast-display libraries using the avidity enhancement of antigen-coated magnetic beads (Margaret Ackerman, *manuscript submitted*). Depletion of binders from yeast-display libraries can be efficiently accomplished through successive rounds of incubation of libraries with target antigen-coated beads without library re-amplification, increasing the likelihood of eliminating binders from the population with each pass. This methodology is similar to the one described by Stavenhagen and coworkers to engineer Fc specificity with yeast display libraries (22), but as discussed later, has some key differences that likely improve specificity screening.

To screen for receptor specificity, we set out to systematically ask what combinations of mutations at Fc contact loops yield FcγRIIIA-specific binding, experimentally exploring the sequence space at these interaction sites in a vastly more comprehensive manner than previous approaches, which have included alanine scanning point mutagenesis (21), screening random mutagenesis libraries of the entire Fc region (22), and *in silico* prediction and validation of variants (20). While mutations distant from Fc:FcγR contact interfaces have been shown to impart specificity (21, 22), likely through conformational changes in the Fc, we reasoned that focusing on sampling amino acid diversity within the loops of the Fc in direct contact with FcγRs would have the greatest impact on specificity.

Here, we constructed saturation libraries about three contact sites within the Fc – the lower hinge, the B/C loop, and F/G loop (**Figure 4.1**) – and screened them by displaying these full-length $hIgG_1$ variants on the surface of yeast. In this display system, the femtomolar affinity scFv 4m5.3 (38) has been reformatted as a $hIgG_1$, allowing 4m5.3 $hIgG_1$ Fc library variants to be captured on fluorescein-labeled yeast from which they are secreted (**Figure 3.2**) by adapting features of a cell surface secretion capture assay (34) and the improved secretion of full-length $hIgG_1$ from *S. cerevisiae* (Chapter 2). Contact interface libraries were constructed by fully-randomizing four amino acid stretches using degenerate NNK codons (N=ATCG, K=GT), which encode all 20 possible amino acids

in 32 codons. This design approach allows for over-sampling the codon diversity ($32^4$ ~ $1x10^6$), and thus amino acid diversity, in these yeast-based libraries, which often have a transformation efficiency on the order of $1x10^7$. The following libraries were constructed and pooled by contact region: lower hinge (234-237, 236-239), B/C loop (265-268, 267-270), and F/G loop (326-329, 327-330, 329-332, 331-334).

Yeast capture libraries were depleted multiple times in succession on FcγRIIB coated magnetic beads, then screened for binding to the FcγRIIIA$^{176F}$ allele, initially on receptor-coated magnetic beads, and during later rounds of screening, at increasing stringency by fluorescent activated cell sorting (FACS). Given its weaker binding for wild-type Fc, FcγRIIIA$^{176F}$ likely represents a more stringent, as well as therapeutically relevant, barrier for improved FcγRIIIA binding.

**Variants enriched for FcγRIIIA$^{176F}$ specific binding.** All variants enriched for FcγRIIIA specific binding from the B/C loop libraries originated from the 267-270 sublibrary, suggesting that this region of the loop dominates specificity (**Figure 5.1a,b**). Among the clones isolated, there is an absolute preference for substitution at D270, predominately to Glu, consistent with previous studies that have shown that the D270E variant slightly strengthens binding to FcγRIIIA$^{176F}$ while reducing binding to FcγRIIB (21, 22). In addition, H268 is altered in virtually all clones, with a slight preference for the acidic residues Asp and Glu, although multiple substitutions are present, with Met and Thr also occurring at this position multiple times. The most abundant residue present at position 269 is Asp, with the similarly negatively charged wild-type Glu also appearing multiple times. Position 267 displays the least variation among the clones enriched from the screen, with a strong preference for the wild-type Ser, or in some variants, Asp.

Similarly, all variants enriched for FcγRIIIA-specific binding from the pooled F/G loop libraries are derived from the 329-332 sublibrary, suggesting that this region of the loop dominates specificity (**Figure 5.1c,d**). Enriched variants display a strong consensus motif, containing P329A, A330L/V/I/E, and I332E/D, with a strong preference for I332E. I332E alone has been shown to increase binding to all FcγRs (20), and A330L, when placed in the S239D/I332E background, improves receptor specificity, slightly strengthening FcγRIIIA binding while weakening FcγRIIB binding (20). A330V alone

has been shown to confer FcγRIIIA-specific binding (22); P329A alone greatly reduces binding to all FcγRs (21).

**Characterization of FcγRIIIA$^{176F}$-specific loop variants.** To characterize the variants enriched from our yeast-based screen, we cloned pools of clones into mammalian expression vectors, sequenced to confirm clone identity, and expressed individual IgG variants from HEK 293 cells. Cell culture supernatants were loaded onto fluorescein-labeled yeast, then variants analyzed for their ability to bind fluorescently labeled FcγR-streptavidin tetramers, and data normalized by relative surface IgG loading. All variants analyzed in this assay display substantial improvements in FcγRIIIA$^{176F}$ binding specificity, although the degree of specificity varies across the clones analyzed (**Figure 5.2**). The F/G loop variants, all highly similar in sequence, have dramatic increases in FcγRIIIA$^{176F}$ binding and large reductions in FcγRIIB binding, with one clone, P329A/A330E/I332E (AE*E) displaying undetectable FcγRIIB binding at the concentration of receptor used in the screening assay (**Figure 5.2b**). Scanning across the F/G loop variants, it appears that the presence of Glu at 332 as opposed to Asp imparts improved FcγRIIIA$^{176F}$ binding in the P329A/A330L background, and that the hydrophobic residues Leu and Val impart similar binding properties in the P329A/I332E background, while an Ile at this position reduces binding affinity.

Substantial variation, in both sequence and binding properties, exists in the B/C loop clones analyzed (**Figure 5.2a**). A subset of clones achieve specificity by virtually eliminating (at the concentration tested) FcγRIIB binding, while maintaining FcγRIIIA$^{176F}$ binding at near wild-type, or even reduced, levels. Another subset reduces, although does not ablate, FcγRIIB binding, yet realizes improvements in specificity through additional increases in FcγRIIIA$^{176F}$ binding. Among the clones analyzed, some observations can be made about the role of individual mutations within the context of other mutations within a variant. Within the S267D/D270S background, the presence of Asp at position 267, as compared to Met, substantially increases binding to both FcγRs; similarly, within the H268E/E269D background, the presence of a Glu at position 268, as opposed to Met, also substantially increases binding to both FcγRs. Within the H268E/E269D background, the presence of Glu at position 270, as opposed to Gln,

imparts increased binding affinity to both receptors. Finally, within the H268T/D270E background, an Asp at position 269, as opposed to the wild-type Glu, allows for greatly improved FcγRIIIA$^{176F}$ binding without a detectible increase in FcγRIIB binding.

**Effect of P329A in F/G loop clones.** To understand the contribution of individual mutations from the most interesting variants identified from our screen, we constructed point mutants and assayed them for receptor binding. The F/G loop variant A330L/I332E has been previously identified and characterized, as part of a triple mutant S239D/A330L/I332E, and we sought to understand the contribution of the P329A mutation that was universally enriched from our screen (**Figures 5.1c,d**). Compared to A330L/I332E, P329A/A330L/I332E appears to yield a slight decrease in FcγRIIIA$^{176F}$ binding, yet weakens FcγRIIB binding to a greater extent (**Figure 5.3**). Similar to the results from the initial screen using cell culture supernatants (**Figure 5.2b**), the presence of Glu at position 330 in the variant P329A/A330E/I332E, compared to Leu in P329A/A330L/I332E, significantly weakens binding to all FcγRs, yielding a variant with virtually no FcγRIIB and FcγRIIA binding, and strengthened (compared to wild-type Fc) binding to FcγRIIIA$^{176F}$. The F/G loop only variants have weakened binding to all FcγRs compared to the previously described S239D/A330L/I332E. In this assay, the S239D mutation, in the context of A330L/I332E, strengthens binding to all FcγRs, albeit appears to enhance binding to FcγRIIB and FcγRIIA$^{131R}$ to a greater extent than to FcγRIIIA$^{176F}$. Overall, the variant enriched from the screen, P329A/A330L/I332E, appears to have weakened FcγRIIIA$^{176F}$ binding compared to S239D/A330L/I332E, yet dramatically reduced FcγRIIB binding.

**Mutational analysis of the B/C loop clone H268T/E269D/D270E.** To understand the contribution of individual mutations in the triple mutant H268T/E269D/D270E (TDE), the most promising B/C loop variant from the initial screen (**Figure 5.2a**), we compared the relative receptor binding of the previously identified variant D270E, which has been shown to confer FcγRIIIA specific binding, to H268T/E269D/D270E and the double mutants H268T/D270E and E269D/D270E (**Figure 5.3**). Similar to previous reports, D270E alone slightly increases FcγRIIIA$^{176F}$ binding while greatly reduces FcγRIIB

binding. Placing H268T in the D270E background reduces binding to FcγRIIIA$^{176F}$, similar to that of wild-type Fc, which is consistent with the data from the initial screen using cell culture supernatants (**Figure 5.2a**). In contrast, placing E269D in the D270E background results in a double mutant with strengthened FcγRIIIA$^{176F}$ binding compared to D270E alone, and with similar, barely detectible binding to FcγRIIB. E269D/D270E binds FcγRIIIA$^{176F}$ to a greater extent than H268T/E269D/D270E, further suggesting that H268T has a deleterious effect on receptor binding. Interestingly, E269D/D270E was among the myriad clones enriched from the yeast-based screen (**Figure 5.1a**), suggesting that further screening of HEK-expressed variants from the enriched population would have uncovered this variant, as well as potentially additional variants with desirable FcγR binding properties.

**Effect of loop grafting on receptor binding properties**. Since the initial library screen for receptor specificity only looked at Fc variants with diversity in four amino acid stretches, which were confined to individual loops at the Fc:FcγR contact interface, we sought to improve the properties of the variant Fcs by grafting B/C and F/G loops from enriched variants into a single Fc (**Figure 5.4**). We reasoned that since the Fc homodimer binds the monomeric FcγR asymmetrically (6, 7) – with the F/G loop from one chain of the Fc making extensive contacts with FcγR and the B/C loop from the other chain of the Fc making extensive contacts – the binding properties of such loop grafted variants would be additive. Both H268T/E269D/D270E/P329A/A330L/I332E (TDE/AL*E) and H268T/E269D/D270E/P329A/A330E/I332E (TDE/AE*E) have slightly strengthened binding to FcγRIIIA$^{176F}$ compared to the F/G loop only variants P329A/A330L/I332E (AL*E) and P329A/A330E/I332E (AE*E), consistent with the B/C loop variant H268T/E269D/D270E (TDE) imparting slightly improved binding to FcγRIIIA$^{176F}$ compared to wild-type Fc (**Figure 5.4a**). Interestingly, the presence of the mutant B/C loop dramatically reduces binding to FcγRIIB (**Figure 5.4b**), as TDE/AE*E appears to have completely ablated FcγRIIB binding and TDE/AL*E substantially reduced FcγRIIB binding.

**Comparison of engineered variants to published variants.** As a final test of our engineering approach, we sought to compare the B/C and F/G loop-grafted variants to the previously reported variants mentioned above: S298A/E333A/K334A, engineered by a group at Genentech using alanine scanning mutagenesis (21); S239D/A330L/I332E, engineered by a group at Xencor using *in silico* prediction and screening (20); and F243L/R292P/Y300L/V305I/P396L, engineered by a group at Macrogenics using yeast display libraries of randomly mutated Fc domains (22). These variants display a range of affinities and specificities in our assay (**Figure 5.5**), and the relative data correlate well with previously reported affinities and specificities (20-22): S298A/E333A/K334A has been reported to increase binding affinity to FcγRIIIA$^{176F}$ while nearly abrogating binding to FcγRIIB; S239D/A330L/I332E to greatly enhance binding to both receptors; and F243L/R292P/Y300L/V305I/P396L to greatly strengthen binding affinity to FcγRIIIA$^{176F}$ while maintaining FcγRIIB binding at near wild-type levels.

As a comparison, we chose the loop grafted variants TDE/AL*E and TDE/AE*E, as well as the variants, E269D/D270E/P329A/A330L/I332E (*DE/AL*E) and E269D/D270E/P329A/A330E/I332E (*DE/AE*E), in which position 268 is maintained as the wild type His, motivated by the slight improvement in FcγRIIIA$^{176F}$ binding for E269D/D270E compared to H268T/E269D/D270E (**Figure 5.3a**). The pairs TDE/AL*E and *DE/AL*E, and TDE/AE*E and *DE/AE*E, display similar binding curves to all receptors (**Figure 5.5**), suggesting that the H268T mutation – in the context of the loop grafted variants – has little effect on receptor binding properties. The properties of the loop grafted variants are most similar to S298A/E333A/K334A, achieving strengthened FcγRIIIA$^{176F}$ binding with similar, near abrogated FcγRIIB binding (**Figures 5.5, 5.6**). TDE/AL*E and *DE/AL*E appear to bind FcγRIIIA$^{176F}$ at levels intermediate that of F243L/R292P/Y300L/V305I/P396L and S239D/A330L/I332E, suggesting an approximately 10-fold to 100-fold improvement in binding affinity to this allele; 10-fold and 100-fold enhancements have been previously measured for these variants by SPR (20, 22). Variants with a Glu at position 330 (TDE/AE*E and *DE/AE*E) have smaller increases in FcγRIIIA$^{176F}$ binding – similar, if not strengthened compared to S298A/E333A/K334A – with undetectable binding to FcγRIIB in this assay.

## Discussion

Previous approaches to engineering improved binding affinity and specificity within the IgG Fc domain for FcγR have varied widely in their methodology, throughput, and exploration of Fc sequence space. In an initial analysis to understand the contribution of individual Fc positions to receptor binding, Shields and coworkers constructed a comprehensive set of surface exposed alanine point mutants within the human $IgG_1$ Fc and individually assayed each variant for relative FcγR binding, then combined mutations identified by their alanine scanning mutagenesis to construct variants with enhanced properties (21). More recently, Lazar and coworkers used computational modeling of Fc:FcγR interactions to screen variants *in silico*, then experimentally validate candidate mutations, individually and in combination (20). Also more recently, Stavenhagen and coworkers used a directed evolution approach, screening randomly mutated yeast-display Fc libraries for improved binding to FcγRIIIA, as well as for loss of FcγRIIB binding followed by enrichment for FcγRIIIA binding (22), then similarly analyzed consensus mutations from enriched clones, individually and in combination, to generate variants with defined properties.

The approach we describe here is similar to the one employed by Stavenhagen et al, yet with modifications in display system design, and importantly, in library construction and screening methodology. Similar to Stavenhagen et al, we chose to use a directed evolution approach to experimentally screen large collections of variants, taking advantage of the eukaryotic protein processing of *S. cerevisiae* to display Fc variants on the surface of yeast. In our system, we have chosen to present the Fc in the context of the fully-assembled human $IgG_1$ using a cell surface secretion capture assay (34). In addition, we chose to build upon this approach by: 1) focusing on better sampling the sequence space about the Fc:FcγR contact loops, which we would predict would have the largest impact upon binding specificity, and before this study had not been comprehensively addressed, and 2) employing an improved methodology for screening for binding specificity from yeast-displayed libraries, based upon recent work from our group (Margaret Ackerman, *manuscript submitted*).

While sites distant from the contact interface have been shown to have effects upon binding affinity and specificity (21, 22), we hypothesized that a large component of the binding properties of the Fc domains could be modulated by focusing directly on the loops of the Fc that make contact with FcγR. While variants within these loops have been previously identified through all of the approaches outlined above, we hypothesized that we could uncover additional mutations missed by these previous screening approaches by a more thorough examination of sequence space, completely sampling all combinations of mutations within these loops in four amino acid stretches.

We also use a stringent screening approach for finding variants with dramatic losses in binding to the inhibitory FcγR, FcγRIIB. As in (22), we use the avidity enhancement of magnetic beads to remove FcγRIIB-binding clones from the library, yet rather than re-amplifying the library before performing positive enrichment for FcγRIIIA binding clones in a second round of screening, we subject the depleted population to additional rounds of depletion on FcγRIIB-coated magnetic beads, then an ultimate positive selection for FcγRIIIA binding, before re-amplifying the sublibrary. Our data have shown absorption of yeast-displayed binding clones in a model system on magnetic beads to be approximately 80% efficient, with successive rounds of depletion before re-amplification pushing the efficiency of absorbing binding clones to > 95%.

The variants enriched from our screen from both the B/C loop and F/G loop libraries are similar to those previously identified, although contain elements that allow for enhanced receptor specificity, in particular through reduced FcγRIIB binding, consistent with our screening approach. In particular, all of the clones enriched from the B/C loop libraries contain substitutions as D270, which has previously been identified as modulating FcγR specificity (21, 22). Our approach reveals a flanking mutation, E269D, that when placed in the D270E background, enhances FcγRIIIA$^{176F}$ binding while maintaining greatly reduced FcγRIIB binding. Within the F/G loop, there is a clear consensus for variants with substitutions at positions 330 and 332 (to Glu), a background that has been previously identified by *in silico* screening (20). Our screen also results in an absolute preference for variants with the flanking mutation P329A, which reduces FcγRIIB binding, with a slight decrease in FcγRIIIA$^{176F}$ binding. In addition, our approach also identifies variants with diversity at position 330, in particular

P329A/A330E/I332E, which, while improving FcγRIIIA$^{176F}$ binding, has undetectable FcγRIIB binding.

Having identified loop variants with desired properties from our screen, we also demonstrate modularity in the engineering of Fc domain variants with desired properties by combining mutant B/C and F/G loops. Grafting in the most specific B/C loop (H268T/E269D/D270E) into two of the most specific F/G loops (P329A/A330L/I332E and P329A/A330E/I332E) yield combined variants with additive properties – enhanced FcγRIIIA$^{176F}$ binding and decreased FcγRIIB binding. These combined variants have A/I ratios that rival if not exceed those of previously reported variants and display virtually no binding to the inhibitory receptor, and thus should prove valuable tools for parsing out the contributions of individual FcγRs to therapeutic response, as well as in the design of therapeutic antibodies with optimal FcγR binding properties.

## Materials and Methods

**Loop saturation mutagenesis library construction.** See Chapter 4, Materials & Methods.

**Oligonucleotides.** See Chapter 4, Materials & Methods.

**Library screening.** Library screening was performed using the cell surface secretion assay (CeSSA) (34). Briefly, pooled loop libraries were grown in SD-CAA (2% glucose, 0.67% yeast nitrogen base, 0.54% $Na_2HPO_4$, 0.86% $NaH_2PO_4 \cdot H_2O$, 0.5% casein amino acids) to an $OD_{600}$ of ~ 5, and then induced in YPG (2% galactose, 2% peptone, 1% yeast extract, 0.54% $Na_2HPO_4$, 0.86% $NaH_2PO_4 \cdot H_2O$) for 12 hrs at 20 °C. Following this pre-induction phase, yeast were labeled with fluorescein-PEG-NHS (Laysan Bio) and re-induced in YPG containing 15% PEG (w/v) at 20 °C for 36 hrs. Cells were then washed with PBS containing 0.1% (w/v) BSA (PBS/BSA).

For the first two rounds of screening, pooled libraries were subjected to multiple, successive depletion steps for FcγRIIB binding followed by positive enrichment for FcγRIIIA$^{176F}$ binding on magnetic beads. Depletion was carried out by incubating pooled libraries with biotinylated hFcγRIIB preloaded onto streptavidin magnetic beads (Invitrogen) for 2 h at 4 °C with rotation, followed by magnetic separation, removal of unbound yeast, and subsequent further incubation of the depleted population again with FcγRIIB-coated magnetic beads, for a total of four successive depletions. Following the final depletion step, positive enrichment for binding to hFcγRIIIA$^{176F}$ was performed by incubating the unbound yeast population with FcγRIIIA$^{176F}$ coated magnetic beads, magnetic separation, washing with PBS/BSA, and elution and propagation of captured clones by growth of captured magnetic beads in SD-CAA supplemented with penicillin/streptomycin at 30 °C. Starting with the third round of screening, following successive depletion, yeast were labeled with biotinylated hFcγRIIIA$^{176F}$ preloaded onto streptavidin-Alexa 647 (Invitrogen). The subpopulations were sorted on either a BD FACSAria (Becton Dickinson) or a MoFlo Cell Sorter (Cytomation Inc) and collected cells grown in SD-CAA supplemented with penicillin/streptomycin (Invitrogen), for three

additional rounds of screening (five rounds in total). Library populations were labeled for FACS sorting at increasingly stringent concentrations of FcγRIIIA$^{176F}$ tetramer as follows: round four (800 pM), round five (200 pM).

**Cloning and Site Directed Mutagenesis.** See Chapter 4, Materials & Methods.

**Characterization of HEK-secreted Fc mutants.** Unless otherwise noted, Fc variants were transiently transfected into HEK 293F cells (Invitrogen) in a 6-well plate format. Cell culture supernatants were loaded onto fluorescein-conjugated yeast overnight at 4 °C; yeast were then washed with PBS/BSA, labeled with biotinylated FcγR preloaded onto streptavidin-Alexa 647 at 4 °C for > 2 hrs, and analyzed by flow cytometry. Labeling with 10 μg/ml Protein A-Alexa 647 (Invitrogen) was performed as a separate IgG loading control for all samples. FcγR labeling fluorescence for individual variants was normalized by the surface IgG loading of a variant relative to that of wild-type IgG, as determined by relative Protein A-Alexa 647 labeling. There was strong agreement (within 10% difference) between this approach to signal normalization and gating on a population of cells to give similar surface loading signals.

**Antibodies and recombinant proteins.** See Chapter 4, Materials & Methods.

**Acknowledgements**

Rene Ott, for providing biotinylated FcγRs; Margie Ackerman, for helpful discussions and suggestions about magnetic bead sorting; Ben Hackel, for helpful discussions and suggestions about saturation library creation; and the MIT Biopolymers and Flow Cytometry Core Facilities.

**Figure 5.1**

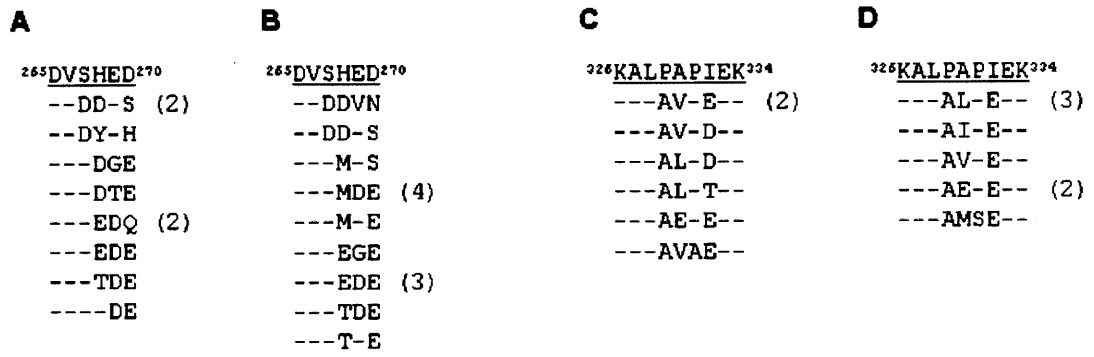


**Sequences of B/C and F/G loop variants enriched for FcγRIIIA$^{176F}$ specific-binding.** Sequences of B/C loop clones enriched after the fourth **(A)** and more stringent fifth **(B)** rounds of screening. Sequences of F/G loop clones enriched after the fourth **(C)** and more stringent fifth **(D)** rounds of screening. Dashes represent the same residue as the wild-type sequence. Numbers in parentheses represent the number of times a particular clone was present in the population sequenced.

**Figure 5.2**

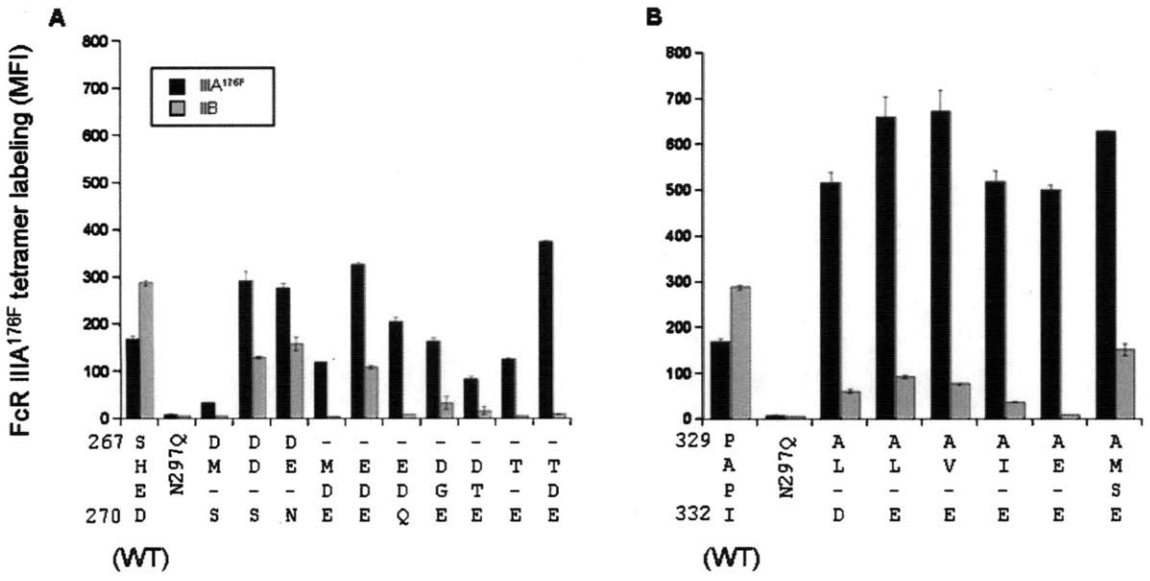


**Relative binding of clones enriched from screen.** B/C loop **(A)** and F/G loop **(B)** 4m5.3 Fc variants enriched for FcγRIIIA$^{176F}$ specific binding from the yeast-based screen were expressed from HEK cells and assayed for relative binding to FcγRIIIA$^{176F}$ and FcγRIIB compared to wild-type (WT). Fluorescein-labeled yeast were incubated with cell culture supernatants, labeled with 5.0 nM of streptavidin Alexa 647 FcγR tetramer, and then cells analyzed by flow cytometry. Data represent the average of two trials, normalized by the relative IgG surface loading of a given variant compared to wild-type, as determined by a separate Protein A 647 loading control. Dashes represent the same residue as the wild-type sequence.

**Figure 5.3**

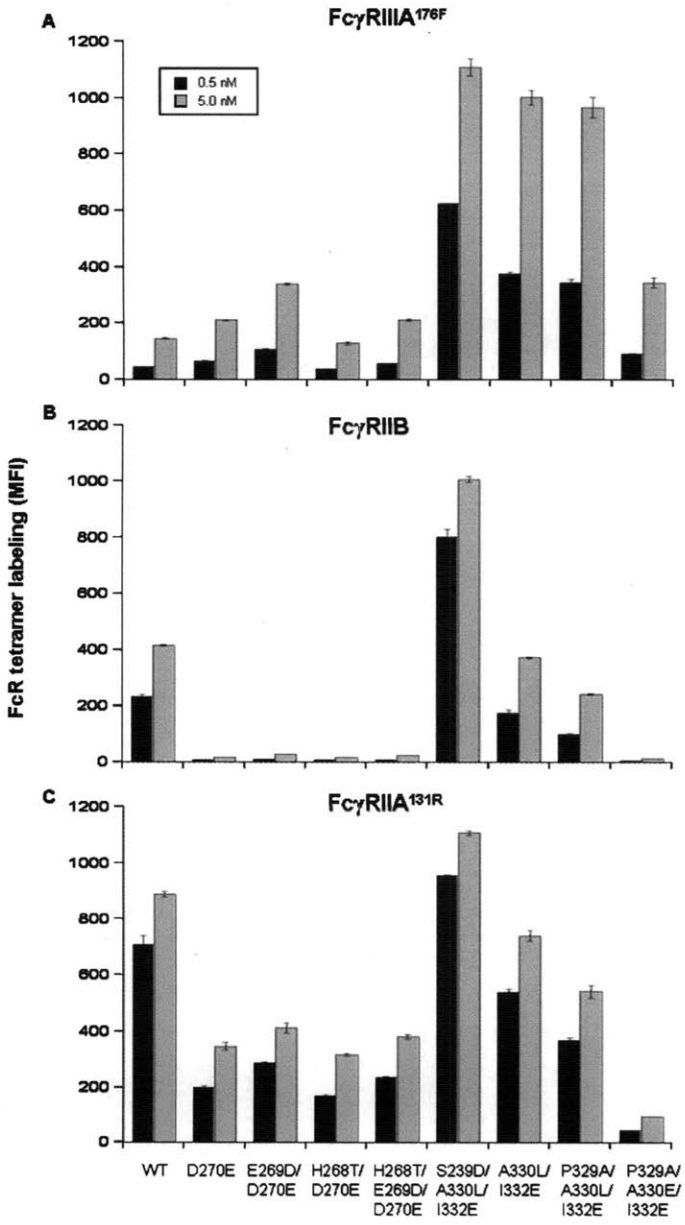


**Mutational analysis of lead clones enriched for FcγRIIIA specific binding.** Relative binding of the previously described D270E variant compared to the enriched B/C loop clone H268T/E269D/D270E and the component double mutants H268T/D270E and E269D/D270E. Similarly, relative binding of the previously described S239D/A330L/I332E variant and the F/G loop only clones A330L/I332E, P329A/A330L/I332E, and P329A/A330L/I332E to **(A)** FcγRIIIA$^{176F}$, **(B)** FcγRIIB, and **(C)** FcγRIIA$^{131R}$. 4m5.3 Fc variants were expressed from HEK cells, purified with Protein A agarose, and 20 μg/ml of antibody loaded onto fluorescein-labeled yeast. Yeast were labeled with streptavidin Alexa 647 FcγR tetramers and analyzed by flow cytometry. Data represent the average of two trials; similar IgG surface loading of a given variant compared to wild-type was confirmed by a separate Protein A 647 loading control.

**Figure 5.4**

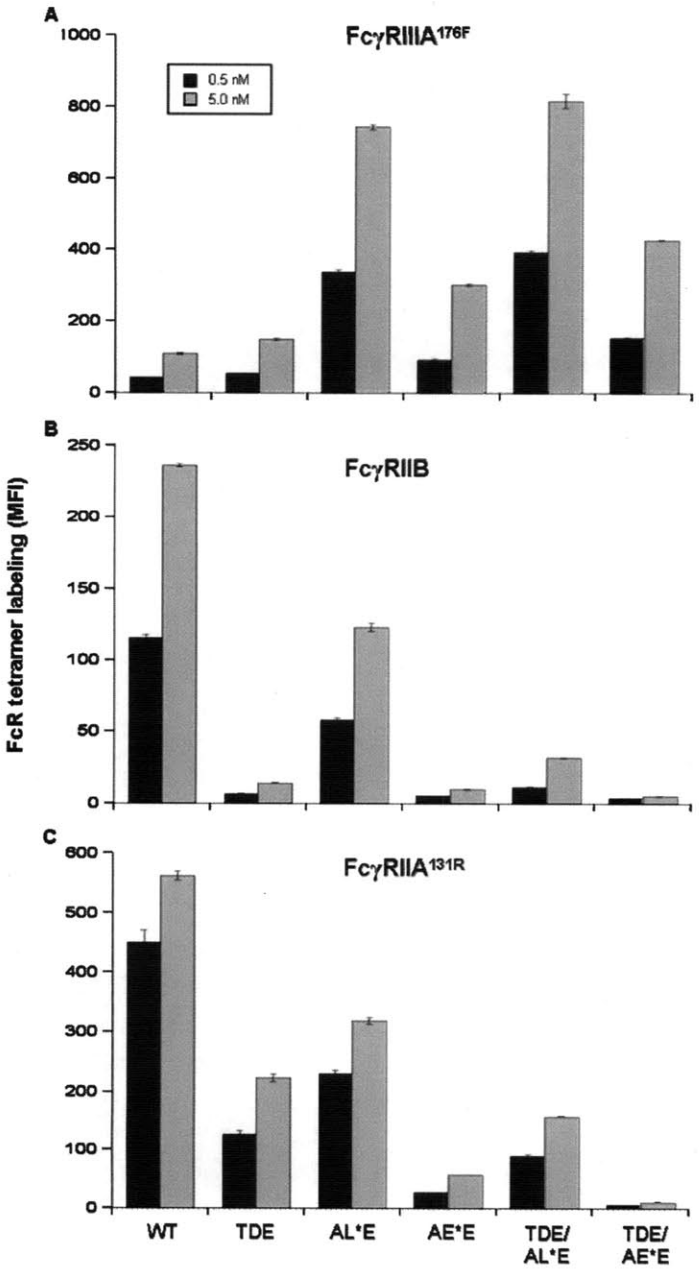


**Effect of loop grafting of candidate B/C and F/G loop variants.** Relative binding of H268T/E269D/D270E (TDE), P329A/A330L/I332E (AL*E), P329A/A330E/I332E (AE*E), and the loop grafted versions TDE/AL*E and TDE/AE*E to **(A)** FcγRIIIA$^{176F}$, **(B)** FcγRIIB, and **(C)** FcγRIIA$^{131R}$. 4m5.3 Fc variants were expressed from HEK cells, purified with Protein A agarose, and 20 μg/ml of antibody loaded onto fluorescein-labeled yeast. Yeast were labeled with streptavidin Alexa 647 FcγR tetramers and analyzed by flow cytometry. Data represent the average of two trials; similar IgG surface loading of a given variant compared to wild-type was confirmed by a separate Protein A 647 loading control.

**Figure 5.5 (a, b)**

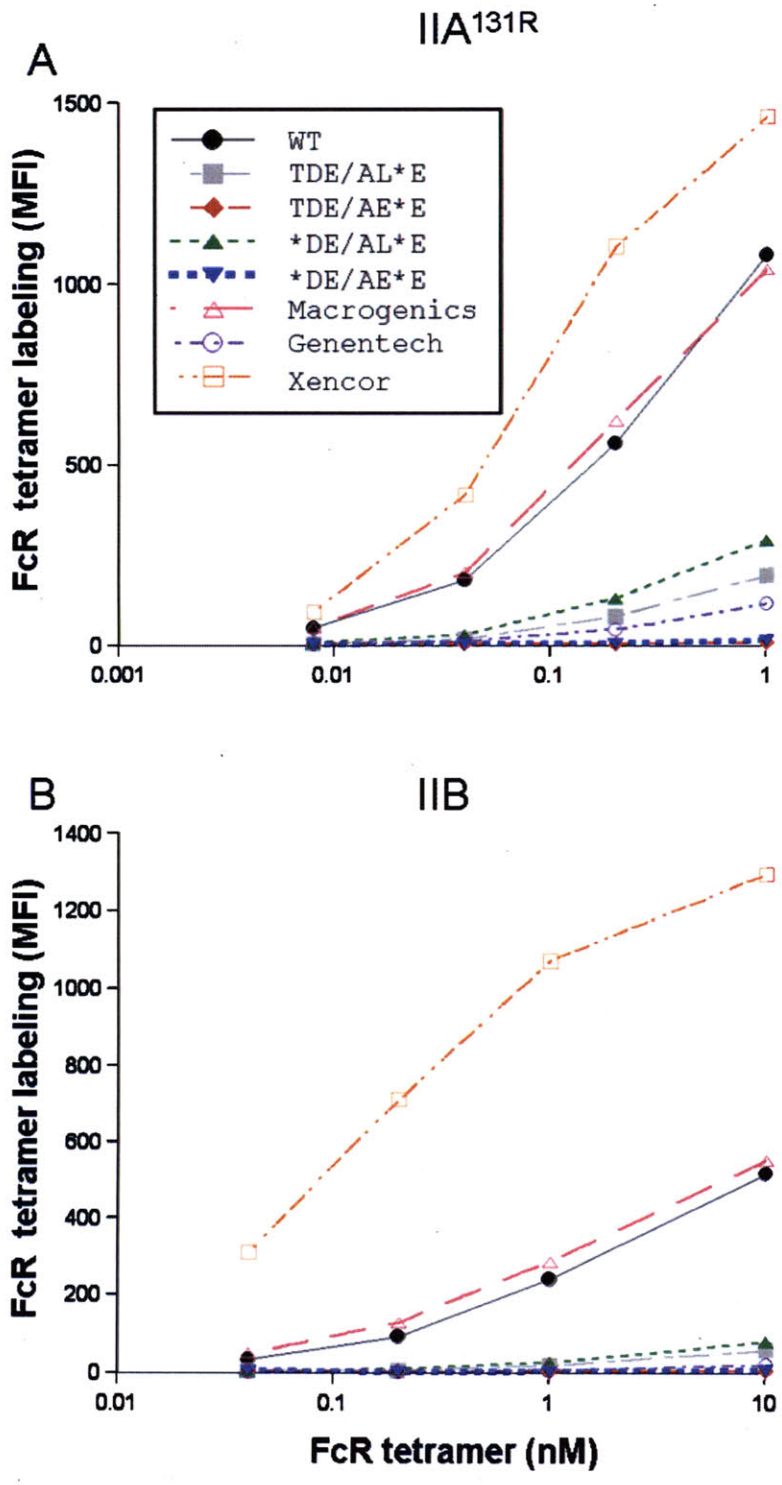
IIA131R
A
FcR tetramer labeling (MFI)
1500
1000
500
0
0.001
0.01
0.1
1
WT
TDE/AL*E
TDE/AE*E
*DE/AL*E
*DE/AE*E
Macrogenics
Genentech
Xencor
B
IIB
FcR tetramer labeling (MFI)
1400
1200
1000
800
600
400
200
0
0.01
0.1
1
10
FcR tetramer (nM)

**Figure 5.5 (c, d)**

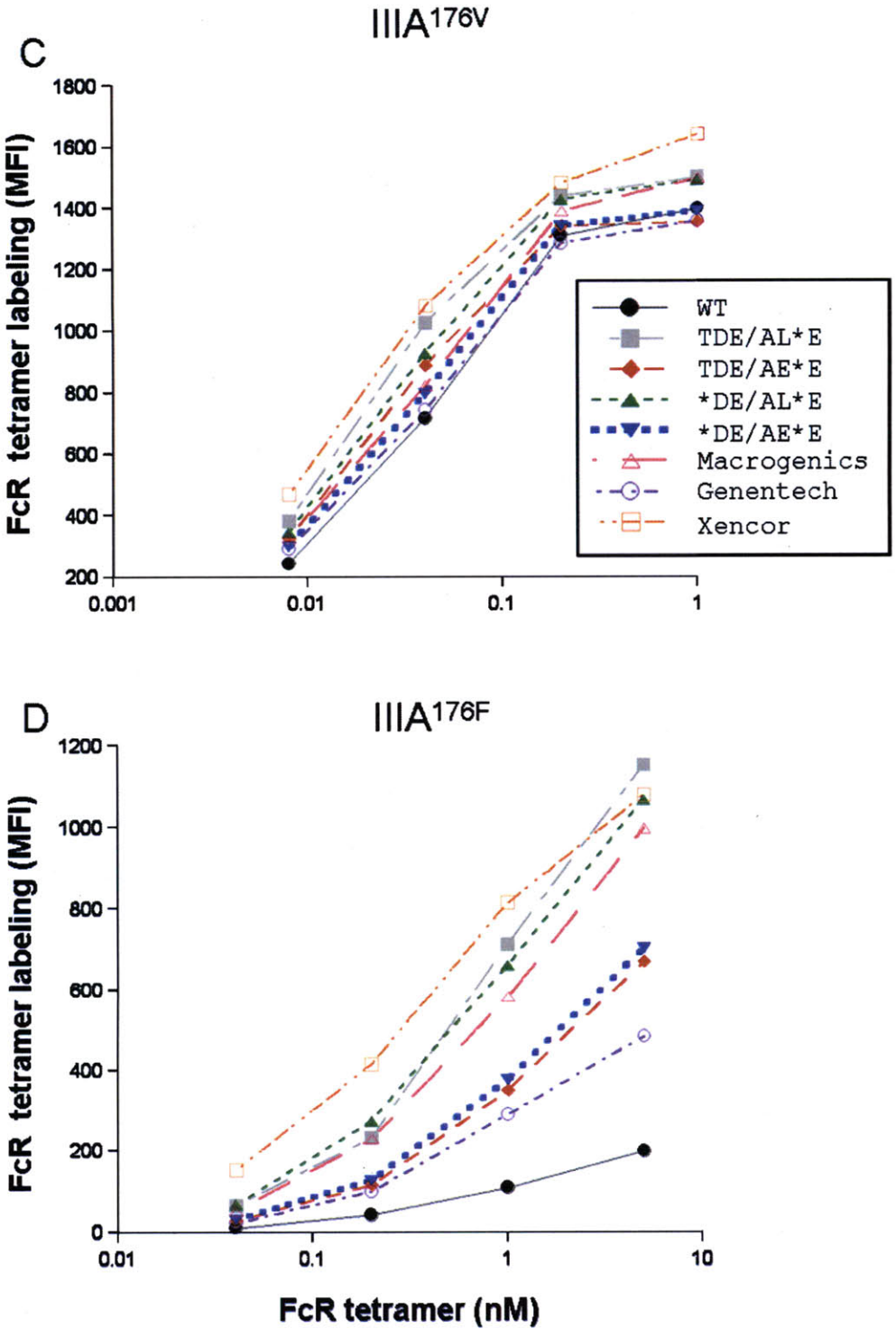
C
IIIA176V
FcR tetramer labeling (MFI)
1800
1600
1400
1200
1000
800
600
400
200
0.001
0.01
0.1
1
WT
TDE/AL*E
TDE/AE*E
*DE/AL*E
*DE/AE*E
Macrogenics
Genentech
Xencor
D
IIIA176F
FcR tetramer labeling (MFI)
1200
1000
800
600
400
200
0
0.01
0.1
1
10
FcR tetramer (nM)

**Figure 5.5 (legend)**

**Comparison of engineered variants to published variants.** Relative binding of the engineered, loop-grafted FcγRIIIA-specific variants compared to previously published variants, to **(A)** FcγRIIA$^{131R}$, **(B)** FcγRIIB, **(C)** FcγRIIIA$^{176V}$, and **(D)** FcγRIIIA$^{176F}$. Variant abbreviations:

| | |
|---|---|
| WT | wild-type |
| TDE/AL*E | H268T/E269D/D270E/P329A/A330L/I332E |
| TDE/AE*E | H268T/E269D/D270E/P329A/A330E/I332E |
| *DE/AL*E | E269D/D270E/P329A/A330L/I332E |
| *DE/AE*E | E269D/D270E/P329A/A330E/I332E |
| Macrogenics | F243L/R292P/Y300L/V305I/P396L |
| Genentech | S298A/E333A/K334A |
| Xencor | S239D/A330L/I332E |

4m5.3 Fc variants were expressed from HEK cells, purified with Protein A agarose, and 20 μg/ml of antibody loaded onto fluorescein-labeled yeast. Yeast were labeled with streptavidin Alexa 647 FcγR tetramers and analyzed by flow cytometry. Data represent the average of two trials; similar IgG surface loading of a given variant compared to wild-type was confirmed by a separate Protein A 647 loading control.

**Figure 5.6**

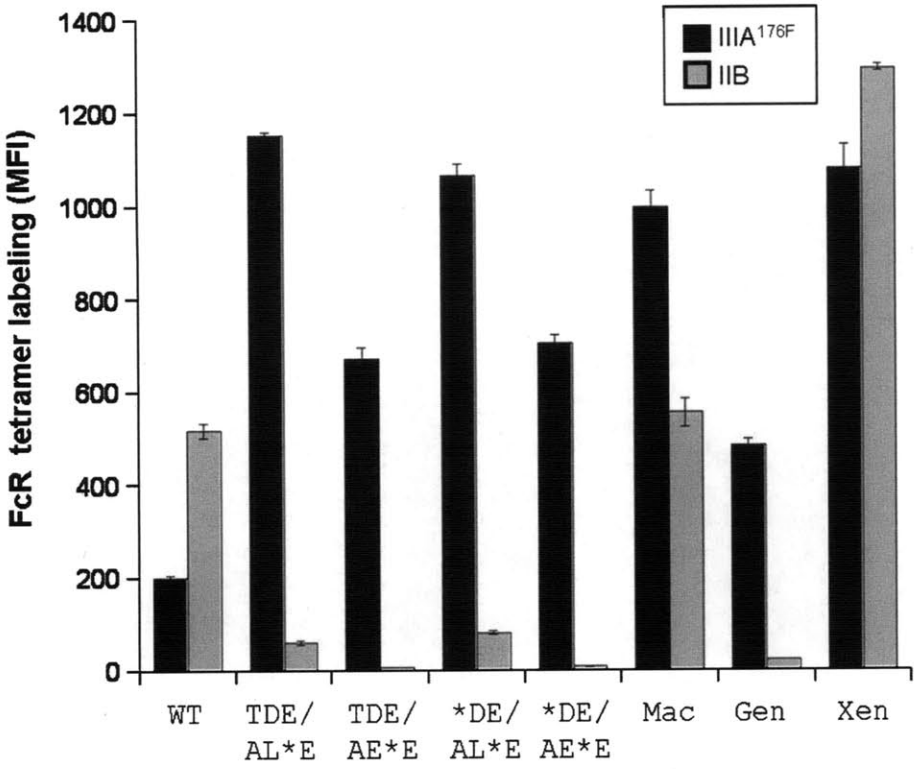


**Comparison of engineered variants to published variants.** Data from Figure 5.5, replotted to illustrate the changes in FcγRIIIA$^{176F}$ and FcγRIIB binding in comparison to wild-type Fc. Data represent the points at 5 nM FcγRIIIA$^{176F}$ tetramer and 10 nM FcγRIIB tetramer. Additional abbreviations from Figure 5.5 legend: Mac (Macrogenics), Gen (Genentech), Xen (Xencor).

## References


1. Adams GP & Weiner LM (2005) Monoclonal antibody therapy of cancer. *Nat Biotechnol* **23,** 1147-1157.
2. Reichert JM & Valge-Archer VE (2007) Development trends for monoclonal antibody cancer therapeutics. *Nat Rev Drug Discov* **6,** 349-356.
3. Waldmann TA (2003) Immunotherapy: past, present and future. *Nat Med* **9,** 269-277.
4. Carter P (2001) Improving the efficacy of antibody-based cancer therapies. *Nature Reviews Cancer* **1,** 118-129.
5. Nimmerjahn F & Ravetch JV (2007) Antibodies, Fc receptors and cancer. *Curr Opin Immunol* **19,** 239-245.
6. Radaev S, Motyka S, Fridman WH, Sautes-Fridman C, & Sun PD (2001) The structure of a human type III Fcgamma receptor in complex with Fc. *J Biol Chem* **276,** 16469-16477.
7. Sondermann P, Huber R, Oosthuizen V, & Jacob U (2000) The 3.2-A crystal structure of the human IgG1 Fc fragment-Fc gammaRIII complex. *Nature* **406,** 267-273.
8. Jefferis R & Lund J (2002) Interaction sites on human IgG-Fc for FcgammaR: current models. *Immunol Lett* **82,** 57-65.
9. Shields RL, *et al.* (2002) Lack of fucose on human IgG1 N-linked oligosaccharide improves binding to human Fcgamma RIII and antibody-dependent cellular toxicity. *J Biol Chem* **277,** 26733-26740.
10. Kaneko Y, Nimmerjahn F, & Ravetch JV (2006) Anti-inflammatory activity of immunoglobulin G resulting from Fc sialylation. *Science* **313,** 670-673.
11. Clynes RA, Towers TL, Presta LG, & Ravetch JV (2000) Inhibitory Fc receptors modulate in vivo cytoxicity against tumor targets. *Nat Med* **6,** 443-446.
12. Nimmerjahn F & Ravetch JV (2005) Divergent immunoglobulin g subclass activity through selective Fc receptor binding. *Science* **310,** 1510-1512.
13. Cartron G, *et al.* (2002) Therapeutic activity of humanized anti-CD20 monoclonal antibody and polymorphism in IgG Fc receptor FcgammaRIIIa gene. *Blood* **99,** 754-758.
14. Musolino A, *et al.* (2008) Immunoglobulin G fragment C receptor polymorphisms and clinical efficacy of trastuzumab-based therapy in patients with HER-2/neu-positive metastatic breast cancer. *J Clin Oncol* **26,** 1789-1796.
15. Weng WK, Czerwinski D, Timmerman J, Hsu FJ, & Levy R (2004) Clinical outcome of lymphoma patients after idiotype vaccination is correlated with humoral immune response and immunoglobulin G Fc receptor genotype. *J Clin Oncol* **22,** 4717-4724.
16. Weng WK & Levy R (2003) Two immunoglobulin G fragment C receptor polymorphisms independently predict response to rituximab in patients with follicular lymphoma. *J Clin Oncol* **21,** 3940-3947.
17. Desjarlais JR, Lazar GA, Zhukovsky EA, & Chu SY (2007) Optimizing engagement of the immune system by anti-tumor antibodies: an engineer's perspective. *Drug Discov Today* **12,** 898-910.
18. Li HJ, *et al.* (2006) Optimization of humanized IgGs in glycoengineered Pichia pastoris. *Nature Biotechnology* **24,** 210-215.
19. Yamane-Ohnuki N, *et al.* (2004) Establishment of FUT8 knockout Chinese hamster ovary cells: an ideal host cell line for producing completely defucosylated antibodies with enhanced antibody-dependent cellular cytotoxicity. *Biotechnol Bioeng* **87,** 614-622.
20. Lazar GA, *et al.* (2006) Engineered antibody Fc variants with enhanced effector function. *Proc Natl Acad Sci U S A* **103,** 4005-4010.
21. Shields RL, *et al.* (2001) High resolution mapping of the binding site on human IgG1 for Fc gamma RI, Fc gamma RII, Fc gamma RIII, and FcRn and design of IgG1 variants with improved binding to the Fc gamma R. *J Biol Chem* **276,** 6591-6604.

22. Stavenhagen JB, *et al.* (2007) Fc optimization of therapeutic antibodies enhances their ability to kill tumor cells in vitro and controls tumor expansion in vivo via low-affinity activating Fcgamma receptors. *Cancer Res* **67,** 8882-8890.
23. Richards JO, *et al.* (2008) Optimization of antibody binding to FcgammaRIIa enhances macrophage phagocytosis of tumor cells. *Mol Cancer Ther* **7,** 2517-2527.
24. Kohler G & Milstein C (1975) Continuous cultures of fused cells secreting antibody of predefined specificity. *Nature* **256,** 495-497.
25. Simmons LC, *et al.* (2002) Expression of full-length immunoglobulins in Escherichia coli: rapid and efficient production of aglycosylated antibodies. *Journal of Immunological Methods* **263,** 133-147.
26. Mazor Y, Van Blarcom T, Mabry R, Iverson BL, & Georgiou G (2007) Isolation of engineered, full-length antibodies from libraries expressed in Escherichia coli. *Nat Biotechnol* **25,** 563-565.
27. Gasser B & Mattanovich D (2007) Antibody production with yeasts and filamentous fungi: on the road to large scale? *Biotechnol Lett* **29,** 201-212.
28. Wood CR, *et al.* (1985) The synthesis and in vivo assembly of functional antibodies in yeast. *Nature* **314,** 446-449.
29. Horwitz AH, Chang CP, Better M, Hellstrom KE, & Robinson RR (1988) Secretion of functional antibody and Fab fragment from yeast cells. *Proc Natl Acad Sci U S A* **85,** 8678-8682.
30. Ogunjimi AA, Chandler JM, Gooding CM, Recinos A, & Choudary PV (1999) High-level secretory expression of immunologically active intact antibody from the yeast Pichia pastoris. *Biotechnology Letters* **21,** 561-567.
31. Ward M, *et al.* (2004) Characterization of humanized antibodies secreted by Aspergillus niger. *Applied and Environmental Microbiology* **70,** 2567-2576.
32. Brake AJ (1990) Alpha-Factor Leader-Directed Secretion of Heterologous Proteins from Yeast. *Methods in Enzymology* **185,** 408-421.
33. Brake AJ, *et al.* (1984) Alpha-Factor-Directed Synthesis and Secretion of Mature Foreign Proteins in Saccharomyces-Cerevisiae. *Proceedings of the National Academy of Sciences of the United States of America-Biological Sciences* **81,** 4642-4646.
34. Rakestraw JA, Baskaran AR, & Wittrup KD (2006) A flow cytometric assay for screening improved heterologous protein secretion in yeast. *Biotechnol Prog* **22,** 1200-1208.
35. Rakestraw JA (2006) A directed evolution approach to engineering recombinant protein production in S. cerevisiae. *Ph.D. thesis (Massachusetts Institute of Technology).*
36. Yeung YA, *et al.* (2007) Isolation and characterization of human antibodies targeting human aspartyl (asparaginyl) beta-hydroxylase. *Hum Antibodies* **16,** 163-176.
37. Sikorski RS & Hieter P (1989) A system of shuttle vectors and yeast host strains designed for efficient manipulation of DNA in Saccharomyces cerevisiae. *Genetics* **122,** 19-27.
38. Boder ET, Midelfort KS, & Wittrup KD (2000) Directed evolution of antibody fragments with monovalent femtomolar antigen-binding affinity. *Proc Natl Acad Sci U S A* **97,** 10701-10705.
39. Robinson AS, Hines V, & Wittrup KD (1994) Protein disulfide isomerase overexpression increases secretion of foreign proteins in Saccharomyces cerevisiae. *Biotechnology (N Y)* **12,** 381-384.
40. Gagnon-Arsenault I, Tremblay J, & Bourbonnais Y (2006) Fungal yapsins and cell wall: a unique family of aspartic peptidases for a distinctive cellular function. *FEMS Yeast Res* **6,** 966-978.

41. Krysan DJ, Ting EL, Abeijon C, Kroos L, & Fuller RS (2005) Yapsins are a family of aspartyl proteases required for cell wall integrity in Saccharomyces cerevisiae. *Eukaryot Cell* **4,** 1364-1374.
42. Bourbonnais Y, Larouche C, & Tremblay GM (2000) Production of full-length human pre-elafin, an elastase specific inhibitor, from yeast requires the absence of a functional yapsin 1 (Ypslp) endoprotease. *Protein Expr Purif* **20,** 485-491.
43. Copley KS, Alm SM, Schooley DA, & Courchesne WE (1998) Expression, processing and secretion of a proteolytically-sensitive insect diuretic hormone by Saccharomyces cerevisiae requires the use of a yeast strain lacking genes encoding the Yap3 and Mkc7 endoproteases found in the secretory pathway. *Biochem J* **330 ( Pt 3),** 1333-1340.
44. Kang HA, Kim SJ, Choi ES, Rhee SK, & Chung BH (1998) Efficient production of intact human parathyroid hormone in a Saccharomyces cerevisiae mutant deficient in yeast aspartic protease 3 (YAP3). *Appl Microbiol Biotechnol* **50,** 187-192.
45. Kerry-Williams SM, Gilbert SC, Evans LR, & Ballance DJ (1998) Disruption of the Saccharomyces cerevisiae YAP3 gene reduces the proteolytic degradation of secreted recombinant human albumin. *Yeast* **14,** 161-169.
46. Shusta EV, Raines RT, Pluckthun A, & Wittrup KD (1998) Increasing the secretory capacity of Saccharomyces cerevisiae for production of single-chain antibody fragments. *Nat Biotechnol* **16,** 773-777.
47. Boder ET & Wittrup KD (2000) Yeast surface display for directed evolution of protein expression, affinity, and stability. *Methods Enzymol* **328,** 430-444.
48. Rakestraw A & Wittrup KD (2006) Contrasting secretory processing of simultaneously expressed heterologous proteins in Saccharomyces cerevisiae. *Biotechnol Bioeng* **93,** 896-905.
49. Gemmill TR & Trimble RB (1999) Overview of N- and O-linked oligosaccharide structures found in various yeast species. *Biochim Biophys Acta* **1426,** 227-237.
50. Munro S (2001) What can yeast tell us about N-linked glycosylation in the Golgi apparatus? *FEBS Lett* **498,** 223-227.
51. Gerngross TU (2004) Advances in the production of human therapeutic proteins in yeasts and filamentous fungi. *Nature Biotechnology* **22,** 1409-1414.
52. Hamilton SR, *et al.* (2003) Production of complex human glycoproteins in yeast. *Science* **301,** 1244-1246.
53. Hamilton SR, *et al.* (2006) Humanization of yeast to produce complex terminally sialylated glycoproteins. *Science* **313,** 1441-1443.
54. Hamilton SR & Gerngross TU (2007) Glycosylation engineering in yeast: the advent of fully humanized yeast. *Current Opinion in Biotechnology* **18,** 387-392.
55. Yeung YA, et. al. (2007) Isolation and characterization of human antibodies targeting human aspartyl (asparaginyl) beta-hydroxylase. *Hum Antibodies* **16,** 163-176.
56. Johnston M, Riles L, & Hegemann JH (2002) Gene disruption. *Methods Enzymol* **350,** 290-315.
57. Xu P, Raden, D., Doyle, FJ 3rd, Robinson, A.S. (2005) Analysis of unfolded protein response during single-chain antibody expression in *Saccharomyces cerevisiae* reveals different roles for BiP and PDI in folding. *Metabolic Engineering* **7,** 269-279.
58. Giard DJ, *et al.* (1973) In vitro cultivation of human tumors: establishment of cell lines derived from a series of solid tumors. *J Natl Cancer Inst* **51,** 1417-1423.
59. Kim YS, Bhandari, R., Cochran, J.R., Kuriyan, J., Wittrup, K.D. (2006) Directed evolution of the epidermal growth factor receptor extracellular domain for expression in yeast. *Proteins* **62,** 1026-1035.
60. Nimmerjahn F & Ravetch JV (2008) Fcgamma receptors as regulators of immune responses. *Nat Rev Immunol* **8,** 34-47.

61. Arnold JN, Wormald MR, Sim RB, Rudd PM, & Dwek RA (2007) The impact of glycosylation on the biological function and structure of human immunoglobulins. *Annu Rev Immunol* **25,** 21-50.
62. Tao MH & Morrison SL (1989) Studies of aglycosylated chimeric mouse-human IgG. Role of carbohydrate in the structure and effector functions mediated by the human IgG constant region. *J Immunol* **143,** 2595-2601.
63. Mimura Y, *et al.* (2001) Role of oligosaccharide residues of IgG1-Fc in Fc gamma RIIb binding. *J Biol Chem* **276,** 45539-45547.
64. Walker MR, Lund J, Thompson KM, & Jefferis R (1989) Aglycosylation of human IgG1 and IgG3 monoclonal antibodies can eliminate recognition by human cells expressing Fc gamma RI and/or Fc gamma RII receptors. *Biochem J* **259,** 347-353.
65. Simmons LC, *et al.* (2002) Expression of full-length immunoglobulins in Escherichia coli: rapid and efficient production of aglycosylated antibodies. *J Immunol Methods* **263,** 133-147.
66. Li H, *et al.* (2006) Optimization of humanized IgGs in glycoengineered Pichia pastoris. *Nat Biotechnol* **24,** 210-215.
67. Krapp S, Mimura Y, Jefferis R, Huber R, & Sondermann P (2003) Structural analysis of human IgG-Fc glycoforms reveals a correlation between glycosylation and structural integrity. *J Mol Biol* **325,** 979-989.
68. Basu M, *et al.* (1993) Purification and characterization of human recombinant IgE-Fc fragments that bind to the human high affinity IgE receptor. *J Biol Chem* **268,** 13118-13127.
69. Garman SC, Wurzburg BA, Tarchevskaya SS, Kinet JP, & Jardetzky TS (2000) Structure of the Fc fragment of human IgE bound to its high-affinity receptor Fc epsilonRI alpha. *Nature* **406,** 259-266.
70. McKenzie SE, *et al.* (1999) The role of the human Fc receptor Fc gamma RIIA in the immune clearance of platelets: a transgenic mouse model. *J Immunol* **162,** 4311-4318.
71. Maxwell KF, *et al.* (1999) Crystal structure of the human leukocyte Fc receptor, Fc gammaRIIa. *Nat Struct Biol* **6,** 437-442.
72. Lee LP & Tidor B (2001) Optimization of binding electrostatics: charge complementarity in the barnase-barstar protein complex. *Protein Sci* **10,** 362-377.
73. Idusogie EE, *et al.* (2001) Engineered antibodies with increased activity to recruit complement. *J Immunol* **166,** 2571-2575.
74. Oganesyan V, Damschroder MM, Leach W, Wu H, & Dall'Acqua WF (2008) Structural characterization of a mutated, ADCC-enhanced human Fc fragment. *Mol Immunol* **45,** 1872-1882.
75. Mimura Y, *et al.* (2000) The influence of glycosylation on the thermal stability and effector function expression of human IgG1-Fc: properties of a series of truncated glycoforms. *Mol Immunol* **37,** 697-706.
76. Anthony RM, *et al.* (2008) Recapitulation of IVIG anti-inflammatory activity with a recombinant IgG Fc. *Science* **320,** 373-376.
77. Nandakumar KS, *et al.* (2007) Endoglycosidase treatment abrogates IgG arthritogenicity: importance of IgG glycosylation in arthritis. *Eur J Immunol* **37,** 2973-2982.
78. Chao G, *et al.* (2006) Isolating and engineering human antibodies using yeast surface display. *Nat Protoc* **1,** 755-768.
79. Lippow SM, Wittrup KD, & Tidor B (2007) Computational design of antibody-affinity improvement beyond in vivo maturation. *Nat Biotechnol* **25,** 1171-1176.
80. Bayly CI, Cieplak P, Cornell WD, & Kollman PA (1993) A Well-Behaved Electrostatic Potential Based Method Using Charge Restraints for Deriving Atomic Charges - the Resp Model. *Journal of Physical Chemistry* **97,** 10269-10280.

81. Sitkoff D, Sharp KA, & Honig B (1994) Accurate Calculation of Hydration Free-Energies Using Macroscopic Solvent Models. *Journal of Physical Chemistry* **98,** 1978-1988.
82. Sondermann P, Kaiser J, & Jacob U (2001) Molecular basis for immune complex recognition: a comparison of Fc-receptor structures. *J Mol Biol* **309,** 737-749.
83. Baudino L, *et al.* (2008) Crucial role of aspartic acid at position 265 in the CH2 domain for murine IgG2a and IgG2b Fc-associated effector functions. *J Immunol* **181,** 6664-6669.
84. Geiser M, Cebe R, Drewello D, & Schmitz R (2001) Integration of PCR fragments at any specific site within cloning vectors without the use of restriction enzymes and DNA ligase. *Biotechniques* **31,** 88-90, 92.
85. Umana P, Jean-Mairet J, Moudry R, Amstutz H, & Bailey JE (1999) Engineered glycoforms of an antineuroblastoma IgG1 with optimized antibody-dependent cellular cytotoxic activity. *Nat Biotechnol* **17,** 176-180.